# Validation of conventional concrete water transport test methods by spatially resolved $^{1}H$ magnetic resonance

**By Noémi Fischer**

Submitted for the engineering doctorate degree from the University of Surrey

Micro and NanoMaterials and Technologies Engineering
University of Surrey

2015

**Declaration of Originality**

I confirm that the submitted work is my own work and that I have clearly identified and fully acknowledged all material that is entitled to be attributed to others (whether published or unpublished) using the referencing system set out in the programme handbook.

I agree that the University may submit my work to means of checking this, such as the plagiarism detection service Turnitin® UK.

I confirm that I understand that assessed work that has been shown to have been plagiarised will be penalised.

**Acknowledgment**

The research leading to these results has received funding from the European Union Seventh Framework Programme (FP7 / 2007-2013) under *grant agreement* 264448.

**Abstract**

Concrete is the most used man made material worldwide with about 1.4 $m^3$ being produced per person every year. As the service life of civil engineering structures is usually 50-100 years, the long-term durability of concrete is a significant issue. The content and mobility of water especially in the surface layers plays an important role in most durability aspects of concrete. Conventional tests of water transport in concrete are empirically derived and usually based on mass increase or visual observation. These tests give no information on the state of water or the saturation within the pore structure of concrete and are not linked to transport theories. Few, if any *in-situ,* non-destructive test method exists that provides spatial resolution of water content as a function of distance from the surface. A recently developed one-sided ‘H nuclear magnetic resonance (NMR) setup allows the investigation of samples larger than the equipment itself and gives spatial resolution of water profiles down to a depth of circa 25 mm. Moreover, in principle, NMR allows the classification of water in porous materials by pore type.

The aim of this work was to use a one-sided NMR with a standard procedure for water content that can be readily applied and easily interpreted and understood. Both the test protocol and the instrument, which were developed under laboratory conditions, required refinement for application in an industrial setting. This required the calibration of the measurement and the optimisation of data acquisition and analysis for concrete and mortar. The practical limitations of the NMR method are discussed.

To provide a scientific background for these tests the water profiles obtained by NMR were compared to conventional capillary absorption and permeability test results. Further investigations of water transport revealed that swelling of the calcium-silicate-hydrate gel is a probable cause for the sorptivity anomaly. The NMR results showed that visual observation is a poor indicator of water penetration depth as there is a significant amount of water present beyond the visual waterfront.

## Table of contents

# 1 Introduction and aim of research

## 1.1 Background to the project

Concrete is the most widely used man-made material. About 20 billion tonnes, around 1.4 cubic metre per person globally manufactured every year [1]. It contributes about 6% of the global $CO_2$ emission by human activities [2] mostly due to the cement production process. Cement is the binder phase of concrete. About half of the $CO_2$ comes from the breakdown of limestone, the main raw material of cement. The other half comes from the heating to burn the raw materials at high temperature, about 1400°C. The production process is highly optimised. To reduce the environmental impact, the options are to use supplementary cementitious materials, especially by-products of other industries and/or improve durability. As service for life civil engineering structures is 50-150 years, long time durability is a significant issue.

Water transport in concrete plays a key role in most degradation processes including freeze-thaw, chloride ionic diffusion and sulfate attack either directly or acting as a transport media for ions. However, most of the methods used for testing water transport properties are based on empirical observations and lack the connection to water diffusion and flow theories. Better understanding for those tests is very important for future use especially for high performance materials with new composite binders.

Several methods for testing water transport exist, the conventional ones measuring the amount of water that ingresses or traverses a test specimen as a function of time. Those tests are usually based on mass change or on a visual water line and are influenced by the pore size distribution and connectivity. Therefore the interpretation of data is not straightforward. This can lead to false assumptions of the transport processes and the the state of water or the spatial variation. Ion transport is enabled by the water present in the porosity and both are essential in aqueous corrosion of steel reinforcement bars. In capillary absorption ions are diffused in liquid water. Ions can also be transported within the pore network driven by the ion concentration gradient.

Nuclear magnetic resonance (NMR) is an established method for both pore structure analysis and water transport in porous media that can provide such information as a function of position making it an appropriate technique for comparison. Most NMR methods require specimens to be put inside a magnet, but recent advances in NMR technology applied to other branches of materials science including rocks for petroleum engineering, have seen the introduction of one-sided magnets that can be place on or beside a large sample. These magnets have obvious advantages for concrete and the concrete industry.

The aim of the research program is to compare the performance of one-sided NMR methods with conventional tests used to asses water uptake and movement in cementitious materials. In particular the effect of different pore structures shall be investigated. Validation, providing better scientific background and understanding, of widely used test procedures for moisture transport measurements. Ultimately, this will help to improve durability and life cycle analysis for concrete.

The research project is part of the Nanocem Transcend program funded by the Marie Curie Initial Training Network for better understanding and prediction of water transport in cementitious materials that seeks to integrate modelling and experimental approaches across multiple length and timescales.

## 1.2 Structure of the report

Following the introductory chapter, Chapter 1 contains basic information on cementitious materials, review of previous work on concrete water transport tests, basics of nuclear magnetic resonance, mobile NMR and work done on cement. Chapter 3 contains the improvements on the Surface GARField NMR measurement, data acquisition, data analysis and calibration. NMR methods and cementitious materials used are described in Chapter 4. NMR evidence of the limitation of the sorptivity and permeability is in Chapter 5 including all three basic mixtures used. Chapter 6 is about the results on the long-term sorptivity. Chapter 7 contains the results relating to the relationship between visual water front and penetration depth measured by NMR. Chapter 8 provides a conclusion of the results and also possibilities of future work.

# 2 Review of previous work

## 2.1 Introduction

This chapter includes a summary of the use, microstructure and water in cement and concrete, the conventional water transport test methods and the basics of NMR. Water transport in concrete is governed by the microstructure and porosity. The pore structure of the concrete mostly depends on the binder, water to cement ratio and curing and can change significantly with age and water content. Therefore, basics of supplementary cementitious materials and the current understanding of pore structure is essential. Part of this thesis focuses on developing a new water transport test method for concrete using nuclear magnetic resonance, therefore the principles of the measurement and previous work on cementitious materials is included.

## 2.2 Concrete history

### 2.2.1 Historic cements

The word cement comes from the Latin *caementum* “rough-cut stone”. Concrete comes from the prefix com “together” and cresco, “grow”.

Although concrete is thought of as a Roman invention, pozzolanic concrete had been used earlier in Greece around 500 BC for the cistern of Kameiros on the Island of Rhodes [3]. Calcium from lime and silica from the volcanic ash mixed with water gives calcium silicate hydrate, which is still the main “glue” in cement paste. This hydraulic binder was then mixed with natural or artificial aggregates depending on availability such as natural sand and gravel, crushed limestone and volcanic pumice. Famous early concrete structures include the Hagia Sofia in Istanbul, the Pantheon in Rome and the Pont du Gard aqueduct in Southern France [4]. The technique spread quickly in the empire. Hydraulic cement was commonly used and was the preferred material for aqueducts.

With the fall of the Roman Empire, most of this knowledge of materials technology was lost from the common use and today's concrete and mortar can be traced back to the 17th century. For example, a type of concrete was used in the construction of the Canal du Midi in France [5]. The Eddystone Lighthouse (1756) led to the development of "Portland cement". Joseph Aspdin patented the technology of burning together finely grounded limestone and clay manufacturing the first artificial cement [6]. The key advantage of this material was the constant quality when compared to "natural" cement, which depended on the geographical location from where the materials were sourced. In addition, Portland cement tended to have better workability than Roman cement concrete, which was very dry and had no slump.

Reinforced concrete was invented by Joseph Monier. He used iron mesh in concrete garden pots and exhibited his new product at the Paris Expo in 1867 [7]. Steel and concrete was a good combination. Steel is used for resisting the tension forces in the structures while the concrete takes up the compression forces and protects the reinforcement bars physically and chemically from damage.

### 2.2.2 Modern use

Concrete is the most common material for building purposes as it is cheap, easily available and can be shaped in any form [8]. The properties vary according to the application: density, consistency or compressive strength. Density usually varies between 800-3500 kg/m$^3$ though aerated concrete have a density as low as 200 kg/m$^3$. Lightweight concrete (800-2000 kg/m$^3$) is used for masonry walls, bridge decks and high buildings to reduce dead load. Heavy concrete (above 2500 kg/m$^3$) is mostly used for radiation protection and ballasting. Compressive strength can reach 150-200 N/mm$^2$, though tensile strength is still very low and reinforcement is needed. Aggregate also varies from gravel and crushed stones to recycled materials (crushed bricks, glass and polymer) [9].

Durability is very important for civil engineering structures. Typically, maintenance costs over lifetime are around 30-50% of the total budget [10]. Buildings and smaller structures are designed for 30-50 years of service and

larger, more important structures such as bridges, dams and tunnels are usually designed to last for 100-150 years. There, the performance of the concrete and protection for the reinforcement over a long time is very important even in harsh and aggressive environments, for example seawater, aggressive chemicals, extreme heat or cold.

## 2.3 Composition of concrete

Across Europe and America, concrete is mainly manufactured from Portland cement, fine and coarse aggregates (usually sand and gravel), water and sometimes admixtures and additives. Admixtures can be used to alter the fresh concrete properties like workability, air content, setting time or colour and also make an impact on the performance of the hardened concrete. Additives are mineral additions, usually cementitious materials that improve or replace Portland cement. For special concrete, metal or polymer fibres are added for improved tensile strength or fire resistance [9].

### 2.3.1 Portland Cement

There are several key reference books on the chemistry and composition of cement, for example Lea's Chemistry of Cement and Concrete [9] and Taylor's Cement Chemistry [11] Portland cement is made from clinker, which is the sintered product made from heating limestone clay and silica. The main phases present in Portland cement are tricalcium silicate (alite), dicalcium silicate (belite), tricalcium aluminate (aluminate) and tetracalcium aluminoferrite (ferrite) [9]. Cement science has its own nomenclature based on the oxides of the elements (*Table 2.1*).

Table 2.1 Cement chemistry notations [9]

| Name | Chemical formulae | Abbreviation |
|---|---|---|
| calcium oxide | $CaO_2$ | C |
| silica | $SiO_2$ | S |
| aluminium oxide | $Al_2O_3$ | A |
| iron oxide | $Fe_2O_3$ | F |
| water | $H_2O$ | H |

Cement hydration, the reaction of anhydrous cement with water, is a very complex dissolution-precipitation reaction that forms hydrates. The main product or phase is calcium silicate hydrate, abbreviated as C-S-H in cement chemistry. The ratio of Ca/Si varies. C-S-H accounts for 50-60% of the products. The structure of C-S-H is highly variable, highly heterogeneous and amorphous, but with nano-scale crystallinity and abundance of nano-scale porosity [12]. The understanding is still fairly poor. Calcium hydroxide or portlandite, $Ca(OH)_2$ abbreviated to CH in cement science notation accounts for a further 15-20%. AFt (alumina ferrite), most commonly ettringite, plays a part in setting and early stages of hydration. AFm (alumina ferrite mono) is usually formed later and has the same compounds as AFt, though in different proportions.

The total volume of hydrated products is smaller than the volume of water and unhydrated cement that was mixes. This is called chemical shrinkage [9]. The shrinkage leads to the creation of capillary voids that only fill with water if excess water is provided after initial setting (see *Section 2.5.1*).

Though sometimes referred to as the same, setting and hardening are separate phenomena. Setting refers to the paste solidification due to early C-S-H and ettringite formation, locking the hydration products with each other and hardening is the chemical process that continues long after the paste is set and gives the strength of the material.

### 2.3.2 Supplementary Cementitious Materials

Mineral additives are pozzolanic or latent hydraulic materials that improve concrete properties usually by increasing the level of hydration and further

formation of C-S-H. To reduce the $CO_2$ emission of concrete production, the two possibilities are either to improve the process of manufacturing or replacing the clinkers. Cement production is already very efficient, so at the moment the solution seems to be replacing the clinkers by the inclusion of supplementary cementitious materials (SCMs). The most important are blast furnace slag, fly ash, silica fume, finely ground limestone and natural pozzolans [13]. They are often waste or by-products of other industries therefore they not just reduce the environmental effects of the cement industry but also others like iron making.

Granulated blast furnace slag is a by-product of iron manufacturing and has irregular shape. It is glassy and has high latent hydraulic properties. Cement mixed with slag has low early compressive strength, but overall it reaches higher strength than ordinary Portland cement (CEM I). Slag reacts with ettringite creating additional C-S-H and therefore creating a finer pore structure. Advantages of slag addition are the better sulfate-resistance, low heat of hydration and better permeability [9].

Fly ash is a by-product of coal-fires power plants. It is small glassy, spherical particles and only the amorphous part is reactive. Fly ashes have two groups. Class F is pozzolanic and requires the presence of portlandite in the presence of water to react. Class C has cementitious properties in its own right and hardens in the presence of water without cement [13].

Silica fume or microsilica is a fine-grain non-crystalline silica, by-product of the production of silicon metals. It is extremely fine (1/100 of average cement particle) and has very high specific surface. It is a highly reactive pozzolan due to the high surface area [13]. The packing of particles is improved and silica fumes reacts with portlandite creating additional C-S-H, both resulting in a finer pore structure.

A comparison for Ca-Si-Al ratios of Portland cement and SCMs with the possible hydration products are shown on *Figure 2.1*. C and F refer to the two types of fly ash.

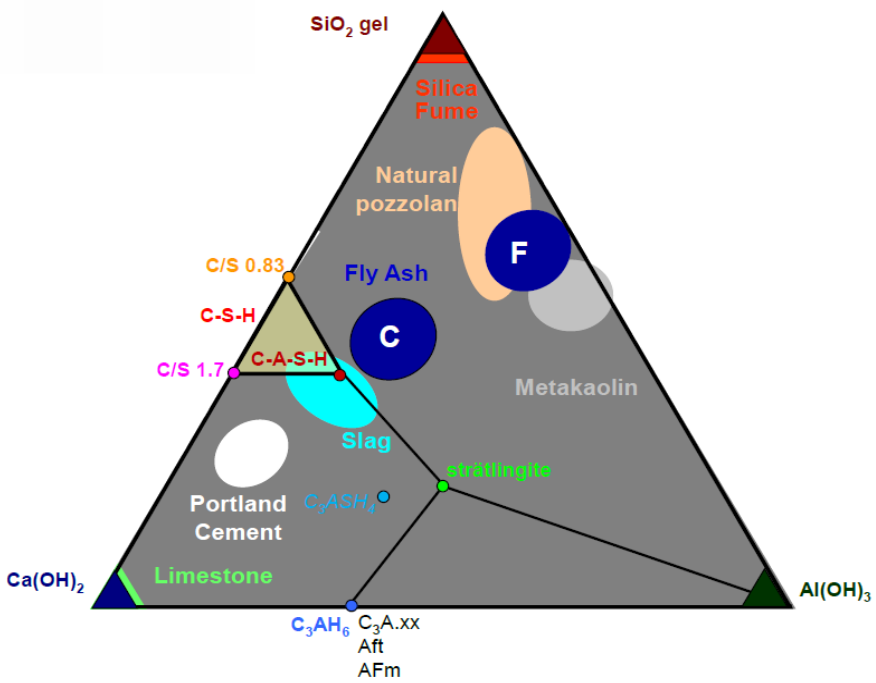


Figure 2.1 Chemical composition and phases of SCMs, reproduced from [13]

Slag reacts with ettringite forming additional C-S-H. The advantages of SCMs are higher strength (at least later strength), higher durability, higher resistance to chloride ingress and sulfate attacks [14-18]. Though some SCMs are widely used, the long-term effects and microstructure that they lead to are not well understood for all SCMs. Also, some of the above mentioned properties are due to the filler effect, that the clinker hydration products have more space to form.

### 2.3.3 Aggregates

The main volume fraction of concrete is aggregates, inorganic granular particles of different sizes. Most common are natural aggregates, such as sand, quartz gravel and crushed rocks (e.g. basalt, dolomite, granite). Other types of aggregates are used for “special”’ applications, such as lightweight or heavy weight concrete. Lightweight aggregates can be natural (expanded clay, volcanic tufa) or artificial (polystyrene or expanded glass, crushed bricks) for making concrete with lower density. Heavy aggregates are hematite, barite and magnetite with high iron content for radiation shielding concrete.

The packing of aggregates is optimized for better performance. The space between the larger particles is filled with smaller and smaller ones. The size

distribution of aggregates is called grading and aggregates are generally put into two categories, fine (below 1-4 mm) and coarse aggregates (above 1-4 mm). The EN 12620:2013 standard [19] defines fine aggregate (sand) below 4 mm and coarse (gravel or crushed rock) with a lower sieve size (minimum size) above 1 mm and the upper sieve size (corresponding to the largest aggregates in the fraction) above 4 mm. So in a graded coarse aggregate with 2/8 fraction the aggregates fall between the 2 and 8 mm sieves with (almost) no aggregates below or above those sieves.

The shape and size of the aggregates influence the properties of both fresh and hardened concrete. Workability, that is how easy the freshly mixed material can be worked in, is dependent on shape and size distribution. The most important characteristics of aggregates are bulk compressive strength, density (bulk and particle density) and possible water absorption (in case of porous lightweight aggregates) or alkali resistance [9].

## 2.4 Structure of concrete from nano- to macroscale

Concrete is a composite material on many length scales from nanometres to centimetres. However, the cement matrix itself is made of different solid phases, pores and water, where only the crystal structure and stoichiometry of calcium hydroxide is fully understood. C-S-H can have foil-like or fibrillar structure that are thought to equate to different Ca/Si ratios. It can also have a more dense and a less dense form that are believed to be related to whether it formed between the original water filled space or in between the other particles [12]. The water to cement ratio influences the amount and connectivity of capillary porosity. High water to cement ratios lead to excess water not required for hydration that fills up space between particles creating a network of larger porosity. [20]. Also, the age, and hence the degree of hydration, influences the microstructure as the hydration products are created. Supplementary cementitious materials in concrete also change the structure of the hardened cement resulting different Ca/Si ratio and additional phases and different pore distribution [15, 21]. For instance, adding silica fume leads to a phase assembly with less portlandite and a lower Ca/Si ratio C-S-H [22].

### 2.4.1 Models

Several models of hydrated cement have been developed, though the exact microstructure is still not clearly understood. Most latter models focus on C-S-H phase only. Other, crystalline phases are better described.

Powers and Brownyard (1948) were the first who worked extensively on a cement model allowing volumetric quantification of the unhydrated cement, hydration product, free water and gel and capillary porosity [23]. Powers modified the model later based on water vapour isotherms and sorption. The model distinguishes non-evaporable below 105°C (chemically bound), gel (physically bound) and capillary water (free). He also noted the effect of different drying techniques on the results [24, 25]. Unlike most of the latter models, the Powers-Brownyard model is not limited to C-S-H only. Mueller et al [26] revised the composition diagrams of the model with different hydration products and water populations and showed that the volume fraction did not depend linearly on the degree of hydration as Powers had assumed.

The current understanding of C-S-H is that it consists of nano-crystalline regions of material similar to tobermorite and jennite. These minerals are composed of sheets of calcium and oxygen atoms and silicate tetrahedra. There is water in three different places. Intra-C-S-H or sheet water is between the silica and calcium layers in C-S-H. Inter C-S-H or gel water is between the locally aggregated C-S-H sheets and water between the nano-crystalline regions. It is still unclear whether these regions are separate granules (colloidal model, [27, 28]) or larger networks of quasi continuous sheet structures sheets (Feldman-Sereda). McDonald et al [29] suggest a model similar to Feldman-Sereda. C-S-H is made of tetrahedral silica layers with calcium and water ions in between. This water is referred as intra-C-S-H water. The C-S-H sheets are stacked with water in between, referred as inter-C-S-H gel water. Both intra (sheet) and inner (gel) pores are considered as planar pores. A comparison for different models is shown on *Figure 2.2*.

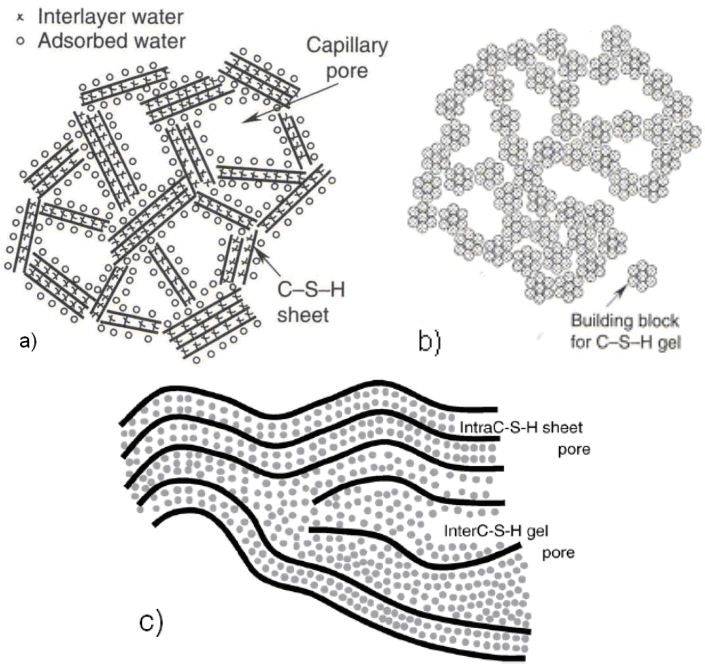


Figure 2.2 Cement and C-S-H models a) Powers b) Jennings, reproduced from [20], c) McDonald et al, reproduced from [29]

Common terminology for future reference is important. Layers are referred to the inner, atomic structure of C-S-H. Sheets refer to the planar structures .For water, the terminology used by McDonald et al will be considered with sheet, gel and capillary/interhydrate pores distinguished.

Concrete is a composite material on several scales, which makes modelling more difficult as it is ranges from nano- to centimetre size pores and particles [30]. To step up to a larger scale from cement paste, concrete material models consist of three phases: cement paste, aggregates and the interfacial transition zone (ITZ) between aggregate particles and bulk cement paste [30-33]. The aggregates are dispersed in the continuous cement matrix with ITZ as interface (*Figure 2.3*).

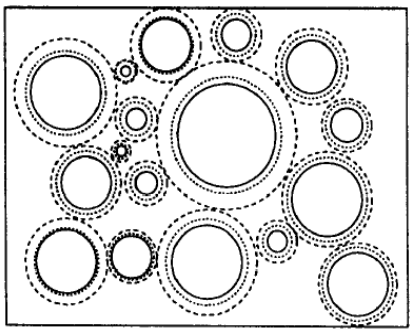

Figure 2.3 Spherical aggregate particles with ITZ around in cement matrix, reproduced from[32]

The ITZ is usually quite different from the bulk paste due to the wall effect of the aggregate. ITZ has usually higher porosity and higher portlandite fraction. It is difficult to determine the ITZ as it has no clear boundary and is dependent on several factors, but it is usually around 10-40 μm thick [33]. The ITZ microstructure is shown schematically in *Figure 2.4*.

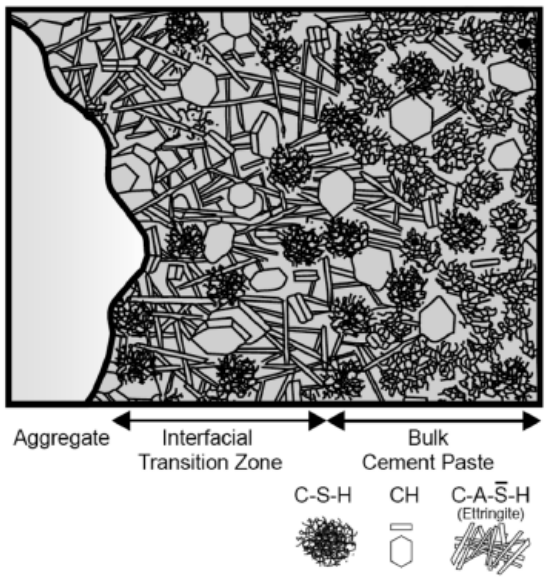


Figure 2.4 Schematic for ITZ microstructure, reproduced from [34]

The packing of aggregates is very important, as aggregates take up about 70-75 vol% of concrete. The perfect packing of aggregates is achieved the cement paste needed to fill the gaps between the aggregates is minimal.

Microcracks (cracks up to about 50 μm width) play an important role in the behaviour of the material, especially on water transport [35]. Microcracks are mainly caused by drying shrinkage and are influenced by many parameters such as the drying rate and temperature, sample thickness the difference in stiffness of the paste and aggregate and the aggregate-paste bond [36]. Chemical shrinkage results from the fact that the total volume of the hardened paste is smaller than the total volume of the ingredients, can also cause cracking. Larger cracks can also be present due to tensile stresses in the concrete under load. Cracks are difficult to include in models. However, they act as a highway for water ingress [37] and can be a much more important factor than the bulk paste Most concrete used in civil engineering is under load that results in tensile stresses larger than the tensile strength and hence the concrete is cracked.

### 2.4.2 Pore structure

Water moves in the pore system of concrete and water transport properties strongly depend on the pore structure characteristics. Therefore the properties of the pore structure are very important. The pore structure of cement is already very complex, but in concrete the ITZ, microcracks and sometimes the porosity of the aggregate (as in the case of porous lightweight aggregates) makes it even harder to determine. Also, larger air voids (up to 4-5 mm) are trapped due to inefficient mixing or additives for special purposes such as increasing freeze/thaw resistance. Creating more confusion is that the nomenclature describing porosity varies widely as shown on *Figure 2.5*.

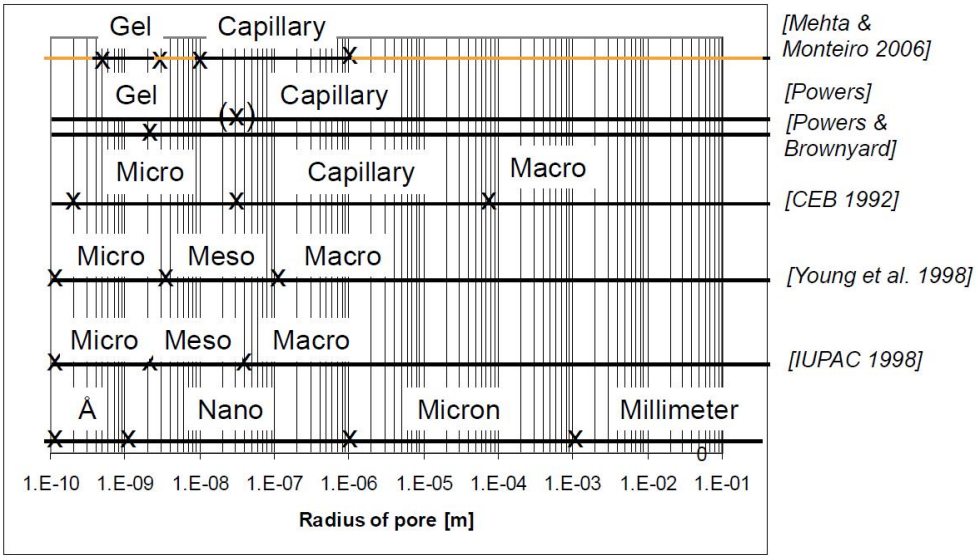


Figure 2.5 Terminology for pore sizes by different authors, reproduced from [38]

The relative proportions of the different pore sizes in cement and concrete depend on several factors, such as the water to binder ratio, cement type, degree of curing and aggregate shape and type. Sheet and gel porosity depends on the amount of C-S-H For full hydration, about 0.4 water to cement (w/c) ratio is needed for cement paste [24] and slightly higher for concrete to take into account the water adsorbed on the fine aggregate surface. When the w/c is high, there is water not taking part in the hydration filling up the space between the hydration products and hence there will be more capillary porosity. Also, as there is additional water and particles further apart in higher w/c mixes, the capillary porosity will be more connected than in lower w/c mixes where hydration products were closer formed. In case of blended cements, the

supplementary cementitious material, e.g. slag of fly ash reacts creating additional hydration products (and gel porosity) that fill the available capillary space. The overall porosity is usually finer in blended cements compared to CEM I. Curing also effects the porosity as the internal stresses of the cement paste will be different for a sealed sample that dries out and an under water cured that has a constant supply of water filling the voids [39]. The ITZ can vary depending on the aggregate. For example, porous lightweight aggregates have a rough surface and better bond between the aggregate and the cement paste with smaller ITZ than normal aggregates.

There are numerous techniques used to determine the pore structure and pore size distribution. However, none is ideal from every conceivable viewpoint including, range of sites covered, destructive, pore connectivity and cost. Moreover, the results from different techniques can contradict and hence lead to controversy. The reason is that indirect methods are used because the pore system is in the submicron level. The important characteristics are total porosity, pore size distribution, pore shape and connectivity and tortuosity (the “twistedness” of path) of pores. The more traditional techniques are gas adsorption, low-temperature calorimetry, mercury intrusion porosimetry (MIP) and more recently introduced methods such as nuclear magnetic resonance or electron microscopy. There are several studies and discussions about the effect of sample preparation and drying methods in the microstructure [40-44].

## 2.5 Water in cementitious materials

### 2.5.1 Importance

Water is essential for cement and concrete as part of the main chemical reaction and it is present in all phases with different ratios. Free water can move between the capillary pores and plays an important role in most degradation processes of concrete.

Freeze/thaw is directly related to water content. Freezing in the pores increases the pressure causing microcracks. Then when the water melts, it penetrates the concrete even further through the freeze-induced cracks. Carbonation and chloride ingress is responsible for the corrosion of reinforcement and the chloride is usually transported in water. Carbonation is due to the $CO_2$ in the air reacting with the calcium hydroxide forming calcium carbonate. The problem with carbonation is that the pH of cement paste (pore solution) drops and no longer protects the steel reinforcement from corrosion. Chloride ingress plays an important role on the initiation of steel reinforcement corrosion. [45]

Therefore, water transport measurements are key indicators for potential degradation and service life. For a long time, the measurements mostly focused on vapour diffusion into dry materials and liquid water into saturated samples. However, neither of these states is common in real-life structures and in most cases unsaturated flow is the way of transport.

### 2.5.2 State of water

Water is present in concrete in many different forms. Sheet or intra-layer water is an integral part of the main hydration product, C-S-H and is very difficult to remove by drying only. Often high temperature is used instead to remove water that involves change in the chemistry. Interlayer or gel water is present between the layers of C-S-H and can be removed by strong drying processes. As the water is removed, the layers collapse and the result is shrinkage of the cement paste. Adsorbed water is physically bound on the surface and can be removed by drying and accounts for most of the shrinkage.

Absorption/desorption isotherms describe the equilibrium water content at different relative humidities. In cementitious materials, there is a hysteresis. The water content corresponding to a relative humidity depends on if the sample is in desorption of adsorption. A schematic of a typical adsorption-desorption isotherm is shown on *Figure 2.6.*

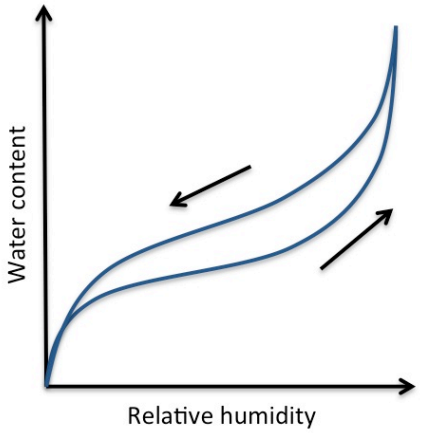


Figure 2.6 Schematic of absorption-desorption isotherm with hysteresis

The hysteresis is caused by how the pore system is filled with water and emptied. The different stages of water transport are shown on *Figure* 2.7 for different saturation levels. In a dry material, water vapour is first adsorbed on the pore surface (a). At higher water content, vapour is travelling through the pores and condensate in the narrower sections (b). With more water, the main transport method becomes liquid flow (c-d). The circle symbolises that the pore is only partially saturated. When the pores fill, there is an absorbed layer and condensation at the pore neck. Then further layers are absorbed on the pores (e). When the pores empty from one side but there are 1-2 layers of absorbed water (f) based on [29].

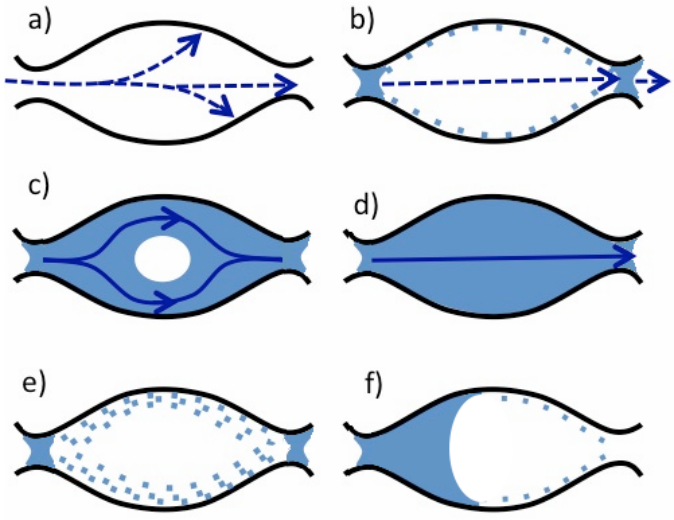


Figure 2.7 Water transport at different saturations, a) vapour adsorbing on pore surface, b) vapour transfer and condensated water at pore neck c) partly saturated flow d) saturated e) pore filling and f) pore emptying. a)-d) redrawn from [46]

At desorption, water is first removed from the large capillary porosity, then the gel and then from the sheet. *Figure 2.8* shows the water content by drying temperature measured by NMR for total (squares), mobile (triangles) and solid (circles) fractions.

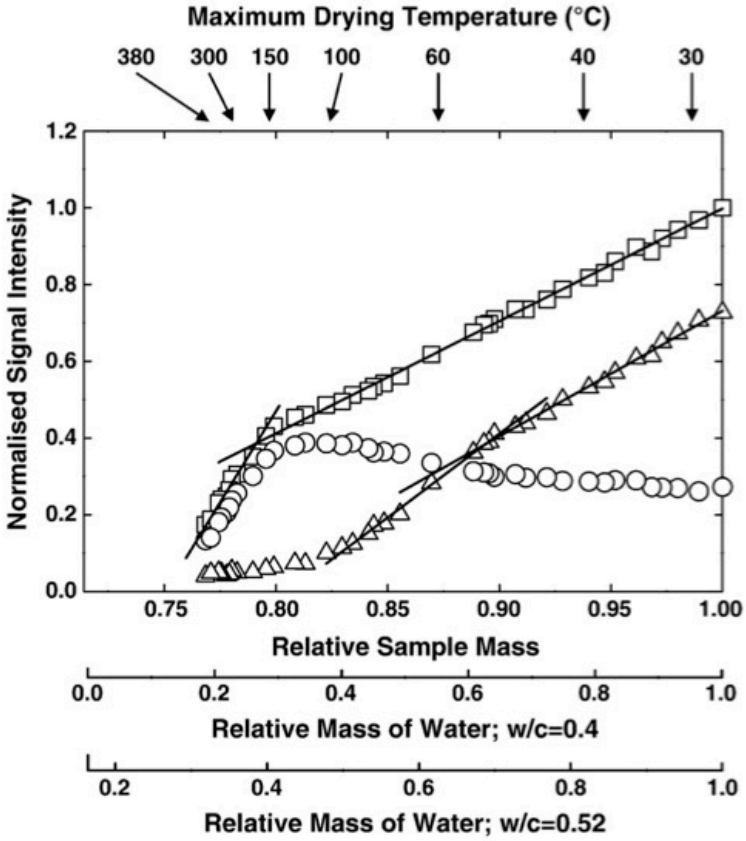


Figure 2.8 Desorption isotherm of Portland cement paste with total (squares), solid (circles) and mobile (triangles) signal fractions at different drying temperatures. reproduced from [29]

The mobile fraction decreases in two steps, it is faster above 60°C. The reason that the mobile water is lost in two stages is that there are two main (by volume) pore types: gel pores and intra layer. The reason the solid water apparently increases with reducing RH is that the residual monolayer on pore surfaces is no longer mobile and hence appears solid like. This allows estimates of the pore sizes: 3 and 1 nm diameter/width respectively.

### 2.5.3 Principles of transport

#### 2.5.3.1 Diffusion

Diffusion occurs when a relative humidity gradient drives vapour into a porous material. For diffusion in steady-state condition, Fick's First Law of diffusion is generally used. The flux goes from the higher concentration to the lower concentration. It states that the mass flux, $J$ (m/s when c is a fraction or kg/m$^2$/s if c is kg/unit volume), is proportional to the concentration gradient, $\frac{dc}{dx}$ where $c$ is the concentration, $x$ is the distance and the diffusivity coefficient, $D$.

$$J = -D \cdot \frac{dc}{dx} \qquad 2.1$$

Fick's Second Law predicts diffusion in non-equilibrium condition, describing the concentration field as a function of time, $t$.

$$\frac{\partial c}{\partial t} = D \cdot \frac{\partial^2 c}{\partial x^2} \qquad 2.2$$

Both equation *2.1* and *2.2* assume that $D$ does not depend on the concentration. However, diffusivity in concrete depends on the concentration. Therefore

$$J = -D(c) \cdot \frac{dc}{dx} \qquad 2.3$$

$$\frac{\partial \mathrm{c}}{\partial \mathrm{t}} = \frac{\partial \mathrm{c}}{\partial \mathrm{x}} \cdot \left[ D(c) \cdot \frac{\partial \mathrm{c}}{\partial \mathrm{x}} \right] \qquad 2.4$$

Many authors have developed models for diffusion in cements and concretes [47-51] including hysteresis [52] and a coupled vapour and liquid water transport by Baroghel-Bouny [53].

#### 2.5.3.2 Capillary absorption

When the overall energy of the system is lower for solid-liquid than solid-air surface interaction it is called wetting. The surface tension is present to minimize the surface area as molecules are at lower energy levels when connected to each other compared to surface with higher energy. The simplest

case when liquid is absorbed into a vertical cylindrical tube. The height of the column, $h$ is

$$h = \frac{2 \cdot y_s \cdot \cos\theta}{\rho \cdot g \cdot r} \qquad 2.5$$

where $\gamma_s$ is the surface tension between the air and liquid and $r$ is the radius or the pore. $\theta$ is the contact angle (in case $\theta < \frac{\pi}{2}$ the curvature is negative), $\rho$ is the density of the liquid and $g$ is the local gravitational field. The Washburn-equation [54] gives the height of column as a function of time in a bundle of cylindrical tubes

$$h^2 = \frac{2 \cdot y_s \cdot \cos\theta}{\rho \cdot \eta} \cdot t \qquad 2.6$$

where $\eta$ is the viscosity and $t$ is the time. The $h^2$ dependence on time means that capillary transport can be seen mathematically as diffusion. In concrete, the pores are small enough for capillarity, however, the pore structure is more complex than simple cylindrical tubes. The negative gauge from lower pressure in liquid causes the capillary suction. Water vapour diffuses into the empty pores of the material. Capillary condensation happens because of the favourable pressure from vapour to liquid above a certain point of saturation. The Kelvin-equation

$$r_K = -\frac{2 \cdot \sigma \cdot M \cdot \cos\theta}{R \cdot T \cdot \rho \cdot \ln\psi} \qquad 2.7$$

gives the critical radius, $r_K$, of a pore that is filled with water at a relative humidity, $\psi$, and temperature, $T$. In this equation $M$ is the molar mass, $\sigma$ the surface tension, $\rho$ the density and $\theta$ the contact angle of the liquid in the pore and $R$ is the gas constant. Therefore, the radius, (the pore size) that will spontaneously fill with liquid water by condensation from vapour can be calculated.

In case of unsaturated pore system, the equilibrium is at lower pressure than the ambient. At low water content, the curvature is high, liquid phase occupying the smallest pores and necks. At higher water content, the pressure drop is smaller and the curvature is smaller too.

#### 2.5.3.3 Permeability

In construction materials, such as concrete, unsaturated flow is more common than saturated. Permeability refers to saturated flow due to pressure difference and conductivity refers to unsaturated flow. Darcy's law describe flow in porous media. The volumetric flow rate, $Q$ ($m^3/s$) depends on the difference in hydrostatic pressure, $p$, the length of the specimen, $L$, the cross sectional area, $A$ and $k$ is the Darcy permeability.

$$Q = \frac{k \cdot A \cdot \Delta p}{L} \tag{2.8}$$

Unsaturated flow is due to capillarity and the extended Darcy equation for local flow, $u$ (m/s) is

$$u = K(\Theta) \cdot F \tag{2.9}$$

where $K$ is the conductivity and $F$ is the capillary force and $\Theta$ is the water content. In case of one-dimensional flow, it can be written as

$$u_x = -K(\Theta) \cdot \frac{\partial \psi}{\partial x} \tag{2.10}$$

where $\frac{\partial \psi}{\partial x}$ is the gradient of liquid tension ($\psi$ is the pressure head), the pulling force for the transport.

#### 2.5.3.4 Sorptivity

Sorptivity is one of the most important properties of porous materials. In theory, sorption is a one-dimensional flow with sharp wetting front. The Sharp Front model [55] assumes that the wetted region has a rectangular, "shock-front" and constant water content at least close to saturated state. For construction materials, sorptivity has been used since 1977, when Hall described that the cumulative water absorbed per surface area increases by the square root of time, $t$, [56]. Therefore, the infiltration, $i$ ($m^3/m^2$) is

$$i = S \cdot t^{1/2} \tag{2.11}$$

where $S$ is the sorptivity, given as $m^3/m^2/s^{0.5}$ or $m/s^{0.5}$. Mathematically, it is also closely linked to diffusion. Taking account the surface effects when the specimen is put on water

$$i = a_0 + S \cdot t^{1/2} \qquad 2.12$$

is used where $a_0$ is a positive intercept. The intrinsic sorptivity is independent of liquid characteristics and only depends on the water content. Gravitation effects can be neglected in most cases. Measuring sorptivity assumes that the flow is strictly one dimensional, the initial water content is uniform, the material is homogeneous and it is not changed by water. Fulfilling all requirements can be a difficult task, but is essential for accurate results.

Two- and three-dimensional flow from a finite source is important as most in situ measurements use cups or drilled holes. The following approximations for sorptivity are from [57]. In case of cylindrical drilled source the cumulative absorbed water volume per unit area, when hole radius, $r_0$ and advancing cylindrical wet front radius $r$, is

$$i = \frac{f_e \cdot (r^2 - r_0^2)}{2 \cdot r_0} \qquad 2.13$$

and $f_e$ is the water content of the wetted area (effective porosity). For short time (few minutes), flow is same as one-dimensional. Sorption from a circular source is very complex, the wetting front is a semi-ellipsoid.

As has been seen in the foregoing, in cementitious materials, most forms of water transport lead to a general form of an ingress equation, mass as a function of square root of time. Therefore, the transport can be described by a Fickian type differential equation relationship. Hence, measuring the effective diffusivity does not give information about the mechanism of transport, such as capillary or vapour transport.

The current all encompassing models are somewhat empirical, based on macro properties such as sorption isotherm and not on the nanostructure [53, 58]. Some other models include a more nanoscopic materials aspect, such as by Baroughel-Bouny [53], but in theses cases there are many unknown parameters. Knowing the mass uptake or water penetration depth is insufficient to test models that all look “Fickian-like”. More information on the filled pore size distribution as a function of space and time is required to help distinguish between models in the future. Such information is potentially provided by spatially resolved magnetic resonance.

## 2.6 Tests determining water transport in concrete

### 2.6.1 Water vapour diffusion test

Water vapour diffusion in concrete is usually measured with the “cup-test”. The test specimen is placed on top of a cup containing a desiccant (or saturated salt solution) and then sealed. Then it is placed in an environment with different relative humidity (RH) therefore vapour passes through the specimen and is absorbed by the desiccant. The weight of the cup and the sample is measured periodically to determine the water uptake. It is called “dry-cup” for 0-50% RH, when moisture diffuses into the cup and “wet-cup” for 50-100% RH when moisture flows from the cup to the salt. Diffusion coefficients, *D*, depends on the for example water-cement ratio or RH, and therefore on concentration [53]. *Figure 2.9* shows a typical setup for the cup test. Typical sample thickness is a few millimetre to a centimetre. A typical effective water vapour diffusion coefficient for concrete measured by the cup test is in the range of $10^{-7}$ $m^2/s$ [53].

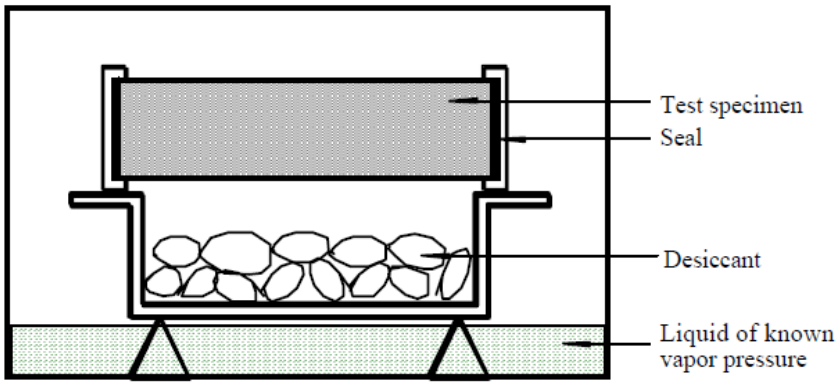


Figure 2.9 Test set-up for water diffusion, reproduced [46]

### 2.6.2 Liquid water sorption tests

Water absorption capacity and sorptivity are both based on capillary suction. The absorption capacity gives information on the open porosity of the material. A specimen is dried to constant weight then immersed in water for a certain duration.

For sorptivity, the usual setup is that the specimen is placed in contact with water where the only force is the capillary suction. The weight of the specimen is measured at intervals. Sorptivity is calculated from *Equation. 2.10*. The sides are usually sealed to prevent water transport through the sides. The smallest measure should be at least three times the maximum aggregate size. An improved measurement technique was suggested by [59] with constant weight measurement by computer. Typical setup for sorptivity test is shown on *Figure 2.10*. The recommended sample height for concrete is minimum 100 mm, ideally about 150 mm and the sample diameter or edge is maximum half of the height. A typical sorptivity for an 0.5 w/c concrete is about 0.1 mm/min$^{1/2}$ measured by mass uptake [60].

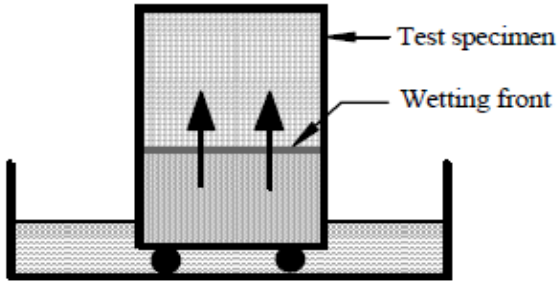


Figure 2.10 Typical setup for water sorption test, reproduced from [46]

Sorptivity can be calculated from the depth of water penetration, as

$$d = d_0 + S \cdot t^{1/2} \qquad 2.14$$

where $d_0$ is an intercept depending on the surface finish. However, the sorptivity obtained from penetration depth is different from the one measured from water uptake. The test set-up is the same with the same specimen preparation, but the specimens are split at certain time after the beginning of the test and visual inspection. Usually test length is 24 hours, longer test do not follow *equation 2.13.*

Capillary absorption of water in concrete shows strong time dependence. The sorption anomaly has been evidenced by many authors [61-65]. Results generally show two timescales, liquid water uptake uptake significantly slowing down after 24-60 hours. The water uptake first follows *equation 2.10*, it is linear with the square root of time, but then slows down. The water uptake beyond is not proportional to square root of time but display a smaller sorptivity. This effect was not seen when organic liquids were used [63] and this observation

was suggested by the authors as indicative of chemical reaction with water on rewetting. ESEM micrographs suggest swelling in reaction to water during the second period [61].

Sorptivity depends on compressive strength, hydration and curing conditions [14, 59]. The effects are more prominent with lower strength concrete. Supplementary cementitious materials reduce the water sorption [62, 65].

### 2.6.3 In-situ tests

Sorptivity tests require one-dimensional flow and necessarily require laboratory environment. Water absorption tests are carried out under low pressure with no assumption on the direction of the water transport. Therefore it is possible to use them on site to determine sorption properties. There are two main types, surface absorptivity and drill-hole absorptivity tests. The former uses a water reservoir mounted on the sample. In the later case, water is absorbed from a filled drilled hole.

One of the common tests is the Initial Surface Absorption Test (ISAT), which became a standard primarily laboratory test in the United Kingdom in 1983 [66]. The samples are oven dried then stored at ambient humidity and temperature prior to testing. *Figure 2.11* shows a typical setup for the tests. Absorption is measured at intervals after the start by closing the tap at the reservoir and observing the movement in the capillary tube for a certain period. ISAT carried out in a laboratory gives reproducible results, though in-situ measurements are strongly dependent on initial water content. It is in good agreement with the Sharp Front sorption theory and gives similar sorptivity values as simple one-dimensional measurements [67].

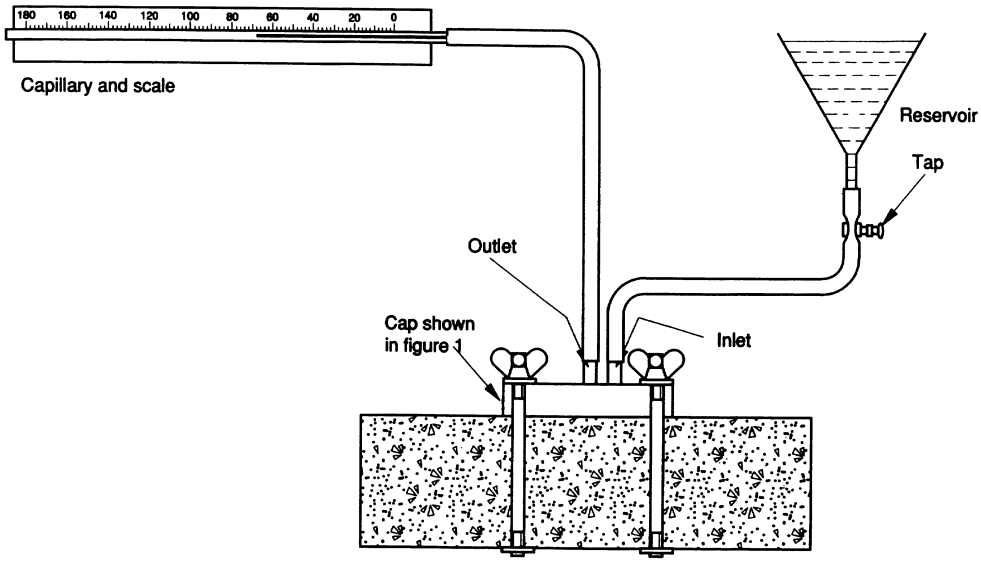


Figure 2.11 Setup for ISAT test, reproduced from [46]

Autoclam sorptivity tests [68] measure the cumulative absorption of water from a circular cap with low pressure. The flow of water is plotted versus the square root of time and the slope gives the sorptivity index. The commercially available Autoclam Permeability System can also test air and water permeability. The results are reliable only under 80% internal RH, above can be misleading [69].

Drill hole tests use a hole of a certain diameter and depth drilled into the surface of the concrete. Then it is sealed on the top surface or at part depth. The cavity is filled with water at low pressure from a capillary tube. The Figg test [70] was introduced in 1973. It is widely used and has several modifications for improvement. The time period is measured from filling the cavity till the meniscus moves 50 mm. The covercrete absorption test (CAT) is very similar to the Figg test, but the hole size is different. The cavity is filled and there is constant water head for low pressure. The movement of the meniscus is measured at a set time. The problem is that drilling can change the microstructure around the hole and initiate micro-cracks. Also, the size of the hole may not be representative of the average microstructure, although it has the advantage that the absorbing surface does not have the top surface layer.

### 2.6.4 Permeability tests

Liquid permeability of concrete under pressure can be measured as a steady or non-steady flow, though in most cases the material is too dense to determine the permeability coefficient and instead water penetration is used. The coefficient of permeability and the intrinsic permeability can be calculated from steady state water flow. The flow due to a pressure gradient is measured in a saturated sample. The permeability cell seals the sides of the sample to ensure no leakage through the sides. The inflow or outflow is measured, sometimes both. The duration of the test is usually around few weeks. The usual setup for test is shown on *Figure 2.12*.

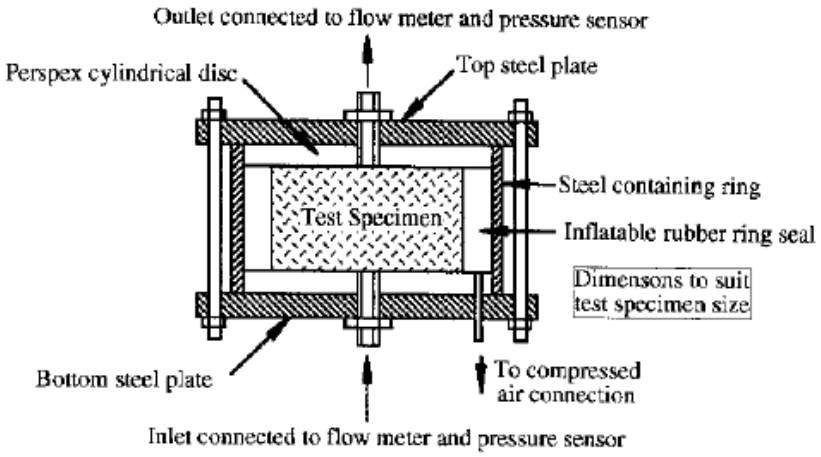


Figure 2.12 Permeability test, reproduced from [46]

As it is difficult to reach steady-state for concrete, usually either the inflow or the outflow is measured. The set-up is the same as for steady state, the pressure and duration of the test varies. The Autoclam water permeability test mentioned at sorption tests is used for on-situ measurements. It uses a cup mounted on top. The inflow data is plotted against the square root of time.

The depth of water penetration test is a standard test method [71]. The samples are cured under water and the minimum testing age is 28 days. Pressure of 500 kPa is applied on one side on a 70 mm diameter area for 72 hours. After the test, the sample is split in two, the water penetration depth is marked and the maximum depth is measured. In some cases it is very hard to determine the penetration front as there is no clear mark and the maximum depth is mostly a good guess, especially for high performance concretes with low permeability.

A different approach of measuring permeability indirectly was developed by [72]. A saturated rod is put under three-point bending with a fixed displacement. A pressure gradient develops in the liquid due to strains in the sample and liquid flows to equilibrate the pressure. The time to equilibrium depends on the permeability. The time and force for maintain deformation is measured. The advantages are short measurement time (minutes to hours) and no need for a pressure vessel. The disadvantages are that to avoid microcracking by using adequate sample dimensions, the samples are difficult to handle and that the measurement is inaccurate when permeability is very high.

Water permeability is a widely studied topic. Liquid water permeability is consistently lower than gas and ethanol, which is inert to cement [73]. Permeability decreases with time due to self-healing and further hydration [74]. The magnitude of the gradient depends on many factors, but the most important is the curing and previous wetting-drying cycles [57]. Permeability is the most sensitive water transport property to microcracking and shows significant influence of sample thickness/aggregate size ratio [75]. Also, the quality of the mortar in high strength concrete significantly affects the permeability [76]. Typical value for water permeability, K or $K_w$, for concrete is in the range of $10^{-11}$-$10^{-12}$ m/s [77, 78].

### 2.6.5 Problems with water transport tests in concrete

Water transport is not easily described in concrete for several reasons. Concrete chemically reacts with water. Even in mature material continuous hydration is possible. Sample preparation for testing such as drying can damage the microstructure. Loss of water causes drying shrinkage, which is not fully reversible and above 60-70°C decomposition of ettringite and C-S-H is an issue. However, the initial water content of the sample and the testing temperature affect the water uptake of the sample significantly. It is difficult to find a balance for drying that is sufficient for water removal and minimises microstructural damage.

Also, swelling during water uptake affects hydraulic barrier properties. Air trapped in “end pores” and between filled pores can be under pressure changing the transport properties. It can escape through liquid by diffusion very slowly. The thin surface layer of concrete is different from bulk and can affect the measurements. Cut samples from middle section or drilled holes eliminate the problem, although in most cases the top layer is present in real life. However, microcracking and other changes can be introduced by the cutting process.

The results of in-situ test measurements are strongly dependent on the initial water content and are usually associated with three-dimensional flow, complicating any clear understanding of the transport mechanisms. In contrast, laboratory tests usually measure one dimensional flow.

The precision and accuracy for the tests vary. In case of laboratory tests, precision is down to the equipment used (can be 0.001 g) and is usually not an issue as the variation from sample to sample in most cases is minimum a magnitude greater. Accuracy is more complicated as some of the tests are indirect and do not necessarily have scientific proof that the results provide correct measurement of the transport properties. For practical issues, the variability of the data will be more dependent on the variation between the samples, the quality of the seals and the environment in case of the in-situ tests.

## 2.7 Nuclear magnetic resonance on cement and concrete

### 2.7.1 Basics of nuclear magnetic resonance

A good introduction of NMR for engineers is Blümich: *Essential NMR for Scientists and Engineers* [79]. Nuclear magnetic resonance is an effect when magnetic atomic nuclei such as $^{1}H$ are present in a static magnetic field and exposed to a second, oscillating magnetic field. Not all nuclei have this phenomena, it depends on the spin (magnetic moment) of the nuclei. $^{1}H$ proton have a spin, therefore water can be studied by NMR. In a magnetic field, the

spins align with the field in equilibrium. The aligned nuclei are disturbed from equilibrium, that is rotated away from or flipped from alignment with the magnetic field and the magnetisation recovery is measured. The recovery takes two forms: the spins precess or rotate about the magnetic field like a gyroscope precesses about a gravitational field and the spins return to alignment with the field direction. According to the Larmor equation, when a magnetic nuclei is placed in a magnetic field, strength is $B$, the frequency of precession, $\omega$ depends on the gyromagnetic ratio, $\gamma$, which is a constant for a particular nuclear species according to

$$\omega = \gamma \cdot B \qquad 2.15$$

The intensity of the signal depends on the amount of water in the pore. The lifetime of the signal is the time for coherence of the precession (i.e. the spins rotating together) to be lost. It depends on the mobility of the molecules.

The spin-lattice relaxation time, $T_1$, characterises the time required for the nuclei to return parallel with the magnetic field and reach thermodynamic equilibrium with the lattice by an exchange of energy. It ranges from milliseconds to seconds.

The spin-spin relaxation time, $T_2$, characterises the decay of the signal (return of to equilibrium between the nuclei). It ranges from microseconds for bound $^1$H (e.g. CH, ice) to seconds for bulk water. In porous media it is often the case that

$$\frac{1}{T_2} \propto \frac{Surface}{Volume} \qquad 2.16$$

since spins diffuse to pore surfaces and the relaxation occurs predominantly at the pore surface [80]. The $T_2$, relaxation time of solids is very short and comes from inter-nuclear interactions.

### 2.7.2 Basic measurements

The simplest experiment is when a pulse tips the magnetisation 90° from alignment with the magnetic field. The response, the free induction decay (FID) signal is measured (*Figure 2.13*). The lifetime of the signal, $T_2^*$, is very short. The spectrometer deadtime following pulse can hide the shortest $T_2$

components. It is a combination of $T_2$ and $T_2^{\Delta B}$ a measure of field inhomogeneity ($\Delta B$).

$$\frac{1}{T_2} = \frac{1}{T_2} + \frac{1}{T_2^{\Delta B}} \qquad 2.17$$

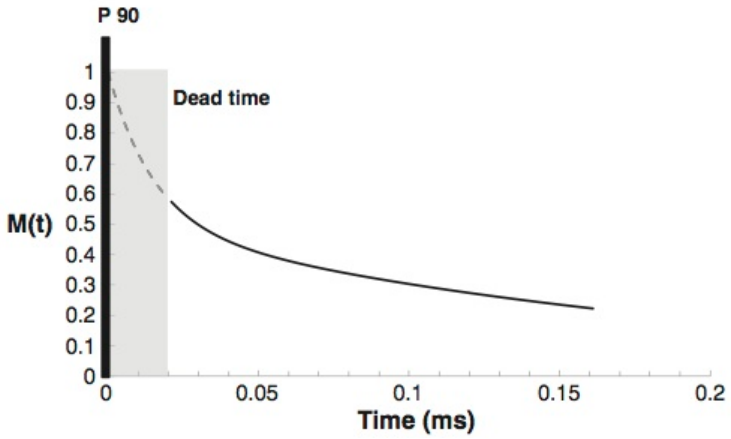


Figure 2.13 FID pulse, reproduced from [81]

The field inhomogeneity that leads to dephasing of the spins and a short value of $T_2^{\Delta B}$ can be reversed using a Carr-Purcell-Meiboom-Gill (CPMG) experiment [82]. It uses a 90° pulse followed by 180° pulses (*Figure 2.14*). The time between the 90° and the first 180° pulse is $\tau$, and the time between the 180° pulses is $2*\tau$. The first 180° pulses refocus the magnetisation to echo signals. The time between the echoes, $2*\tau$ is called echo time in the data software and later in this work.

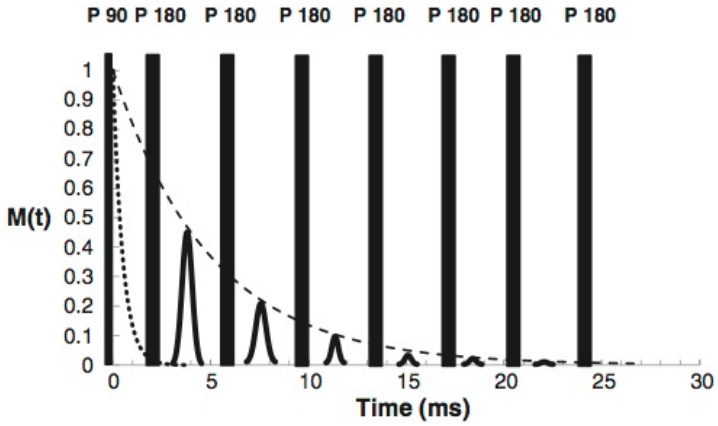


Figure 2.14 CPMG pulse sequence with echo train reproduced from [63]

There are two methods to measure $T_1$ relaxation time, the saturation and the inversion recovery pulse sequences (*Figure 2.15*). In the former, the system is saturated by 90° pulses that force the bulk magnetization to zero, in the later, the magnetisation is inverted. The magnetisation recovers for a variable $\tau$, then

a 90° pulse is applied and FID signal acquired. The signal detected depends on and $\tau$ and $T_1$.

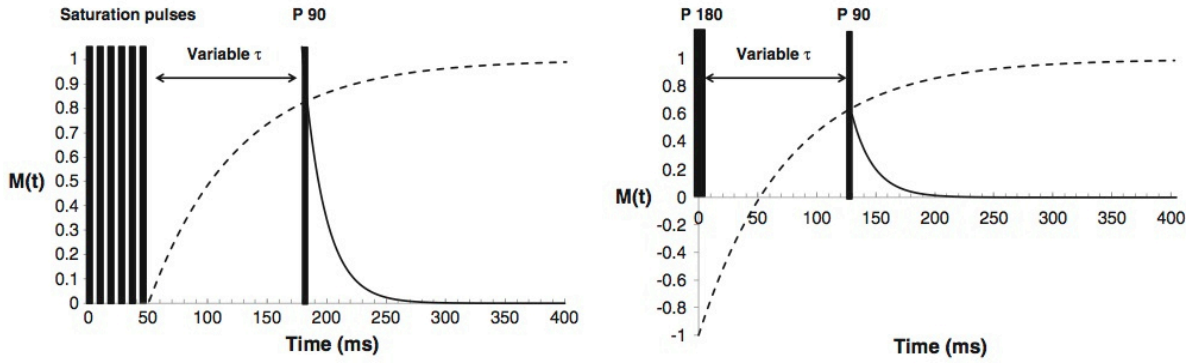


Figure 2.15 Saturation (left) and inverse recovery (right) pulse sequence, reproduced from [63]

### 2.7.3 Spatially resolved NMR

A gradient is applied to the magnetic field (*Figure 2.16)*. The field strength varies with location, so that $B(r) = B_0 + g \cdot r$ where $g = \frac{dB}{dr}$. The resonance frequency, $\omega$, depends, on the field strength therefore it is proportional to the position, $r$

$$\omega(r) = \gamma \cdot (B_0 + g \cdot r) \qquad 2.18$$

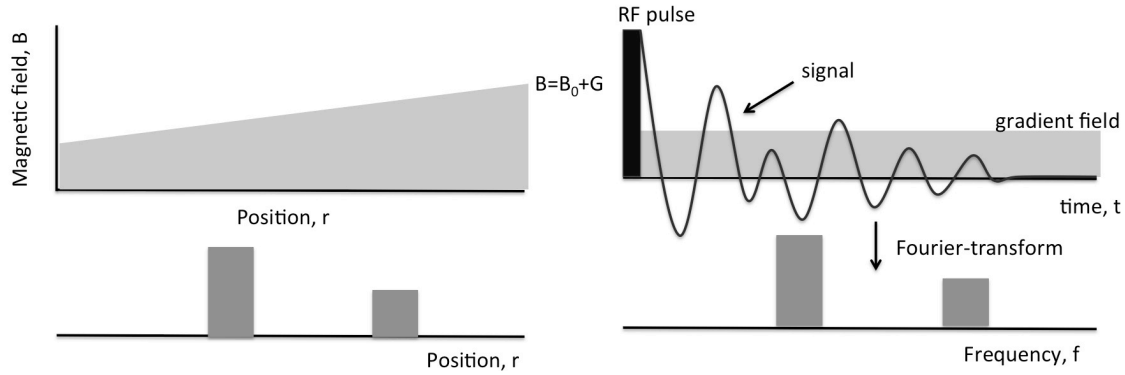


Figure 2.16 Frequency encoding for imaging

The magnetic field varies by location, therefore the resonance frequency is proportional to the position. The signal, $S$ is

$$S(t) = \int c(r) \cdot \exp(-\gamma \cdot g \cdot r \cdot t) dt \qquad 2.19$$

where $c$ is the concentration. In equation 2.18, the constant precession at $\omega_0$ around $B_0$ is not included. This is removed by the spectrometer receiver.

For imaging, an FID is acquired in presence of a gradient. The frequency of the signal gives the position of the nuclei and the amplitude gives the amount. A lot of sequences are used for imaging. The resolution for frequency encoding is given by $\frac{2 \cdot \pi \cdot \Delta f}{\gamma \cdot g}$ where $f$ is $\frac{1}{N \cdot \Delta t}$ where $N$ is the number of points and $\Delta t$ is their spacing. The maximum acquisition time is $T_2$ that limits the resolution. Some vary the gradient strength instead which is known as phase encoding or the combination of frequency and phase encoding.

The 90° pulse can be applied in the presence of a gradient so that it only contains a narrow range of frequencies. The bandwidth of frequency is inversely proportional to the pulse length. Therefore if a pulse is applied in a strong gradient, the bandwidth of frequency of the pulse is much less in the sample. Hence only a narrow band that has the same frequency as the RF pulse is excited and a slice is selected.

In slice selection of GARField the resolutions is determined by the strength of the gradient and by the bandwidth of the pulse. The pulse bandwidth is about $\frac{1}{t_{pulse}} \approx \frac{\gamma \cdot g \cdot r_{slice}}{2 \cdot \pi}$. In GARField, there is a strong gradient and even with short $T_2$ a decent resolution (0.25-1 mm in the GARFields that were used in this work) can be achieved. However, the gradient is still not enough for frequency encoding and therefore slice selection is used by moving the sample or the magnets.

### 2.7.4 Portable NMR

Taking NMR to built structures and allowing larger samples then the magnet itself had great interest as a possibility for a new, non-destructive testing method. An overview of one-sided mobile NMR systems and applications by Blümich was published in 2008 [83]. One-sided open access portable magnets started in the oil industry characterizing porous stones and rocks. Most portable NMRs are one-of-its-kind magnets still in development. The first NMR-MOUSE [84, 85], a unilateral NMR developed in Aachen [86] and the Surface GARField [87-89] that will be used in this thesis, all use a high gradient for spatial resolution in depth. As the further development and refinement of the Surface

GARField in the thesis, there is a separate chapter on the setup and starting state (*Chapter 3.1*). The second NMR Mouse [90] and the NMR-MOLE [91, 92] have a “sweet spot”, a volume with the most possible homogeneous field.

The well logging tools are commercial (Schlumberger) as well as the NMR-MOUSE (for small depth, few millimetres).

### 2.7.5 Laboratory GARField

In the Laboratory GARField [93] a small sample, usually in the form of a core, is placed between the shaped poles of a permanent magnet *(Figure 2.17*). The magnet is about 50 cm high. There are two coils available, one is used for larger samples with a diameter of 18 mm, but maximum measured length is about 35 mm and another where the sample diameter is 10 mm but the length is not limited.

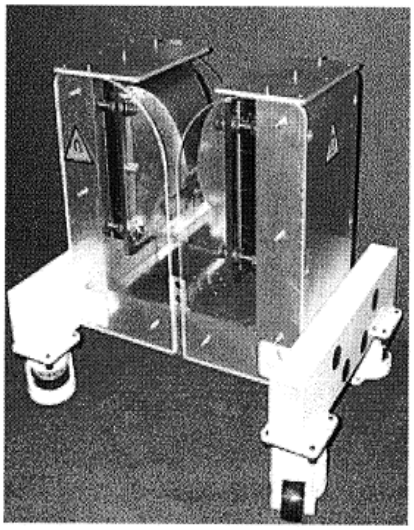

Figure 2.17 Laboratory GARField, reproduced from [93]

The shaped poles ensure a uniform magnetic field strength in the horizontal plane and a uniform gradient in the vertical direction. However, the field strength (0.5 T) and gradient strength (12 T/m at the optimum position) are much greater than with the Surface GARField (0.06T and 3.25 T/m respectively) so that a thinner slice can be selected with greater sensitivity. Also, because the sample is smaller, a smaller coil can be used and the dead time is much shorter so that smaller values of echo time can be used. This enables the interlayer water and gel pore water to be better measured in cement paste.

### 2.7.6 Previous work on cement and concrete

NMR has been used for cement characterisation for a long time in several topics. $^{1}$H proton NMR relaxometry is used to determine porosity, hydration and water transport. $^{27}$Al and $^{29}$Si NMR spectroscopy are used to determine hydration products and phases. The theory by Brownstein and Tarr was that the relaxation time of fluids in a confined space is dependent on the size of the space [94]. Then later experiments found that the relaxation time in a porous media is an average of bulk and surface water that are exchanging e.g. *Equation 2.16* [95]. The early works were mainly on white cement paste due to its low iron content [96, 97] and comparing the results for pore-sizes distribution with other test methods, such as MIP [98, 99]. Mostly a three compartment model was used based on the relaxation time [100].

Valori et al reviewed studies of pore structure of cement paste investigated by NMR [81]. The composition of cement paste as a degree of hydration refined the Powers model [26]. NMR was used for pore-size resolved desorption isotherm and determining the density of C-S-H [101]. It was also shown by Muller et al [26] that NMR can detect all water in cement paste: chemically bound and pore water in all pore sizes, sheet, gel, interhydrate and capillary. NMR can provide information on the water ratio in different pore sizes.

Moisture and drying profiles were investigated by MRI [102, 103], for drying of concrete [104, 105], evaporation and drying in cement paste [105] and for capillary uptake with different curing conditions and w/c ratio [106]. The influence of superplasticiser on hydration and freezing was studied by single point imaging by [107]. Internal curing and water transition between superabsorbent and gel water was observed by [108, 109].

$T_1$-$T_2$ and $T_2$-$T_2$ experiments of hydrating cement paste showed a cross-peak, off the diagonal and it was suggested by McDonald et al that it was due to an exchange of water between gel and capillary pores [110]. It was confirmed by detecting the exchange in $T_2$-$T_2$ experiments estimating the characteristic pores sizes and exchange time [111]. Korb used $T_2$-$T_2$ experiments to detect water exchange and proposed a 2D walk on the pore surface of water molecules in the vicinity of iron impurities [112]

## 2.8 Concluding remarks

Although concrete is a widely used material, the microstructure on the nano level is still not clearly understood and there remains an ongoing debate on the three dimensional structure of C-S-H. Most degradation processes of concrete are related to water transport and water content and the mechanisms depend on the pore structure characteristics. Better understanding of the transport properties and the test procedures measuring water sorption characteristics is important for making durable materials and understanding the deterioration of existing concrete structures.

Many of the most widely used testing methods of water transport in cementitious materials, especially the ones used for concrete in practice, are fairly basic and rely on indirect measurements of transport, such as visible penetration depth for permeability.

$^{1}H$ proton NMR is a useful method to compare to the conventional gravimetric test results on water transport, and give information on the state of water and distribution. It has been established, that all water in the paste (chemically bound and pore water in all pore sizes) can be measured by NMR methods.

Based on the literature reviewed it is clear that vapour tests are extremely long for concrete samples and as a consequence the research has focused on liquid water tests. The most important tests are determining sorptivity and permeability. Both tests can be carried out on 150 mm test cubes, a standard specimen size and also appropriate for the NMR measurements. The effect of w/c, cements and curing conditions were investigated. All these affect the pore structure by different chemical composition, degree of hydration, water content and phase distribution. Further investigations related to water transport were also carried out on mortar samples.

# 3 The Surface GARField measurement

## 3.1 Introduction

At the outset of the project, the Surface GARField NMR measurement was still under development for concrete. Both the test protocol and the Surface GARField machine itself, which were developed under laboratory conditions, required commissioning in an industrial setting and appropriate refinement. This chapter describes the improvements to, and calibration of, the measurement.

With the Surface GARField one-sided NMR, the magnets can be moved up-down while the detector coil remains in the same position, on the top of the specimen. Water content as a function of depth (profile) can be determined. The magnet is around 16 kg and about 25x30x25 cm. It is capable of measurements up to 30 mm depth, and showed minimal effects from rebars [89]. *Figure 3.1* shows the setup and the GARField magnet on a sandstone sample.

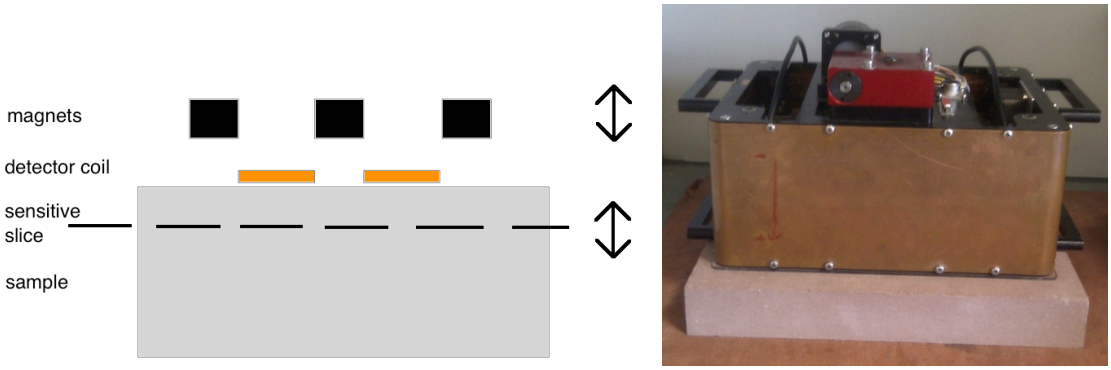


Figure 3.1 Surface GARField: schematic of profiling, sensitive slice is at different position as the magnets move up and down (left) and photograph of magnet on a sandstone slab (right)

The Surface GARField machine was installed at HeidelbergCement Technology Center (*Figure 3.2*). A sample holder was constructed to give reproducibility and ease of handling. The sample holder keeps the position of the magnet frame and sensor coil fixed above the sample. The material of the holder was carefully chosen to minimise interference with the magnet and minimise NMR signal from the frame. Wood, and certain polymers are mobile $^{1}H$ rich and give large signals. Metals can interfere with the RF signals and so ferrous components cannot be used for obvious reasons. The holder frame was

made of polymethyl methacrylate (PMMA). It gives no detectable signal as the relaxation time of PMMA is sufficiently short and does not contribute to the CMPG measurement with Surface GARField. Also it can hold the weight of the magnet. The sample holder was designed to hold 15 cm cubes and also thinner samples cut from the 15 cm cubes.

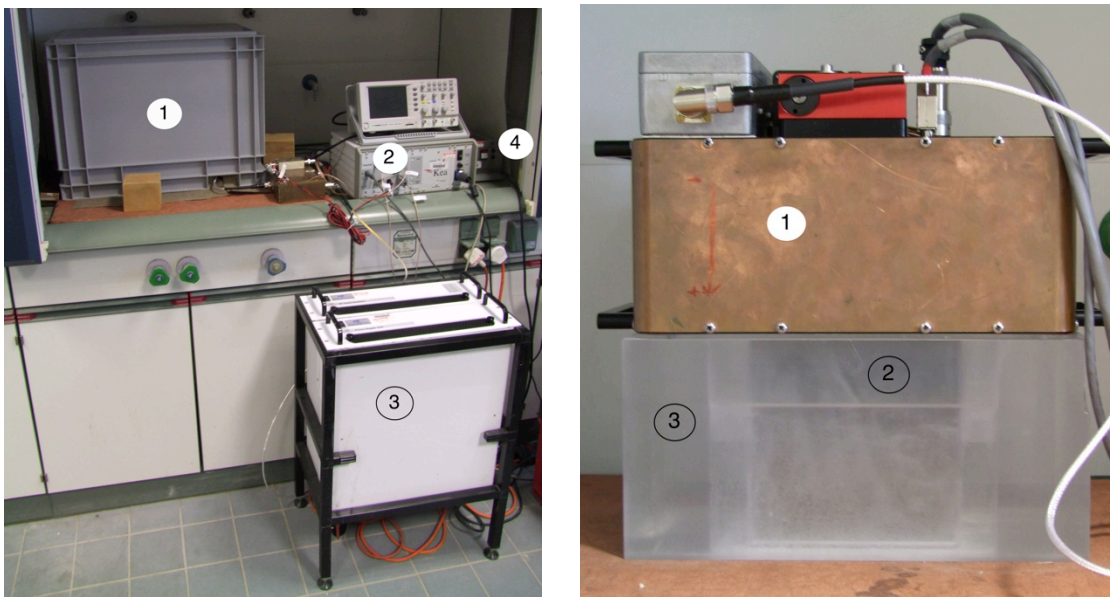


Figure 3.2 left: equipment setup of magnet under shielding (1), spectrometer (2), amplifier (3) and motor controller (4) and right: GARField magnet (1) with concrete cube (2) and sample holder (3)

## 3.2 Starting state of test procedure and objectives

The Surface GARField was improved considerably by Valori [105] in a laboratory context. It is fully portable and it has been briefly tested on a construction site. A brief user's guide was written by Valori [113] with operating instructions and a data acquisition parameter set for concrete. A macro was written for profiling, using CPMG at each slice and moving the magnets with the motor between sequential slices.

The optimum parameters used for the NMR measurement were not set. Results for the same mixture measured under different NMR parameters can be very different and are not easily comparable without expert knowledge. There was no standard protocol for the experiments .The aim is to be able to use the machine on-site with a standard procedure that can be readily applied and easily interpreted and understood.

The objectives were to develop a standard test protocol including the parameters for data acquisition and for data analysis, calibrate the machine for absolute water content and to further develop the analysis software for ease of use.

### 3.3 Basic measurement at starting state

*Figure 3.3* shows a CPMG echo train recorded for a wet (dried and rewetted by capillary absorption for 1 day) concrete at a depth of 4 mm (position 3) using a pulse length of 12 µs, 8 echoes with an echo time of 200 µs, a repetition delay of 250 ms with 2048 scans. This was a parameter set suggested by Valori in [89] and is clearly not the optimum. Only the first echo is really visible above the noise and this echo has artefacts to be discussed. Data is phased real data only. Phasing is discussed in *Section 3.6.1*. Each echo was recorded with 48 points for 48 µs in total. The middle of the echoes were at 200,400, 600 µs etc. The data was recorded by summing all scans point by point (standard mode in the Prospa spectrometer software).

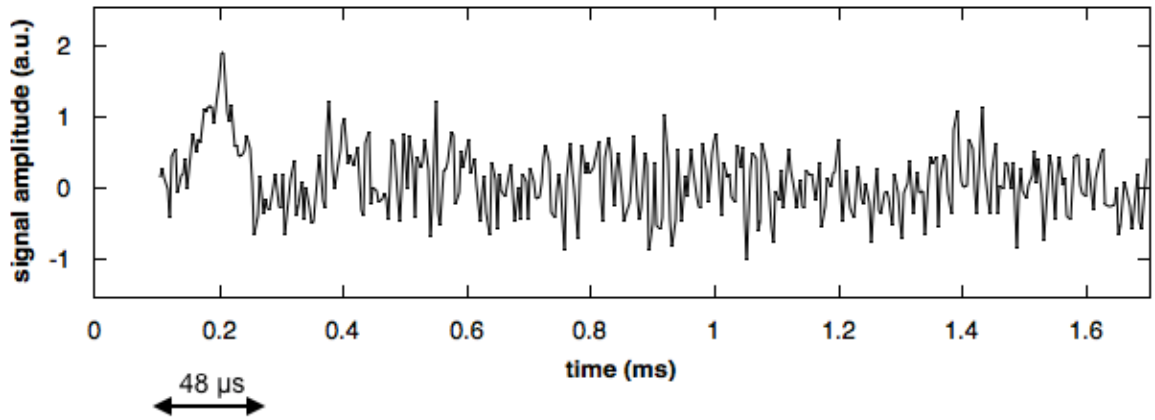


Figure 3.3 real phased CPMG echo train data at 4 mm depth of CEM I concrete measurement using acquisition parameter set suggested by Valori

For better signal to noise ratio, instead of exponential fitting of the echo train, an echo sum was used. The echo sum is a point by point sum for all echoes of the echo train. So the first point of each echo is added together for the first point, then second point of each echo is summed, etc. *Figure 3.*4 shows the echo sum for the echo train of the previous figure, *Figure 3.3*. The echoes were

recorded with enough points to see the baseline before and after the echo shape.

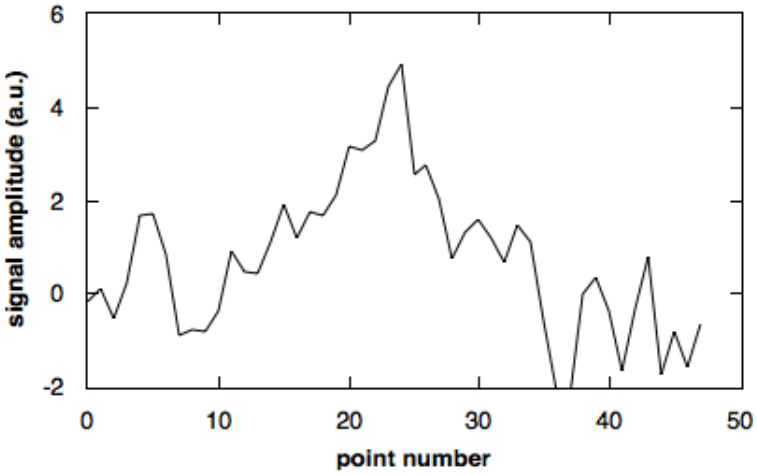


Figure 3.4 echo sum of the CPMG echo train shown on Figure 3.3

*Figure 3.5* shows a CPMG echo train recorded for concrete at a depth of 20 mm. The echo train is not clearly visible on *Figure 3.5*, only the first echo could be easily recognised. The data acquisition parameter set for concrete was not optimised for each depth and the signal-to-noise ratio was low.

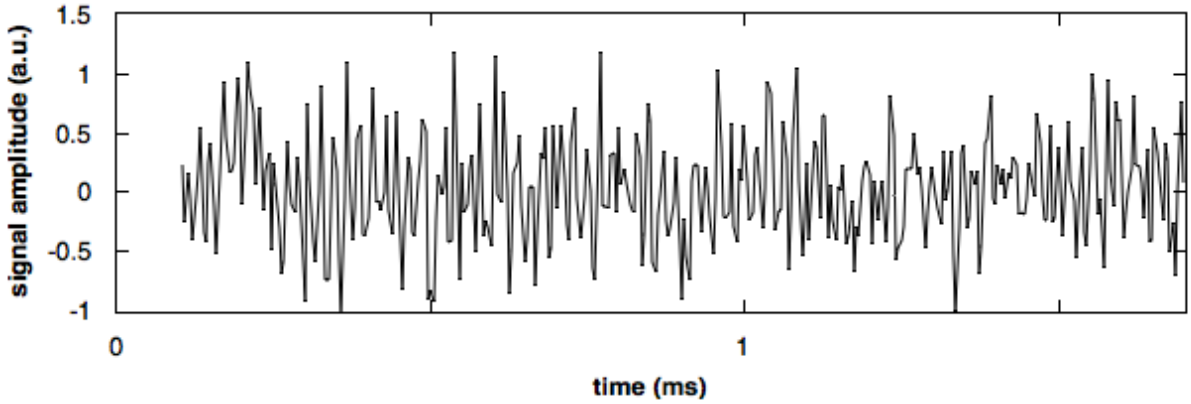


Figure 3.5 real phased CPMG echo train data at 20 mm depth of CEM I concrete measurement using acquisition parameter set suggested by Valori

These simple experiments indicated that there was a need to improve the system performance and this is in the following section.

## 3.4 Comparison of old and new probe

### 3.4.1 Original coil

Originally, a single detector coil was provided with a small gap to the back plate. Data acquisition parameters were optimised for maximum signal to noise at all positions. The coil had an internal background ringing that increased by depth. Phased real data of a wet concrete at 20 mm depth with optimised parameters is shown on *Figure 3.6*. The optimised parameters for the coil at that depth were 15 µs pulse length, recording 8 echoes with an echo time of 200 µs and a repetition delay of 150 ms with 4096 scans. The measurement for each slice took about 10 minutes. The number of scans were doubled compared to the measurement at the starting state for better signal to noise ratio. Measurement on no sample, only air, called here “empty” at 20 mm depth with the same parameters as used for concrete is shown on *Figure 3.7*. There is significant ringing where the first 3 echoes are normally.

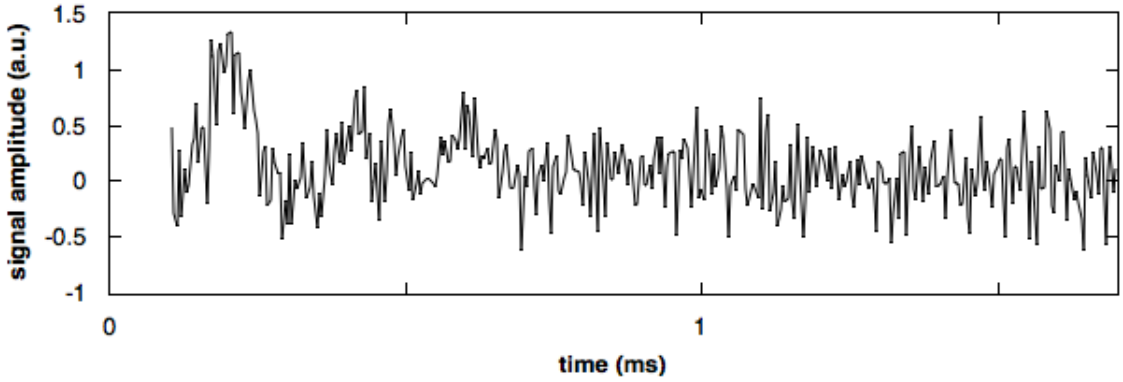


Figure 3.6 real phased CPMG echo train at 20 mm depth of CEM I concrete measurement.

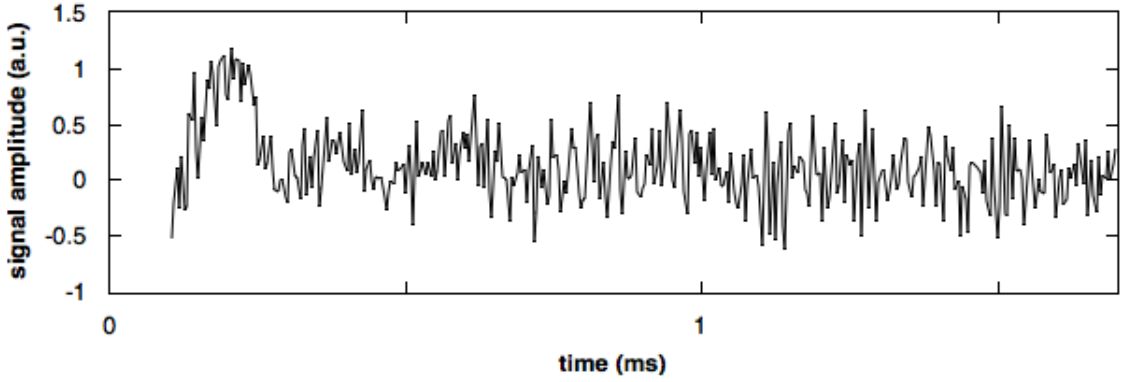


Figure 3.7 real phased CPMG echo train at 20 mm depth of “empty” measurement recorded with same parameters as for the concrete above

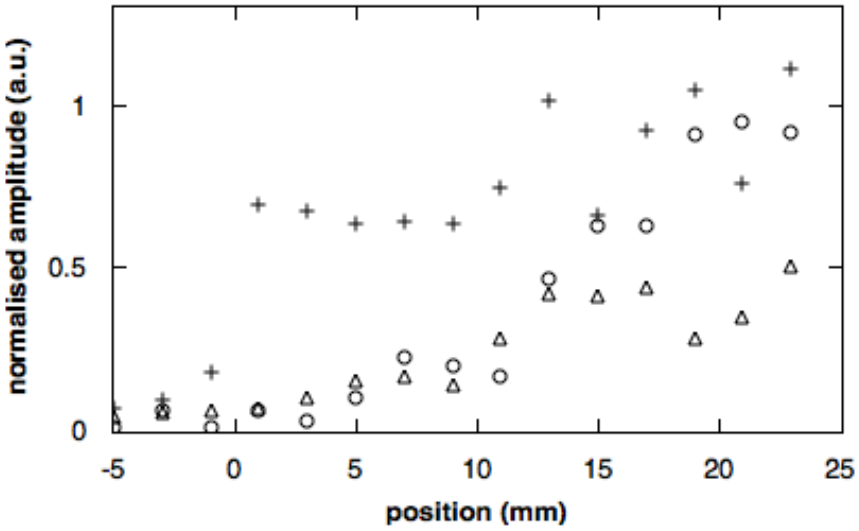


Figure 3.8 Echo sum analysis of internal ringing by depth for empty cavity with echo time of 150 μs (circles) and 200 μs (triangles) echo time. Concrete with 200 μs echo time is shown with crosses

*Figure 3.8* shows the increase of the ringing by depth for echo sum data. The data has been normalised to the signal intensity from a saturated sandstone reference to compensate for the signal loss by depth. Also shown is the signal from concrete acquired with the same parameters. The ringing increased when the echo time, the spacing between the echoes and therefore the pulses, was decreased. The ringing was about 50-60% of the concrete signal at 20-25 mm depth with 200 μs echo time. A shorter echo time increased the ringing significantly therefore the echo time was set to 200 μs. This allowed 8 echoes to be recorded for profiling. The ringing is possibly due to an electronic interference effect because the magnet is close to the coil when larger depth is measured. The ringing was reproducible and therefore subtractable. However, since a large fraction of the signal came from the ringing the data was not reliable at larger depth with subtraction.

### 3.4.2 New coil

A new coil was made and tested during this work. The new coil was a cross transmit-receive coil based on the idea from the NMR MOUSE [84, 91]. It was more rigid and better built. The outer (closer to sample) coil was used to receive and the inner (close to magnet) was used to transmit. The other way round the signal was too weak as the inner coil was too far from the sample. However,

there was significant ringing in the signal (*Figure 3.9*). There could be many reasons for the additional ringing. The coils could be mechanically coupled or not well crossed electronically. Also, the two coils are not in the same physical plane as is required ideally.

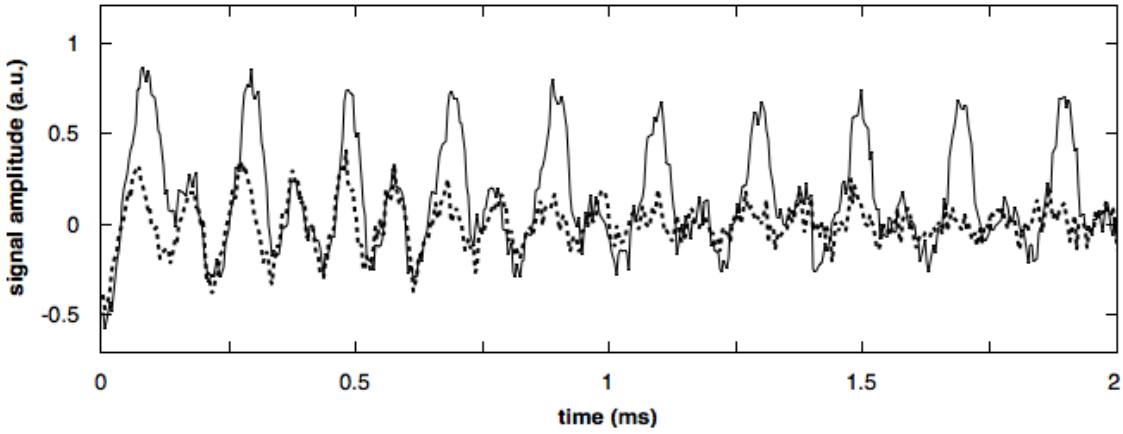


Figure 3.9 real phased CPMG echo train of rubber sample with 200 µs echo time at 3 mm depth. Dashed line is measurement of empty cavity with same parameters

NMR coils are tuned with capacitors. The outer coil was tested as a single coil with both the original and new coil tuning box. The new “out” coil with the old tuning box had no internal background, only acoustic ringing at the first echo. The echo time could be reduced to 130 µs from the previous 200 µs and 12 instead of 8 echoes could be recorded for profiling increasing the signal to noise for echo sum significantly. All results shown in the material chapters (*Chapters 5-7*) were acquired with the new coil.

## 3.5 Improvements on data acquisition

### 3.5.1 Elimination of noise from different sources

The signal to noise ratio is relatively low for the Surface GARField measurement and depends largely on the material (amount of protons measured) and the acquisition parameters (number of scans and therefore acquisition time). In this work, a series of tests and changes have been

performed to improve the signal to noise ratio. The noise comes from several sources. There is noise from the environment of the equipment (RF noise from e.g. other equipment), from the samples (electrical ringing in weakly conducting samples) and acoustic ringing from the coil itself.

The signal strength exponentially decreases by depth. Also, the noise is high due to the open setup of the magnet and that the sample is slightly conducting and therefore yielding a signal ringing.

The RF noise from the background was reduced by an improved copper shielding box about 15-20%. The plastic cover-box is covered with two overlapping layers of copper fabric and it is large enough to cover the magnet on the sample holder frame. Also, „empty" tests were carried out on the sample holder to determine the background signal. There was minimal background signal in the first echo, but the first echo is not used in the analysis for several other reasons (see *Section 3.6.3*).

### 3.5.2 Optimisation of data acquisition parameters

All the following optimisation process was first carried out on the original coil and then repeated for the new 'outer' coil as a single coil. As all materials results in the following chapters were acquired with the new coil, only the parameters for that is shown below.

The current use of the magnet is water profiling using a CPMG experiment at different depths to build a profile. A separate CPMG measurement close to the surface with more scans is used for relaxation time analysis.

Profile resolution depends on the larger of the excited slice width or stepper motor separation of positions. Ideally, the pulse length is set for a slice width equal to the stepper motor to maximise signal. The excited slice width and the excitation are both inversely proportional to the pulse length [87]. The longer the pulse length the thinner the excited slice, so the signal comes from a smaller volume, but a longer pulse is needed to flip the magnetisation over to the horizontal plane at greater depth. The combined effect of the two has a different optimum at different depth. Previously, a constant pulse length and constant pulse amplitude was used. The amplitude is still the maximum to not waste

valuable power, but long pulse length gave better results at larger depth. The optimal pulse length and the applied function for that are shown on *Figure 3.10*.

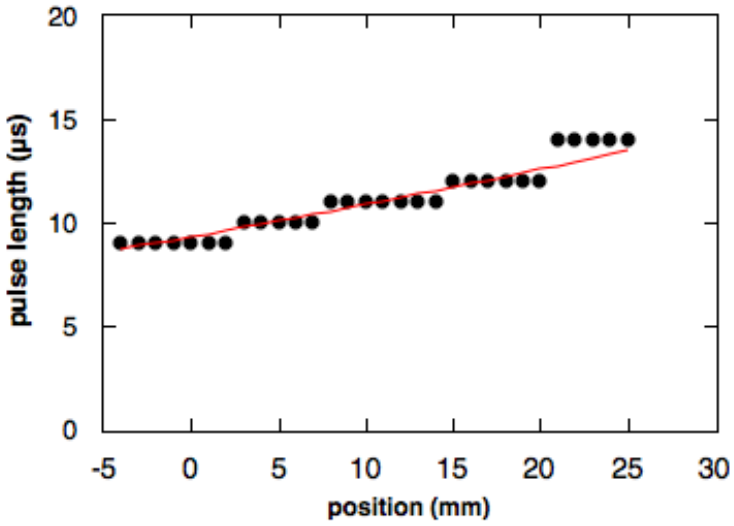


Figure 3.10 The dots are measured data points for maximum single to noise at that position. Red line is the polynomial fit of the optimum pulse length

The optimum pulse length, $p_{length}$ in µs is found to be

$$p_{length}=0.0007\cdot x^2+0.1425\cdot x+8.5682 \qquad 3.1$$

where is $x$ position from the top in mm.

A capillary absorption test on CEM I base mixtures was used for NMR optimisation and calibration. Several CPMG experiments were carried out to determine the optimal NMR parameters for the measurements. The repetition delay, the number of echoes, the “echo time” (time between echoes, $2\tau$) and sufficient number of scans were all studied.

Water profiling parameters were optimised for maximum signal strength. Due to the setup of the equipment, the signal intensity decreases approximately exponentially further away from the surface. The signal lifetime in concrete is relatively short, so short timing between the echoes allowed more echoes to be recorded for better quality data. However, with short echo times, interference appeared. The interference could be caused by the pull and mechanical movement of the coils caused by the pulses. As a compromise, 130 µs was used.

$T_2$ spin-spin relaxation time depends on the pore size, the smaller the pore, the shorter the signal lifetime. For $T_2$ analysis, a short echo time is used to record more echoes specifically for better fitting. Optimised NMR parameters

were determined for $T_2$ analysis at 3 mm from the sample surface where the signal intensity is large and surface drying will not affect the measurement on the measurement timescale. The parameter sets for both profiling and relaxation time analysis are shown in *Table 3.1*. A full profile with 1 mm steps takes about 6 hours and a $T_2$ analysis about an hour to acquire. Due to the duration of the measurement, dynamic water movement cannot be tested by Surface GARField.

Table 3.1 Set parameters for data acquisition

| **NMR parameter** | **Set value for profile** | **Set value for $T_2$ analysis** |
|---|---|---|
| NMR frequency | 2.795 MHz | 2.795 MHz |
| Pulse length | Varied by depth | 9.2 μs |
| Echo time | 130 μs | 130 μs |
| Number of echoes | 12 | 20 |
| Repetition delay | 250 ms | 250 ms |
| Number of scans | 4096 | 16384 |

### 3.5.3 Effect of sample size

The setup of a Surface Garfield allows the sample to be larger than the sensor. At the same time, a small sample can result in loss of signal strength. The chosen sample surface size for permeability and the sorptivity test is 150x150 mm. Therefore, in both cases, 150 mm cubes were cast and for the capillary absorption slabs were cut from the middle section of the cube.

The signal strength was tested with the saturated sandstone, using two blocks from the same sandstone assuming the same porosity. The „large" sandstone was 400x350x50 mm and the small was 150x150x50 mm, same surface area as the concrete specimens. There was no only a small loss between the small and the large samples in signal strength of the total echo sum, the sum of every echo of every slice. The amplitude for the small sandstone is 96±1 and 101±1 for the large (both in the same arbitrary units) with the same data acquisition and processing parameters. The signal loss due to the sample size is 5% assuming that both samples were equally saturated.

This information can help determine the water content in situ, where the sample is likely to be larger than the 150x150 mm area.

## 3.6 Improvements on data analysis

### 3.6.1 Software

The data analysis comprises two steps. The first is phasing and filtering of individual echoes. The second is either computing the echo train intensity sum or fitting exponential $T_2$ decay curves to the echo decay.

The filtering of data includes several questions that are reviewed. Each step can be reviewed and modified with more fitting options then at the outset of the work. The new software includes Gaussian and sinc (sin$t$/$t$) fit to the echo sums by slice or to each individual echo. It also includes exponential fitting to $T_2$ with 1 or 2 components. It is easier to use and needs less time to analyse the data as it can be changed at every stage. Inverse Laplace transform cannot be used to determine the relaxation time distribution due to low signal to noise ratio. The custom analysis software available at the outset was written in GNU Octave language, a share-ware version of MATLAB®. Part of this work was to improve the data analysis and make it more user-friendly. A new code was written. It works in MATLAB® and instead of giving the analysis options in a macro at the beginning, now it can be done interactively.

### 3.6.2 Data filtering

*Figure 3.11* shows the filtering steps with an example CEM I sealed concrete dataset after 1 day of capillary absorption at 3 mm position on the left. The echo numbers are recalculated when echoes are discarded. The first echo was discarded, so at the next step, the second echo becomes the first and all echo numbers were shifted. Therefore, the x-axis was shifted for the last two filtering steps, so that the echoes at each step are at the same position on the example figures, but the echo number is different.

Improvement by data filtering is shown on *Figure 3.12*. First echo was discarded and the echo numbering changed in the software, therefore x-axis is shifted for filtered data so that the echoes line up for each step on the figure for easier comparison.

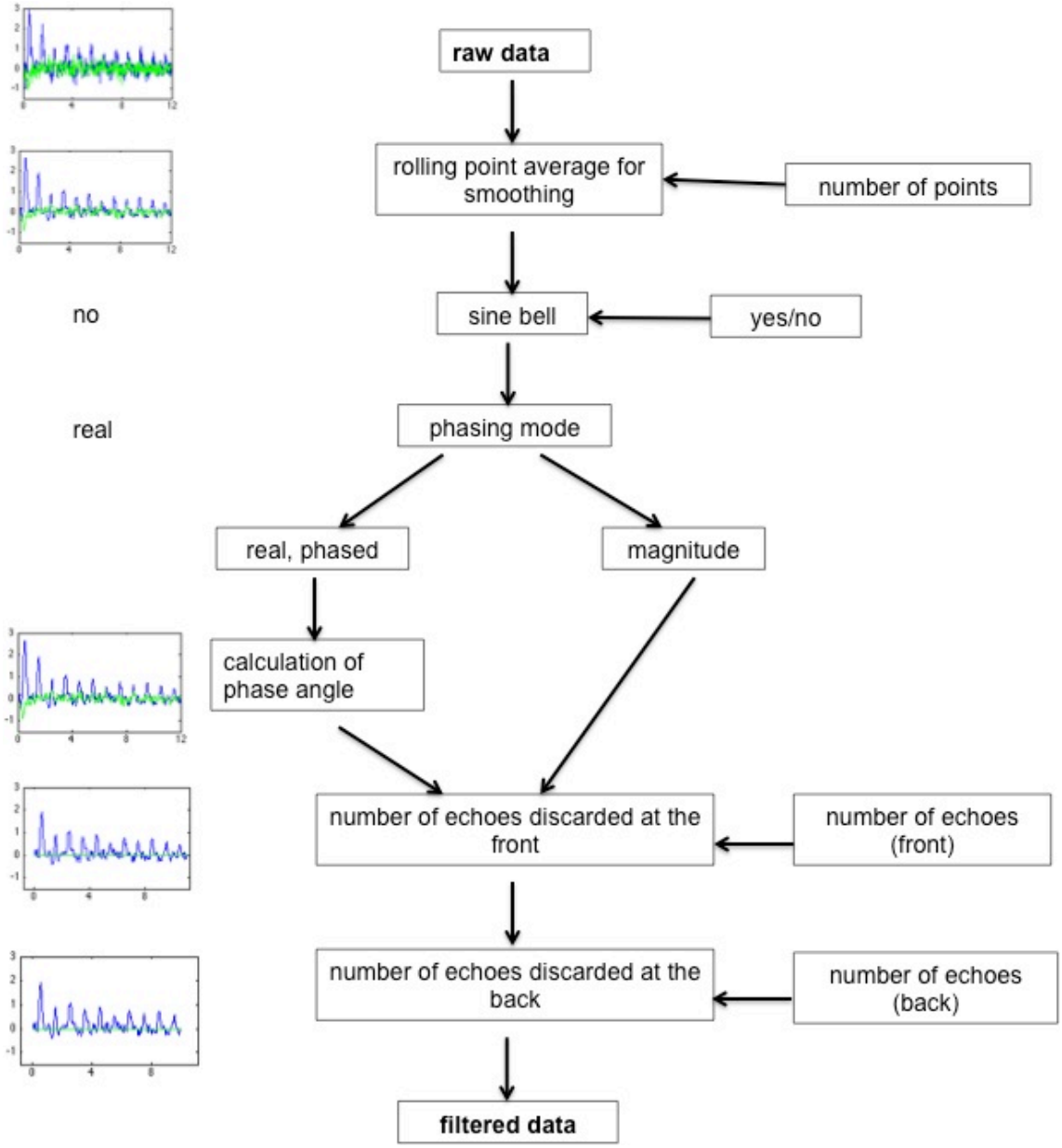


Figure 3.11 Data filtering steps with input. A slice from CEM I sealed cured sample 3 mm from the surface after 1 day of capillary absorption is shown on the left with the standard filtering steps for profiling; 7 rolling points, no sine bell, real phased data with automatic calculation of phase angle, first and last echo discarded.

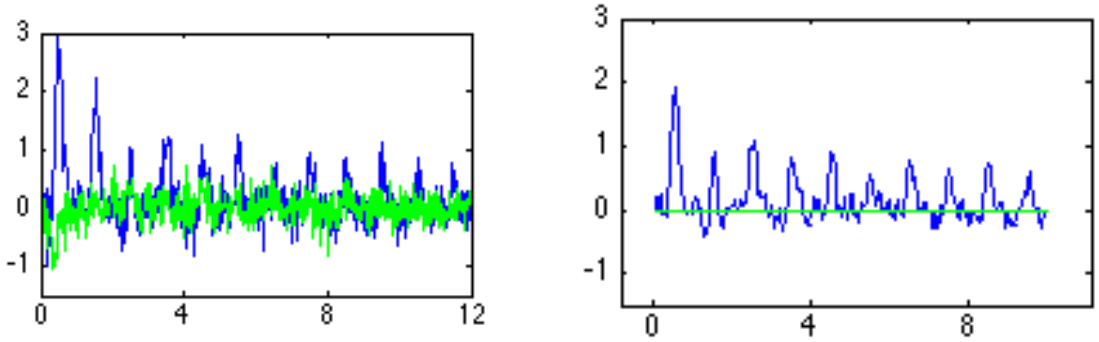


Figure 3.12 Raw data (left) and filtered data (right) from software for the same sample as on Figure 3.11.

### 3.6.3 Data analysis options

For water content, the filtered data is fitted by slice, using echo sum. For relaxation analysis, individual echoes are fitted for $T_2$ exponential decay. $T_2$ data can be acquired for each slice with up to three components. The Surface GARField can measure gel and capillary water, two distinct pore sizes. A three-component option is included to check that there are no more than two components. However, only the first two echoes contain signal from gel water. The first echo is never used because it has a large coherent ring signal that in principle can be subtracted (by measuring “empty”, no sample for the internal ringing of the system), but in practice it is too large. Also, the first echo is affected by systematic modulation due to the magnet setup [114]. Therefore it cannot be reliably fitted as it has additional ringing so the echo is larger than that comes from the signal but at the same time about 30% smaller due to the modulation. This leaves only one echo with signal from the gel water, therefore cannot be fitted to an exponential decay. For relaxation time analysis, only echoes 3-20th were used and a single exponential fitting for capillary water.

Fitting options for both profile analysis and $T_2$ analysis are summarised in *Table 3.2*.

Table 3.2 Data fitting options

| Option | Description | Use |
|---|---|---|
| Option 1 | Echo sum by slice with Gaussian fit of echo sum shape | water profile |
| Option 2 | Echo sum by slice with sinc fit of echo sum shape | water profile |
| Option 3 | Gaussian fit to total echo sum (sum of all slices) | total signal intensity |
| Option 4 | Gaussian fit to individual echoes for exponential decay analysis | $T_2$ analysis |
| Option 5 | Sinc fit to individual echoes | $T_2$ analysis |
| Option 6 | Same as 1, but baseline forced to zero | water profile |

All fitting options include manual correction for the echo fit amplitude. When the signal to noise is low, the fitting for the echoes is not always adequate. The most important for the water content calculation is the signal amplitude. Concrete data can be very noisy that is difficult to fit and the automatic amplitude is not correct. Using real phased data and 0 baseline, the fitting improved compared to variable baseline. In theory, in a linear gradient for a “top hat” RF pulse a sinc shaped echo is expected. However, the pulse is not perfect because the field and the gradient are not perfectly homogeneous. Therefore, a Gaussian fitting works better in practice for echo-shape fit.

One of the new features is that the data can be „normalised” against another dataset. Normalisation means that it compensates the signal loss with the normal approximately exponential signal decay measured on a homogeneous sample. The normalisation runs automatically on the reference sandstone data set and uses the same filtering and fitting as on the original (concrete) data set. In this case, concrete can be normalised against a measurement made on saturated sandstone.

There is a small program to compare the water profiles that also calculates the amount of water in the sample. The signal amplitude relates to the amount of water in the sample at different depth. The profiles can be displayed for both permeability (single sided experiment) and the sorptivity test (both sides).

## 3.7 Calibration

### 3.7.1 Concept

The sensor-coil to examined-slice distance is not constant. Therefore the signal intensity per unit volume approximately exponentially (fourth power) decays by depth in the sample, but changing the pulse width partially compensates for the signal loss. To be able to take that into account, several calibration tests were done on rubber and saturated sandstone.

The NMR was calibrated on water saturated sandstone because the amount of water is uniform on a length scale of millimetres, is easily measured independently, is reproducible and is not time varying due to chemical reaction. The amount of water measured reflects the „real" amount of water in the pore system. The advantage to calibrate on sandstone and not on concrete is that the latter hydrates in contact with water and changes the microstructure. Saturated sandstone is used since it is most similar in terms of NMR response to concrete compared to other standards such as rubber, bulk water or oil, plastic blocks etc. The sandstone used had two distinct pore sizes, the smaller comparable to gel pore size in cementitious materials and the larger comparable to a very large capillary pore. Sandstone is the best known reference, though difference in pore size and hence relaxation time has to be compensated for. Also, Surface GARField cannot detect water in small pores, and the ratio of small to larger pores in sandstone and concrete can raise an issue. The pore structure of limestone could be closer to concrete, but in most cases the total open porosity is very low and so is difficult to use as a reference material.

The rubber is homogeneous and was used to confirm that the sandstone was evenly saturated, even in the middle of the specimen. Two 15x15x5 cm prisms were cut from the same sandstone block. For practical reasons, as saturating a relatively large sandstone piece takes a long time, one was saturated, the other oven-dried. The microstructure and porosity can be assumed to be the same for the two blocks. The microstructure of the sandstone used was stable, with no noticeable leaching or chemical reactions.

The NMR measurement has a resolution in depth, but not in the other two dimensions, therefore the water amount was used for a certain area and multiplied by the slice width measured. The concrete samples used had the area of 15x15 cm, hence the size of the calibration.

The water profile for calibration was acquired with several scans and echoes for good quality data with 1 mm steps. An exponential function was fitted to the saturated sandstone profile from the 7th slice as the first 5-6 slices are above the sample surface. All profiles were corrected by this fitting function for normalisation. The signal decay by depth was similar for sandstone and never dried under water cured concrete (*Figure 3.13*). However, empirically, it is found that dried and re-wetted concrete samples have slightly different signal decay by depth regardless of curing method for the tested sample. The minimum curing was 30 days, but mostly curing exceeded 90 days or more. The normalised profiles are overcompensated for the first few slices and slightly undercompensated for never-dried samples due to the different relaxation times affecting the echo sum.

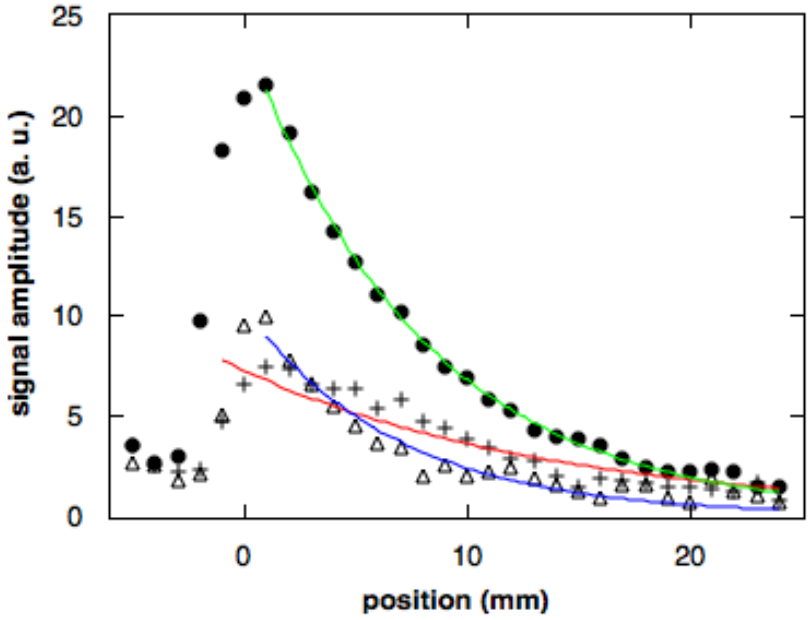


Figure 3.13 Exponential fits to saturated sandstone (circles), never dried concrete (triangle) and dried and rewetted concrete (crosses) profile

The slice width of the NMR measurement is not necessarily the same as the motor steps. The calibration can only be used with the same motor steps, in this case 1 mm. The correction factor for depth, $A^{corr}$, is calculated from the inverse of the exponential fit of the sandstone data.

$$A^{corr} = \exp(k \cdot (x - x_0)) \quad 3.2$$

where $k$ is 0.131 mm$^{-1}$, $x$ is the position in mm and $x_0$ is 6 mm.

Water content was calculated from the difference in density of the dry and saturated sandstone pieces. The total water content of the saturated sandstone was 171.35 g. The saturated sandstone was 49.3x150x2x150.1 mm. Therefore, the accessible porosity was 15.4 vol%. Considering 1 mm slice, the water content for a 1 mm slice was 3.48±0.01 g.

Profiles were acquired with 1 mm motor steps. However, the excited slice width was smaller than the motor step and also changed by depth due to different pulse length (see *Section 3.5.2*). For calibration, each excited slice was a representation of the 1 mm thick sample section. Also, profiling uses echo sum to improve the signal to noise ratio of the profile, but is affected by changes in $T_2$. The relaxation time of concrete and sandstone is different. The reference sandstone was measured by NMR and showed two distinct relaxation times, hence two pore sizes. The smaller pore size of the sandstone was about the same size as gel pores in concrete, the larger pore size is of the same order as a very large capillary pore.

Spot measurements were taken at 3 mm depth from the surface to be able to compensate for the difference in relaxation time between sandstone and concrete. *Table 3.3* shows the NMR data of the spot measurement for the reference sandstone and a sealed cured CEM I sample after 1 day of capillary absorption. The first two echoes were discarded and the (long) component was fitted with single exponential decay. Then the echo sum of echoes 2-11$^{th}$, same echoes as used for profiling, was calculated for the same dataset.

Table 3.3 $M_0$ and $T_2$ of sandstone and concrete

| NMR data | Sandstone | Concrete |
|---|---|---|
| $M_0$ long component | 5.767 | 3.442 |
| $T_2$ long component | 16.55 ms | 1.84 ms |

Gel water is present in the first two echoes of the CPMG echo train. The first echo is always discarded, but the second is used for profiling. The first echo is not reliable and not used for data analysis. Therefore, the second echo is the only echo used that contains signal from gel water, but a single point cannot be

fitted with an exponential to determine the $M_0$ and $T_2$. Instead, to take gel water into account, echo sum-to-$M_0$ ratio was calculated. The signal amplitude and the echo sum of concrete were compared to the reference sandstone:

$$M_{0\_ratio} = \frac{M_{0\_concrete}}{M_{0\_sandstone}} = 0.597 \qquad 3.3$$

$$sum_{ratio} = \frac{echo\_sum\_concrete}{echo\_sum\_sandstone} = 0.49 \qquad 3.4$$

The difference is due to the different relaxation time and also the gel/small pore water content in the echo sum data. At this depth, the echo sum data for concrete has to be multiplied by $f_{corr}=M_{0\_ratio}/sum_{ratio}$ that is 1.22 to compensate. The $M_0$ of the reference sandstone was 5.767 and the echo sum was 59.18 that represent 3.48 g for a 1 mm motor step slice. So to calculate the water content for concrete for each motor step slice (1x150x150 mm) in the profiling,

$$water\_content_{c\_slice}(\mathrm{g}) = \frac{echo\_sum\_concrete}{echo\_sum\_sandstone} \cdot f_{corr} \cdot 3.48(\mathrm{g}) \qquad 3.5$$

The correction factor, $f_{corr}$ was calculated for several samples for all concrete mixes used. The mean of the correction factors for individual samples was 1.2. The concrete profile echo sum data is divided slice by slice with the fit of the reference saturated sandstone profile ($A^{corr}$ for sandstone). Then the water content is calculated for each concrete slice by multiplying by the, $f_{corr}$ and 3.48 g. Water content profiles are shown later in vol%. The NMR signal of each slice corresponds to a 1 mm thick sample slice. Water content by vol% assumed that each slice has a volume of 1x150x150 mm.

The comparison of the sandstone reference and the concrete was at fixed depth, 3 mm from the surface. However, the relaxation time of the same sample changes by depth in a high gradient, such as the Surface GARField[114].

### 3.7.2 Validation of the measurement

40 mm thick samples were used for validation as NMR profile of the full cross-section could be acquired by overlapping profiles acquired from opposite sides of the sample. The exact sample width was measured to mm precision. The total signal intensity was all echo sums for the sample assuming the first

5 mm (5 slices) of the profile was above the sample. For 40 mm thick samples, the profiles acquired up to 25 mm from the surface from both sides overlapped in the middle. The average of the two profiles was used to compensate for the larger uncertainty at large depth. The total NMR signal by summing the whole profile across the sample was compared to mass change. Water content on concrete samples measured by mass increase and NMR were profiling are in good agreement, within 5% difference (*Figure 3.14*). All three base mixtures were tested (details of the three concrete mixes are presented in *Section 4.3*). CEM I + Si samples show around 5-10% difference from gravimetric data. Probably due to a different relaxation time compared to the other mixes Part of the difference in the water content can be due to the fact that surface is between two measured slices. There is no sharp increase from one data point to the next indicating that the motor step probably does not align perfectly with the sample surface.

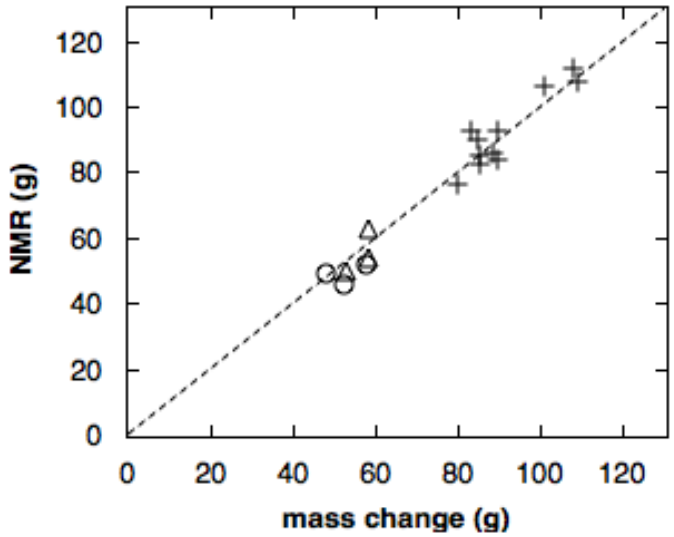


Figure 3.14 Comparison of water content of 40 mm thick samples from different methods, CEM I (crosses), CEM I + Si (triangles), CEM III/B (circles). Dotted line shows equal water content by NMR and mass. $R^2$ is 0.95 for all data

The water profiles were validated on “half wet-half dry” samples (*Figure 3.15*). Two 20 mm thick concrete samples were put together and measured after drying (red profile). Then one sample was saturated with water and both were wrapped in foil separately to protect against moisture transport from one to the other. Water profiles were acquired again from both sides (turning the samples together upside down). The water profile drops at the edge of the wet sample. Due to the uncertainty at higher depth there is a large scatter of data

points, Possibly the motor steps were not exactly matched to the surface of the samples so there is no sharp decline in the middle. The water uptake by gravimetry was 51 g. Water content by NMR from the profile was 48.3 g.

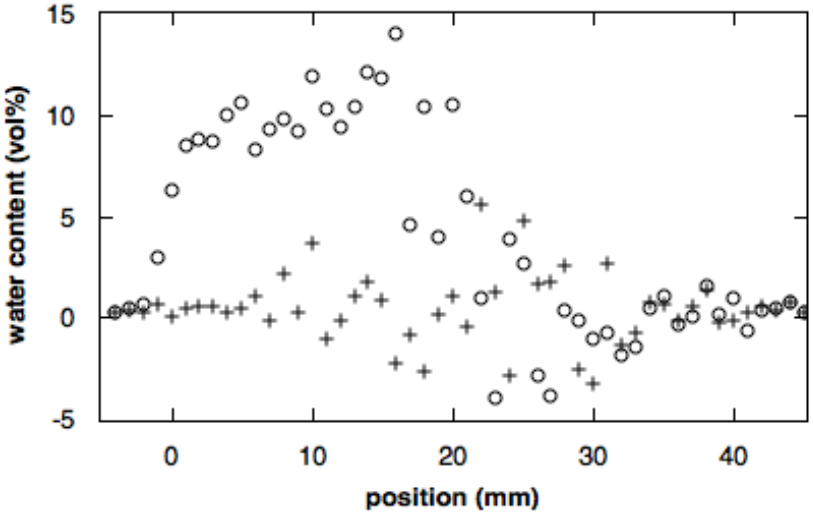


Figure 3.15 Two 20 mm thick samples for profile validation, both dry (crosses) and the left wet, right dry (circles)

### 3.7.3 Error analysis

Error in the measurement was investigated. Repeats were acquired on the same sample and also different samples of the same batch.

Repeated measurements on the same sample show good repeatability of water profiles for the first 15 mm. *Figure 3.16* shows two repeats of same sample with additional measurements at depths of 10, 15, 20 and 25 mm for error estimate. At those depths, the standard error in the mean ($\sigma/\sqrt{N}$ where $\sigma$ is the standard deviation and $N$ is the number of repeats) of the intensity was calculated and used to create error bars. Data was acquired 5-10 times for error calculation. The standard errors in the mean were 1.4%, 5.7%, 10.8% and 15.8% respectively for the saturated sample below. Error bars are not shown on further NMR profiles for clearer figures. The uncertainty is large at higher depth due to weak signal and low signal-to-noise ratio. The error bars were calculated from standard deviation and can be very large, up to 30-40% at depth when the sample is not fully saturated and signal to noise is low. This is one of the limitations of the Surface GARField measurement on concrete that has low water content (compared to mortars and especially cement paste) and hence

signal. This can be partly overcome by increasing the number of scans at larger depth though the experiment duration will increase.

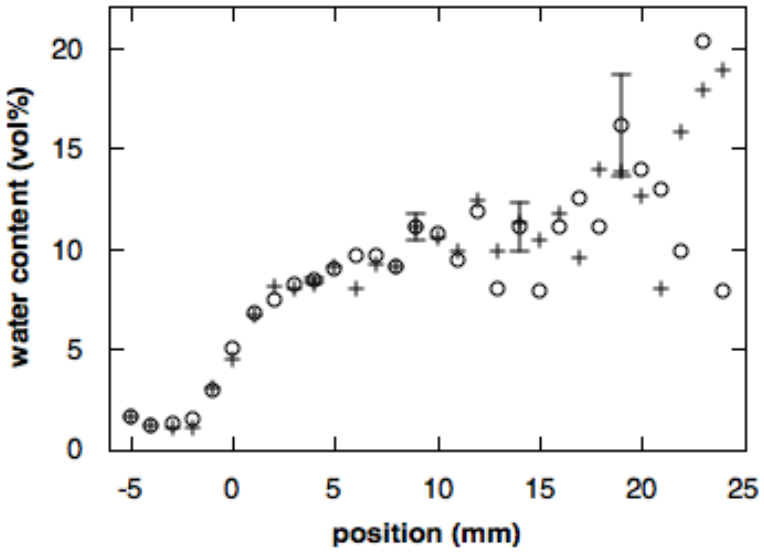


Figure 3.16 Repeated measurements on saturated concrete sample

Measurements on samples from the same mix show good repeatability on "as-cured" and dried and rewetted samples. NMR profiles were acquired after 1 day of capillary absorption on two under water cured CEM I concrete samples from the same batch (*Figure 3.17*).

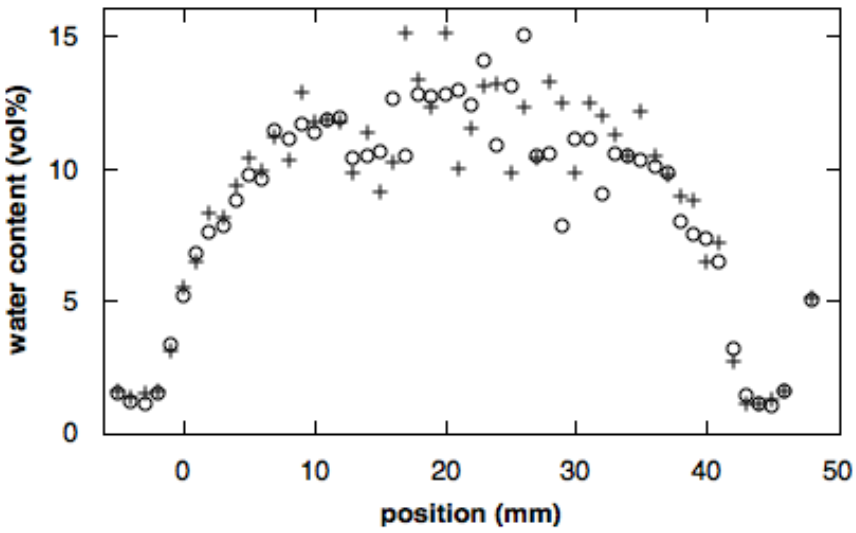


Figure 3.17 Repeated measurements on two samples of same mix, surface in contact with water is at 0 mm

For relaxation time analysis at fixed depth, the standard error in the mean of the fitting of one sample (measured on a sealed cured 0.5 *w/c* sample) measured 5 times was about 1.2 % for the intensity and about 2.5 % for the $T_2$. Across three different samples made from the same original mix, the standard

error for both intensity and $T_2$ was about 3 %. An example for the error of the relaxation time data is shown on *Figure 3.18* measured on a sealed cured OPC sample with 0.8 w/c. It is possible to consider only alternate echoes, e.g. echo 1, 3, 5 etc. due to 180° pulse artefact that is compensated for at even number echoes. Many commercial machines use this approach. Fitting of all echoes and fitting for only odd echoes are also shown on *Figure 3.18.*

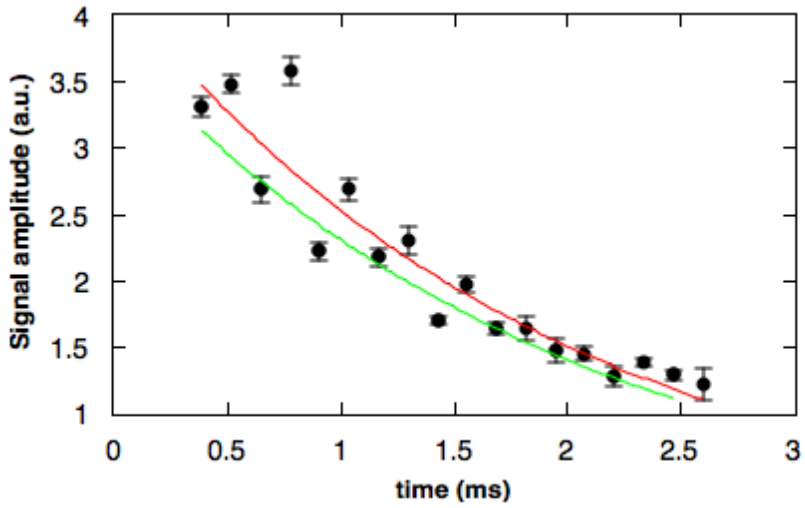


Figure 3.18 Relaxation time data with error from three sample of same mix. Red line is a single exponential fit to all echoes, green line is a single exponential fit to odd numbered echoes only

## 3.8 Concluding remarks

Improvements on the Surface GARField machine has meant that some of the noise can be eliminated and the systematic background noise was measured and then deducted from the signal for the old coil. The new, improved coil has no background noise and so the echo time could be reduced to improve the signal by recording more echoes in the CPMG. The new arrangement can measure part of the gel water, as well as the capillary that was not possible with the previous coil.

The data acquisition has been optimised and a standard test procedure for concrete has been established. With the set parameters for profiling, a full profile with 1 mm resolution takes 4.5 hours. Additional measurement at 3 mm depth from sample surface for relaxation time analysis takes about an hour. This is reasonable in laboratory testing, and can be reduced to 1.5-2 hours for

in-situ testing for profiling where 2-3 mm slice resolution is suitable. Data acquisition was optimised for 4 cm thick samples, where the sample can be measured from both sides with overlapping profiles and the uncertainty at larger depth can be compensated by using the average of the two profiles. For in-situ testing, more scans beyond 20 mm position will be necessary to improve the signal to noise ratio.

A standard data analysis for concrete was developed for both profiling and spot measurement for relaxation time analysis. The analysis software was improved to make it more user-friendly and now provides a possibility to review and change the analysis parameters at every step.

Overall, the NMR measurement technique developed shows good repeatability and it has been calibrated with good agreement to mass increase for five concrete mixes (four cements) Tests on the half wet-half dry sample showed that the profiles provide reliable data even at larger depths.

# 4 NMR methods and cementitious materials

## 4.1 Introduction

Conventional water transport test methods were investigated by spatially resolved NMR. Two NMR systems were used, the Surface GARField described in Chapter 1 and the Laboratory GARField. During the course of this work, the limitations of the Surface GARField measurement made it necessary to use another NMR, the Laboratory GARField for better understanding of test results.

The aim was to examine a variety of microstructures of conventional structural concrete and construction materials, and a number of mix designs were chosen accordingly. Water transport takes place in the porosity of the paste. For better comparison between the various samples tested, the aggregate fractions and overall cement paste volume was the same for all mixes. Three cement types, two water-to-cement ratios and two curing methods were used in various combinations for sorptivity. For the permeability measurements, a similar mix design was used, only the water-to-cement ratio was varied.

This chapter contains description of the Laboratory GARField, the data acquisition and data analysis parameters for NMR both systems and the concrete and mortar mix designs.

## 4.2 NMR methods

### 4.2.1 Surface GARField

The data acquisition and analysis for concrete was optimised for the Surface GARField measurement that was described in *Chapter 3*. The data acquisition parameter sets selected for future work are shown in *Table 4.1* for profiling and spot measurement at 3 mm depth for $T_2$ analysis. Set parameters for both data filtering and analysis for profiling and $T_2$ analysis are shown on *Table 4.2*. The analysis options were discussed in *Section 3.6.1*.

Table 4.1 NMR data acquisition parameters

| NMR parameter | Set value for profile | Set value for $T_2$ analysis |
|---|---|---|
| NMR frequency | 2.795 MHz | 2.795 MHz |
| Pulse length | Varied by depth | 9.2 µs |
| Echo time | 130 µs | 130 µs |
| Number of echoes | 12 | 20 |
| Number of points per echo | 48 | 48 |
| Repetition delay | 250 ms | 250 ms |
| Number of scans | 4096 | 16384 |

Table 4.2 NMR data analysis parameters

| analysis parameter | Set value for profile | Set value for $T_2$ analysis |
|---|---|---|
| Number of rolling points | 7 | 7 |
| Sine bell | no | no |
| Phased/magnitude | Real, phased, automatic angle | Real, phased, automatic angle |
| Discard echoes (front) | 1 | 2 |
| Discard echoes (back) | 1 | 0 |
| Fit option nr. | 6 (profiling, 0 baseline) | 4 (individual echo fit) |
| Further analysis | Normalisation by sandstone | $T_2$ fitting with 1 component |

### 4.2.2 Laboratory GARField

The Laboratory GARField is fundamentally different from the Surface GARField measurement as a sample is positioned between two shaped poles of a permanent magnet. The distance between the poles limits the maximum sample diameter. Notwithstanding, the Laboratory GARField is similar to the Surface GARField in so much as the field strength gradient is perpendicular to the planes of constant, uniform field strength enabling 1D profiling. However, the field strength and gradient strength are much greater than with the Surface GARField, so that a thinner slice can be selected with greater sensitivity. Also, because the sample is smaller a smaller coil can be used and the deadtime is much shorter so that smaller values of echo time can be used. A new coil was

prepared with a glass sample holder tube for the mortar measurement that allowed a maximum of 18 mm diameter instead of the previously used 10 mm to be able to study standard mortar. As a consequence, the maximum measured sample length was about 30-35 mm as the minimum distance between the magnet poles were just slightly over 10 mm hence the originally used sample size, see schematic below (*Figure 4.1*).

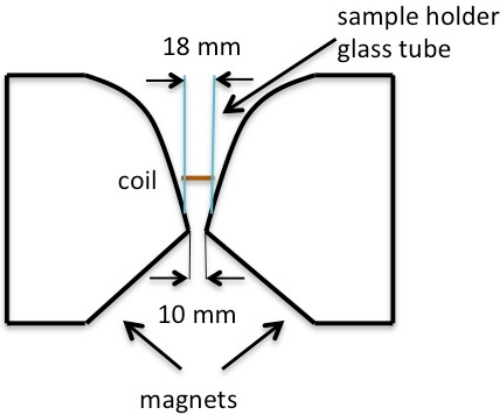


Figure 4.1 Schematic of Laboratory GARField with new coil

NMR profiles were acquired with 2 mm steps for dried sample and 1 mm steps for rewetted samples. The CPMG experiment was carried out at each position. In this NMR system, the coil and the magnet was fixed and the sample was moved to up and down for a profile. Therefore the quality of the NMR data did not depend on the sample position and only 1 data acquisition set was needed.

Parameters for data acquisition are in *Table 4.3*.

Table 4.3 Laboratory GARField NMR parameters

| NMR parameter | Set value |
|---|---|
| NMR frequency | 23.4 MHz |
| Pulse length | 6.5 μs |
| Echo time | 64 μs |
| Number of echoes | 64 |
| Number of points per echo | 16 |
| Repetition delay | 250 ms |
| Number of scans | 2048 |

The data was phased and the points were summed for each echo. The intensity of the first few echoes are systematically modulated in GARField due to pulse length artefacts [111] and so the first three echoes intensities were corrected by reference to a rubber sample for which they are expected to be near constant amplitude. The correction factor was determined for each echo based on a single component fitting for rubber and the difference of the measured intensity and the one calculated from the fitting.

For profiling, the mortar echo train data was fitted with 2 component exponentials and a baseline: a short component between 150-500 μs and a long component 1000-3000 μs plus a baseline in the range of 0-1. The baseline maximum was set to 1, representing about 1% of the maximum signal intensity as real phased data was fitted and longer components than 3000 μs were not seen in any analysis. Higher values for baseline introduced artefacts in the capillary fitting. Fitting the last part of the echo train then subtracting the fitted part from the front half of the echo train (stripping) did not work well with the mortar sample probably due to lower signal to noise ratio than paste samples.

For better signal to noise, the average of the middle 10-11 measured depths along the measured part of the sample length were used for relaxation time analysis. Several fitting parameter sets were investigated, including 2 fixed relaxation times plus a baseline. Details of the fittings used can be found at the description of the particular experiment description as different parameter sets were investigated and the best fit varied.

## 4.3 Cementitious materials

### 4.3.1 Mix designs

The mix design of the materials used in this study was aimed at ensuring that the fresh concrete mix had sufficient workability and flow to compact with minimum vibration. The use of admixtures such as plasticisers can be used to improve the workability and flow by altering the surface chemistry of the cement particles. However, the admixtures can alter the microstructure of the hardened

concrete. This was considered undesirable in the context of this work, therefore no plasticiser or any other admixture were used.

The concrete mixes were designed to be close to commonly used structural concrete, minimum C30/37 compressive strength [115] and 400 mm flow [116] for workability. The aim was to use 0.5 water-to-binder ratio to be able to compare results with standard mortar [117] and the typical 0.4 w/c of cement pastes, (about equivalent to 0.5 in concrete when water adsorbed on the fine aggregate surface is considered).

The base mix design was CEM I (Portland cement, PC), 0.5 water/cement (w/c or w/b for water/binder) with 30% paste volume. The details of the base mix are in *Table 4.4*. The maximum aggregates size used was limited to 8 mm.

The sample thickness should be minimum five times the maximum aggregate. The minimum tested sample thickness was 40 mm for overlapping NMR profiles, so the maximum aggregate was reduced from 16 mm used in the initial testing to 8 mm. The resulting material was then closer to mortar than a conventional concrete used in construction, but still retained the essential features required, e.g. aggregates of different particle size in a cement matrix and significant aggregate-cement interface area.

Table 4.4 Concrete mix designs

| **Component** | **kg/m$^3$ of concrete** | **density (kg/dm$^3$)** | **l/m$^3$ of concrete** |
|---|---|---|---|
| cement | 365 | 3.06 | 119 |
| water | 183 | 1.0 | 183 |
| sand 0/2 | 799 | 2.60 | 307 |
| gravel 2/8 | 981 | 2.61 | 376 |
| air | 15 | | 15 |
| Total | 2328 | 2.328 | 1000 |

Further samples with 0.8 w/c were tested investigating the effect of different gel/capillary porosity ratio. The paste volume remained the same, 30%.

To investigate the effect of cement types, CEM III/B (PC with 70 w% slag premixed) and CEM I with 10 w% silica fume (CEM I + Si) were also tested. The mixes only differed in the binder from the base mix. The cements were chosen

to have similar compressive strength at 28 days. CEM III/B mix had only about 350 mm flow, but was still well worked in the moulds. Samples were prepared according to EN 12390-2 [118] and the air content of the fresh concrete sample measured. A cured sample was tested for compaction by splitting and showed no signs of large air voids. A higher paste volume mix was also tested with 400 mm flow, but was discarded due to high cement content and possible microcracking.

The 0.5 w/c mixes were tested for compressive strength at 28 days according to [119]. The compressive strength was around 50 $N/mm^2$ for all three 0.5 w/c mixes and was above the planned C30/37.

For permeability testing, the mixture was optimised so that the visible water penetration line was within 25 mm of the surface, the maximum for the Surface GARField measurement, and so that the water line was easily visible. The base mixture was tested for permeability (EN 12390-8) and showed limited water penetration, but not clear water penetration line. Therefore, the mix design was altered to 0.6 and 0.55 w/c and all other parameters remained the same. In the former case, the water penetration was about 40 mm, beyond the measureable region of the NMR magnet. For the latter, the visual water line was 18-20 mm and easily visible. The 0.55 w/c mix was chosen as optimal and used for all further testing.

For further testing on the Laboratory GARField, three binders CEM I, CEM I + Si and CEM III/B was used. As the sample size was smaller, instead of concrete, standard mortar with a ratio of 0.5:1:3 by mass for water:cement:aggregate was cast in 150 mm cubes. The maximum aggregate size was 2 mm. One cube was prepared for each mixture and curing method.

### 4.3.2 Curing and pre-conditioning

One day after mixing, the cubes were demoulded and sealed cured with a double layer of plastic sheet for a minimum 90 days at 20°C. Concrete samples were wet cut from the middle part of a 150 mm cubes. Further CEM I samples were under water cured to investigate the effect of curing and initial capillary

water content. Preconditioning was oven drying at 60°C till constant mass to minimise microstructural damage. Drying of the concrete sample required a long time, a minimum 4 weeks until the samples reached constant mass. A sample from each batch was measured by the Surface GARField after drying and the sample was considered dry when there was no signal, hence no capillary water and probably only minimal amount of gel water.

Mortar cylinders of 18 mm diameter and 150 mm length were wet cored from the cubes for the Laboratory GARField experiments. The paste skin that forms on the surface of the sample at casting was not removed from the end of the cylinders. The mortar cylinders were dried to constant mass at 60°C, about 2 weeks, under light vacuum to minimise carbonation.

At 60°C, it is expected that gel and capillary pores empty, but that the inter-layer pore water remains reasonably intact [29].

## 4.4 Concluding remarks

NMR acquisition parameters were set for both the Surface GARField and the Laboratory GARField for concrete and mortar testing. Standard analysis procedure was determined for both NMR systems for profiling. Spot measurement was developed for relaxation time analysis for the Surface GARField measurement at fixed depth. Further data analysis methods were used for the Laboratory GARField using average of 10 slices for better signal-to-noise ratio.

The test samples were designed with a variety of microstructures. All mixtures could be worked in well and had the minimum compressive strength planned. The maximum aggregate size was reduced from 16 to 8 mm as to effects from large aggregates in relatively thin samples. As a consequence, the samples were closer to a mortar than conventional concrete. However, the essential microstructural characteristics were the same. The water uptake was not significantly different for the orientation mix with the larger aggregates compared to what was used later in this work. CEM I with 0.5 w/c and sealed curing became the base mixture with variations of curing, w/c and cement. These were used for sorptivity testing. A similar mixture was designed for

permeability testing, but w/c was optimised for water penetration depth so that the water line was clearly visible and still within the depth the Surface GARField could measure.

Similar mortars were used for testing on the Laboratory GARField, same w/c ratio, but slightly higher paste volume. The aim was to use similar materials on the different systems so that the results could be compared.

# 5 NMR evidence of limitations in conventional testing of water transport

## 5.1 Introduction

Capillary absorption tests were carried out with the usual method: the total water uptake by capillary absorption up to 24 hours measured by mass increase. The NMR relaxation time distributions were measured after the capillary absorption and the results compared to the gravimetry, the NMR giving more information on the saturation and the pore size distribution with water in it. The experiments were then continued up to 4 weeks with further mass and NMR measurements. Both tests were carried out using different microstructures by varying the curing, w/c, cement and sample size. Silica fume improves the microstructure by filling the voids between the cement grains and by pozzolanic reaction. Slag also improves the microstructure by changing the C-S-H formed. Both blended cements tend to have better durability properties than Portland cement, but can be at greater risk of carbonation of residual portlandite.

The water penetration under pressure test was carried out on samples with a minimum measure of 100 mm in the pressurised surface size. The samples can be cylinders or cuboids, though the diameter or shorter side of the surface where pressure is applied have to be at least 100 mm. The test was carried out on 150 mm cubes, the same surface area as the sorptivity testing. For the investigation of size and curing cylinders were used to avoid edge-effects.

## 5.2 Sorptivity

### 5.2.1 Test setup

The sample thickness was based on two factors, the minimum depending on the largest aggregate size and the maximum depending on the range of the

NMR experiment. CEM I samples were used for orientational testing and developing the testing procedure on 3 cm, 4 cm and 4.5 cm thick samples. 4 cm samples were considered optimal for calculating water content as the two profiles measured from opposite sides still overlap, but are least affected by the aggregate size. Due to the cutting process, the exact sample thickness varied between 38-43 mm.

Mass was measured at 1, 2, 4, 8 and 24 hours for cumulative adsorbed water. Further testing was carried out up to 4 weeks at 2, 7, 14 and 28 days. After the capillary absorption measurement, the NMR water profile was acquired on the sample to visualise the water distribution. The first profile was acquired after 24 hours of capillary absorption, then at every mass measurement. Profiles across the full samples were carried out on the 4 cm thick samples and were used for calibration comparing mass uptake and total NMR signal intensities.

A minimum of three samples were tested for each mixture and size. A total of 20 samples were investigated for at least 2 weeks for mass uptake and by NMR.

### 5.2.2 CEM I

In the case of CEM I, the 4 cm thick samples were almost saturated after 1 day, there was no significant water uptake beyond 1 day because the water front reached the top of the sample. Further water uptake was only possible by removing the trapped air bubbles. The gravimetric water uptake of sealed and underwater cured 0.5 w/c and sealed 0.8 w/c samples as a square root of time is shown on *Figure 5.15*. The water uptake was linear with the square root of time up to 2 days of capillary sorption after which there was only minimal change in sample mass. The standard error of the measurement is shown for the 0.8 w/c samples based on 3 samples. The error was smaller for the 0.5 w/c mixes, at about 3%. The water uptake was essentially the same for both curing methods of the same mix and the same batch. Water uptake is shown up to 4 weeks of sorption.

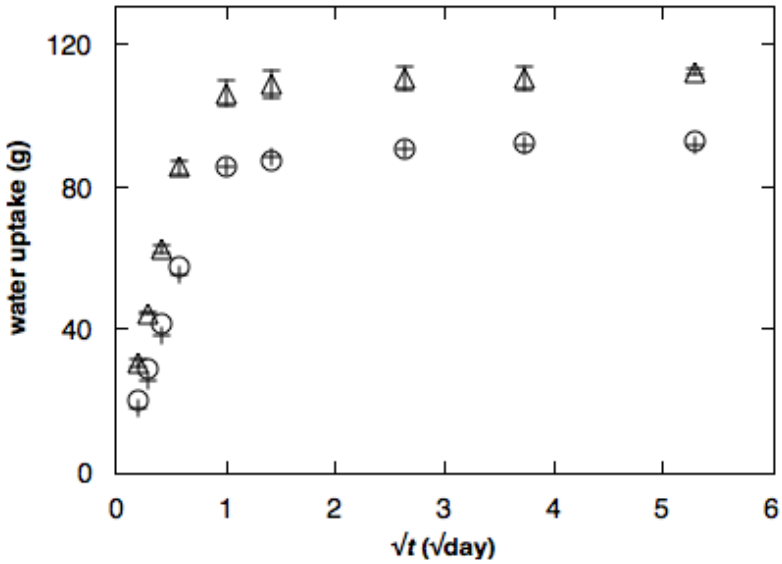


Figure 5.1. Average water uptake of sealed (circle) and underwater cured (cross) 0.5 w/c and sealed 0.8 w/c (triangle) each data point is the average of 3 samples

NMR profiles were acquired on dry samples and after 1 day of sorption. All profiles measured with the Surface GARField are echo sum profiles using the standard data acquisition and analysis described in *Section 4.2.1*. The first 5 slices were above the sample surface. The sample was in contact with water on the left side (*Figure 5.2*). The dry measurement shows high variability due to uncertainty at depth. Underwater cured samples (*Figure 5.3*) had very similar profiles to sealed cured samples of the same mix. The slope in the profile close to the surface is due to the normalisation procedure (see *Section 3.7.1*). Also, neither the sample surface nor the excited slice was entirely flat nor were they perfectly parallel. Another possible cause is that the motor steps were not perfectly aligned with the sample surface and only part of the excited slice was within the sample. The increased water content in the middle of the sample is an artefact due to high uncertainty. The uncertainty of the measurement is also shown on the dry measurement. There is no signal and therefore echo sum to fit, just random noise, but the current version of the software fits a Gaussian/sinc function to the data points in every case. Therefore the profile can be either negative or positive. This can be overwritten manually for each slice by adjusting the amplitude.

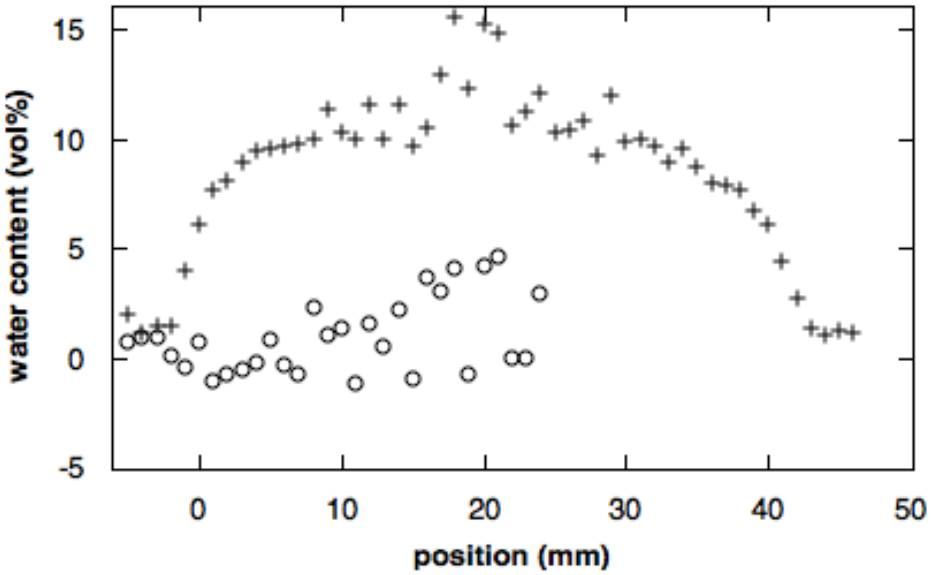


Figure 5.2 NMR profile of 4 cm sealed cured CEM I concrete sample after 1 day of sorption (cross) with dry profile from one side before measurement (circle)

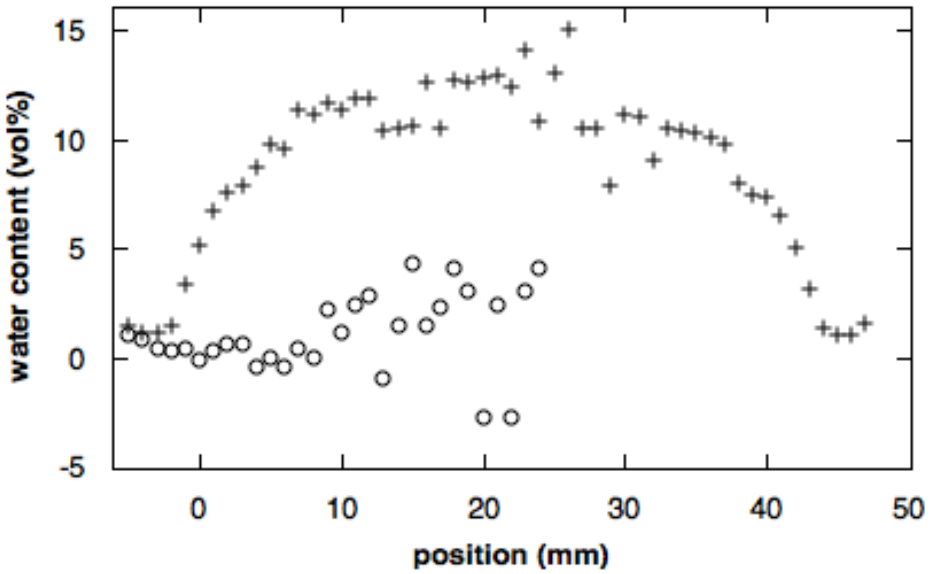


Figure 5.3 NMR profile of 4 cm under water cured CEM I concrete sample after 1 day of sorption (cross) with dry profile from one side before measurement (circle)

The 0.8 w/c sample was also saturated after 1 day of sorption (*Figure 5.4*), but the overall water content was higher than of the 0.5 w/c sealed cured sample as expected from the higher amount of large porosity.

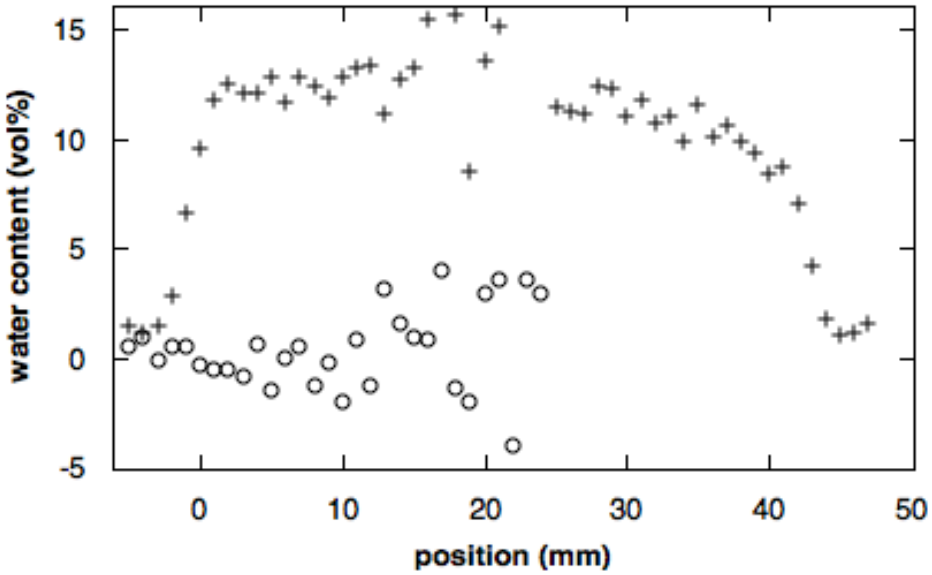


Figure 5.4 NMR profile of 4 cm sealed cured CEM I 0.8 w/c concrete sample after 1 day of sorption (cross) with dry profile from one side before measurement (circle)

Conventional testing worked for the base CEM I mix and sample size up to 1 day of absorption. NMR evidence showed that the mass uptake slowed down because the waterfront reached the top of the sample. The experiment was repeatable and did not depend on sample curing.

However, the capillary absorption test can be carried out by splitting the sample in half and determining the wet front. Therefore, the colour change of the sample was also investigated. All samples had a dark band close to the wet surface. However, the NMR profiles showed that there was no detectable change in the water content after the dark band compared to visibly wet region. On *Figure 5.5*, the NMR profile is shown with the cross-section of the sample beneath.

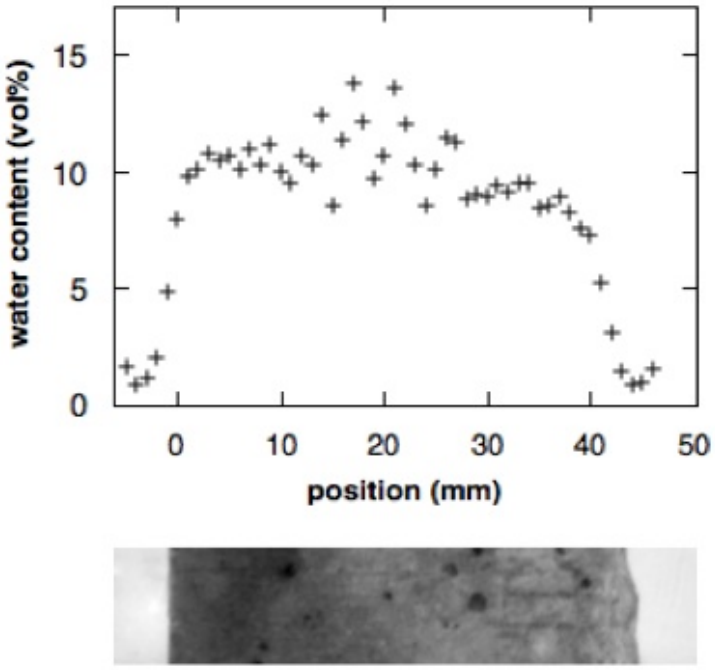


Figure 5.5 Water profile by NMR (top) with photo of cross-section of the sample (bottom), the scales line up

The difference of sorptivity measured by mass increase and penetration depth has been noted in literature and water beyond the visibly wet region was expected [57]. An explanation is that colour change only reflects part of the wet volume. Further investigation of the relationship between the visual water line and the actual waterfront is provided in *Chapter 7*.

### 5.2.3 Effect of sample size

The height of the sample in sorptivity testing is usually round 10 cm, so that the waterfront does not reach the top of the sample during the measurement time. However, due to the depth limitation of the magnet, 4 cm thick samples were used. To investigate the effect of sample thickness (height), 7 and 10 cm thick samples were also investigated. All samples were cut from the middle of 15 cm cubes as the base samples. All three binders were investigated (CEM I, CEM I + Si, CEM III/B), but only sealed cured. Results for the composite binders will be presented in the following *Sections 5.2.4* and *5.2.5*. Mass uptake for all three CEM I sealed cured sample sizes is shown on *Figure 5.6*.

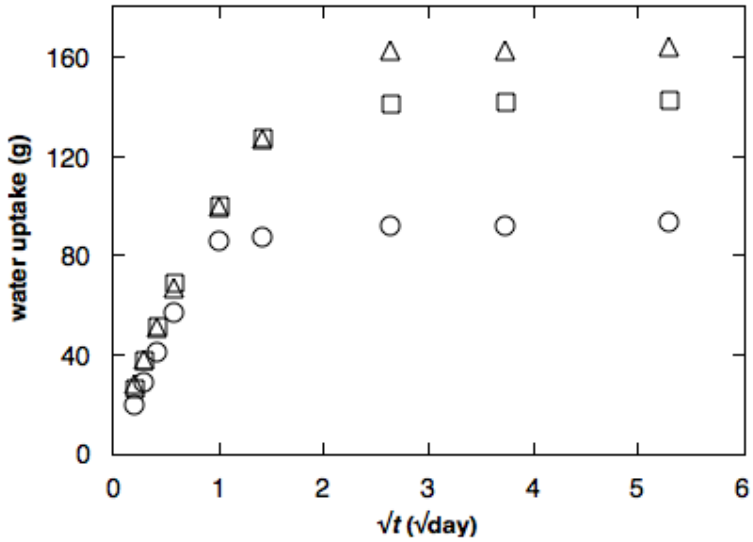


Figure 5.6 Water uptake by time on CEM I samples 4 cm (circles), 7 cm (squares) and 10 cm (triangles) thick

Three samples were tested for each sample size. For all sizes, the water uptake was linear with the square root of time up to 1 day. The water uptake slows down significantly after 1-4 days of capillary absorption. In the case of the 4 cm thick samples, the waterfront reached the opposite side of the sample. A 7 and a 10 cm thick sample were measured 3 mm below the surface on the opposite side after 1 day of capillary absorption and there was no NMR signal. It should be noted that although the mass attained a constant value, this does not necessarily imply that the sample is uniformly saturated.

NMR profiles of the same mix, but different sample sizes are shown on *Figure 5.7*. Only the top 30 mm is shown for the thin sample, though the full cross-section was measured. The water content of the sample close to the wet surface, up to minimum 10-15 mm depth, did not depend on the sample thickness. The profiles at 20-30 mm depth differ due to the low signal intensity and uncertainty of the NMR measurement.

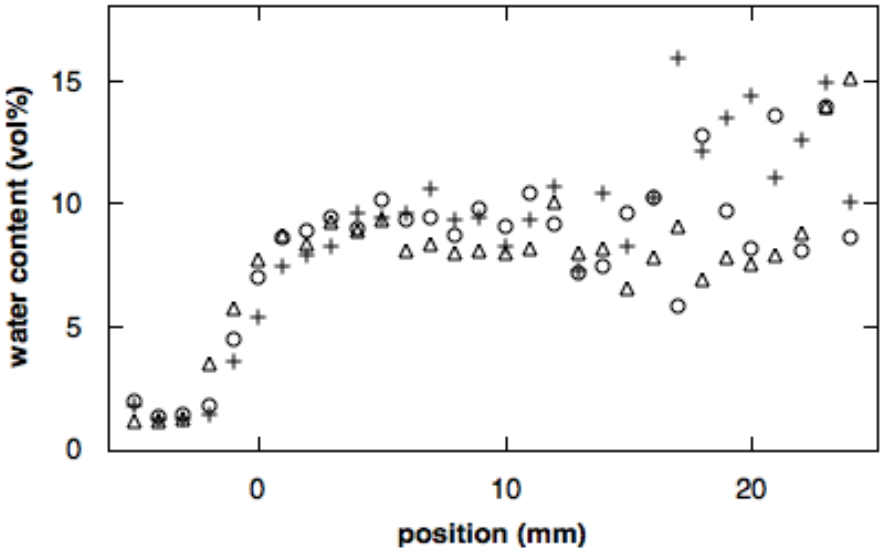


Figure 5.7 NMR profiles of 4 (cross), 7 (circle) and 10 cm (triangle) CEM I samples.

The NMR profiles on *Figure 5.8* show a decrease in water content beyond 1 day of capillary absorption. The scatter in the middle of the NMR profile between 15-30 mm is due to the uncertainty of the measurement at larger depth (see *Section 3.7.3*). The decrease is from about 12 vol% to 8-9 vol% at 1 week, then it remains constant. This is because the NMR only measures water filled porosity.

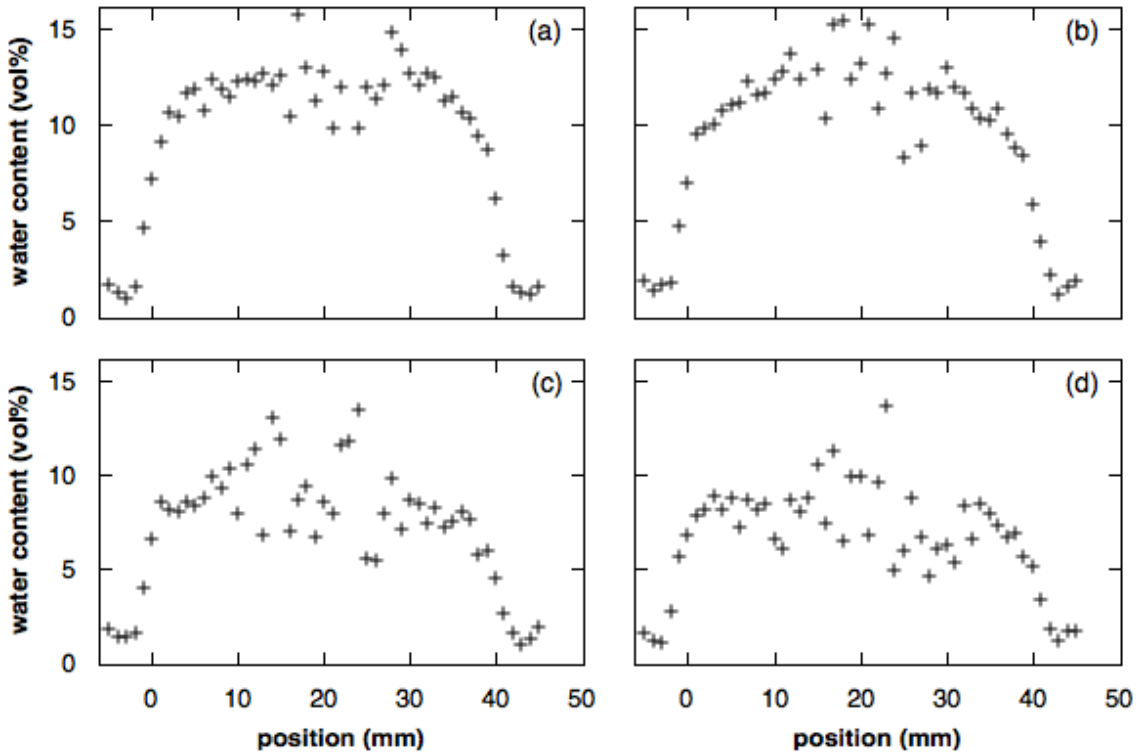


Figure 5.8 NMR profiles of 4 cm thick CEM I sample at (a) 1 day, (b) 2 days, (c) 7 days and (d) 14 days of capillary absorption, water uptake from left side

An initial explanation of this observation suggests that water first enters capillary pores then desorbs once more despite a constant water source. However, this seems unlikely and it will be shown that this is an incorrect interpretation.

Another possible explanation for the sorptivity anomaly could be delayed hydration. However, the samples tested were all minimum of 4 months old at testing with high degree of hydration. XRD showed no change in unhydrated cement content after 4 weeks of capillary absorption compared to a reference sample from the same batch. The unhydrated phase was 4% in both cases. Another possible reason is C-S-H swelling, where the capillary space is filled by swollen C-S-H and therefore the total large pore volume should be reduced. Long-term (beyond 1-4 days) capillary absorption results by NMR are discussed in *Chapter 6.*

### 5.2.4 CEM I + silica fume

The capillary absorption experiment was repeated the same way for all the other mixtures. The CEM I + 10% silica fume mix had slower water uptake, probably because of the finer porosity. For 4 cm thick samples, 1 day water uptake was about 55-60 g for CEM I + Si compared to 85-90 g for CEM I.

The water uptake for the three sample sizes was almost the same up to a day (*Figure 5.9*). This indicates a different behaviour compared to CEM I samples. The 4 cm thick samples took up only slightly less water than the thicker 7 and 10 cm samples. There is no clear difference based on sample size: all three show the sorptivity anomaly, contradictory to CEM I results. The error for the same size measured on 3 samples was about 2-3%. Error bars are not shown on Figure 5.9 as they were smaller than the data symbols and not clearly visible.

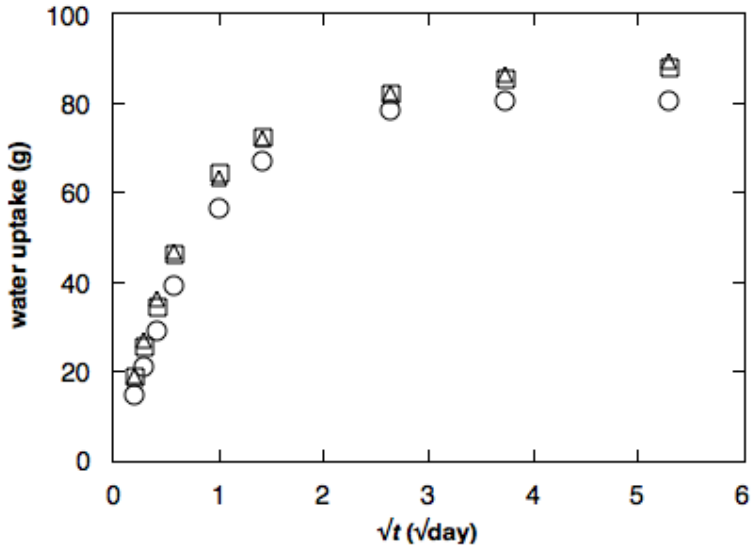


Figure 5.9 Average water uptake by time of CEM I + Si samples, 4 cm (circles), 7 cm (squares) and 10 cm (triangles) thick

The NMR profile shows the decrease in water content with time (*Figure 5.10*). The significant scatter at the middle of the sample between 20-30 mm is due to uncertainty of the measurement at larger depth. The signal to noise ratio is lower at 14 and 28 days as there was less detectable water and therefore less signal. The dry sample was measured only from the side that was to be put in contact with water only as above. It was assumed that the sample dried uniformly.

After 1 day, the water did not reach the opposite side, the waterfront moved more slowly, as after 2 days there is more water close to the “dry” side. Same decrease occurred in the 7 and 10 cm thick samples though water did not reach the opposite end of the sample. However, the amount of water decreased on the “wet” end despite constant water source. The water content measured by NMR decreases up to 4 weeks, from about 11 vol% to 7 vol%. The water uptake slowed down for another reason compared to the CEM I samples. However, the conventional test does not show a difference between the two underlying mechanisms.

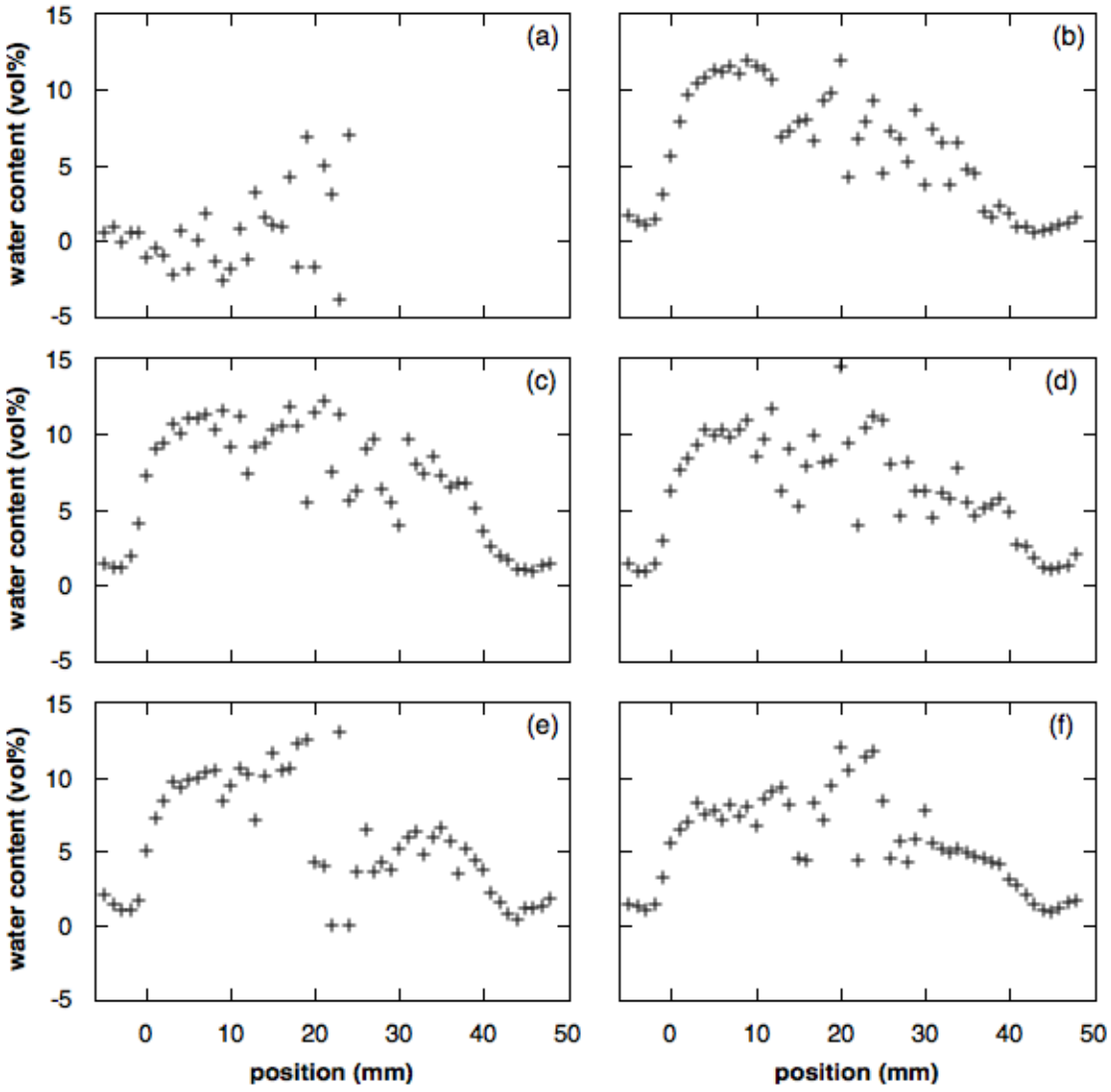


Figure 5.10 NMR profiles of 4 cm thick CEM I + Si sample at (a) dry, measured from left side only (b) 1 day, (c) 2 days, (d) 7 days, (e) 14 days and (f) 28 days of capillary absorption, water uptake from left side

### 5.2.5 CEM III/B

CEM III/B is Portland cement with 70% slag. The water uptake was the lowest with this mixture (*Figure 5.11*). The same three sample sizes were tested. The water uptake was linear up to 1 day, similar to the other mixes. Sample thickness not affected the water uptake, similar to the CEM I + Si samples and different compared to the CEM I samples.

The difference in water uptake measured on 3 samples of the same size was larger than the CEM and CEM I + Si mix. The error was the largest for the thickest, 10 cm sample, about 5-10%. Only one sample was tested longer than 1 week, therefore no error could be calculated at 2 and 4 weeks. The thinner

samples had smaller errors in the water uptake, about 2-3% similar to the other mixes. The large difference in water uptake of the same batch, same sample size suggested a different mechanism during the water uptake or at least a different pore structure and/or pore size distribution. It has been observed that cement containing slag has finer porosity with more small pores and less large capillary pores [120].

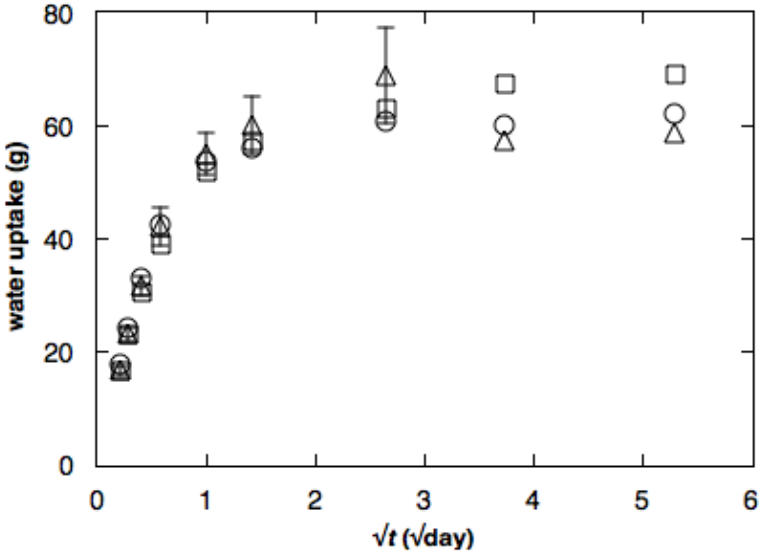


Figure 5.11 Average water uptake by time of CEM III/B samples, 4 cm (circles), 7 cm (squares) and 10 cm (triangles) thick

NMR profiles of a 4 cm thick sample showed decreasing water content after 1 day (*Figure 5.12).* The dry sample was measured from one side only. The large scatter between 15-25 mm is due to the low signal-to-noise at larger depth of the Surface GARField measurement and the decrease in overall capillary water hence signal and signal to noise ratio.

After 1 day, the waterfront was in the middle of the sample. At 2 days, the waterfront slightly moved forward, however, the uncertainty of the measurement is greatest in the middle. At 1 week of capillary absorption, the waterfront was still in the middle of the sample. However, the amount of water near the wet surface started to decrease. The water in the sample further decreased till 4 weeks of capillary absorption, from the original 10 vol% to 6 vol%. The mass of the sample remained constant after 2 days. Pore blocking can cause the waterfront to stop in the middle of the sample. Another possibility is that the sample reached a liquid/vapour dynamic transport equilibrium as the opposite

side was not covered and water could evaporate. From the NMR profiles and mass uptake the actual reason cannot be determined.

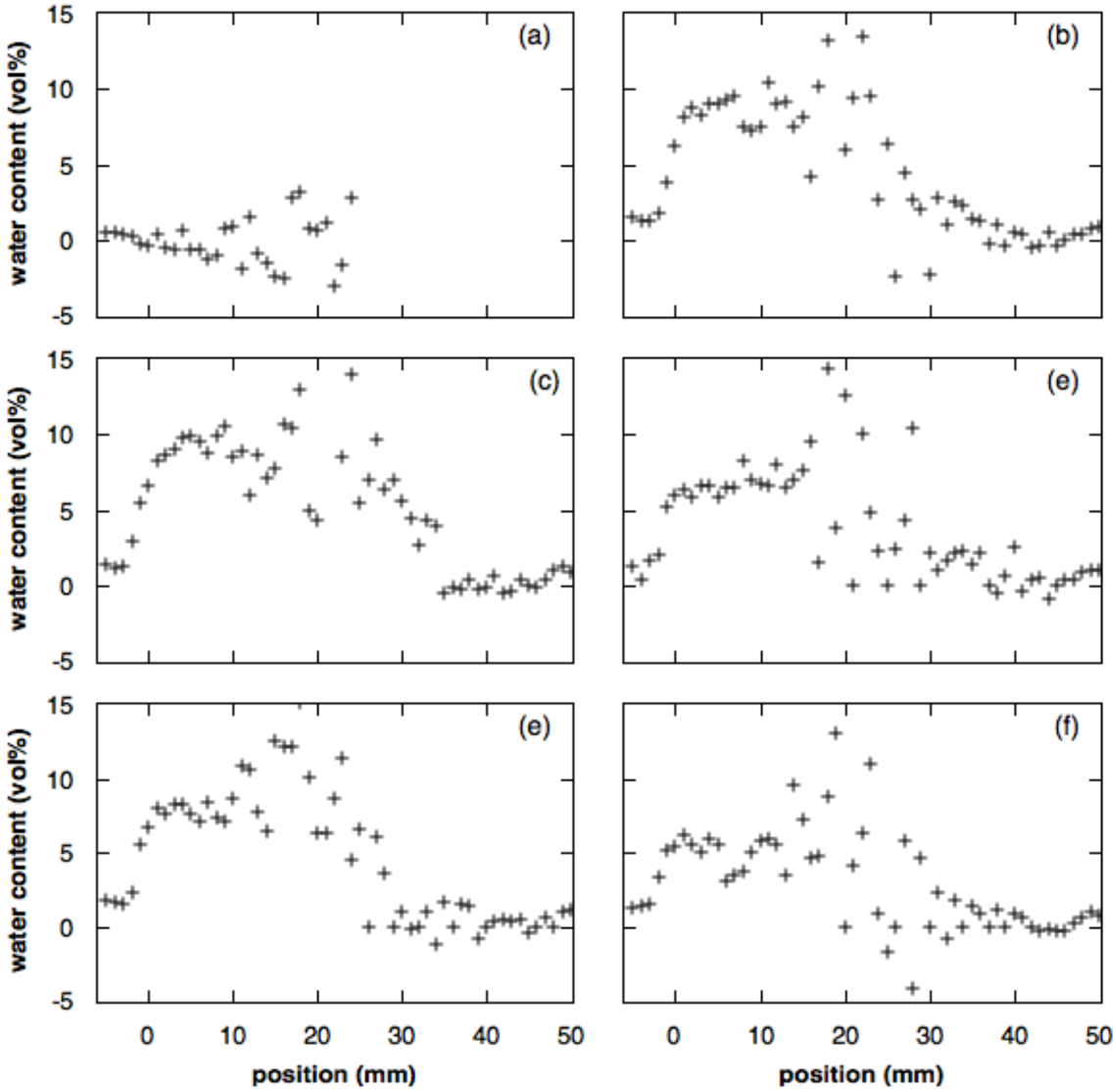


Figure 5.12 Water profile for 4 cm thick CEM III/B sample at (a) dry, measured from left side only (b) 1 day, (c) 2 days, (d) 7 days, (e) 14 days (f) 28 days of capillary absorption, water uptake from left side

The mass uptake measurement shows no change in water content for all three sizes after 2 days. However, it is not due to the saturation of the sample, as the waterfront stopped in the middle of the sample. The decrease in the amount of water close to the wet surface can be due to swelling. Further investigations of long-term sorptivity are in *Chapter 6*.

### 5.2.6 Comparison of results from different cements

The water uptake for 4 cm thick samples for the three tested cements is shown on Figure 5.13 and the NMR profiles are on Figure 5.14.

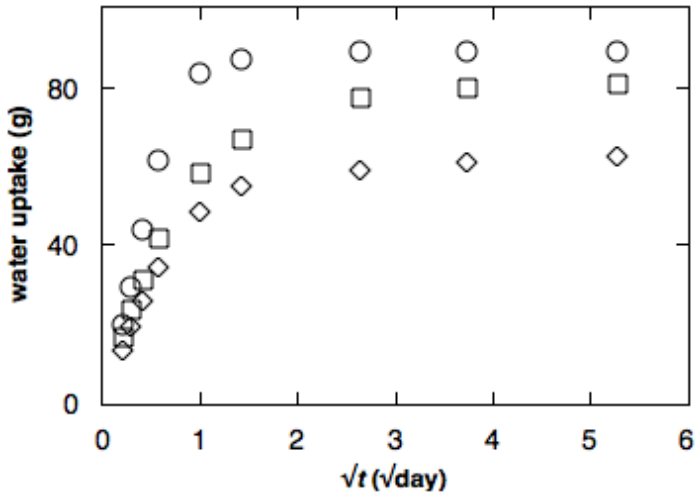


Figure 5.13 Water uptake of 4 cm thick CEM I (circle), CEM I + Si (cross) and CEM III/B (triangle) sample

The profiles on Figure 5.14. are 3 rolling point averages of the measured profile points and lines are presented for a cleaner figure that is easier to understand.

It can be seen on Figure 5.13 that the water uptake measured by gravimetry slowed down for all three mixes after about 2 days. However, the NMR profiles revealed a different behaviour for the three mixes. In the CEM I sample (Figure 5.14*a*), the water front reached the top of the sample after 1 day then the overall water content decreased across the sample. In the CEM I + SI sample (Figure 5.14*b*), the water front did not reach the top after 1 day, and slowly moved forward at 2 days, then decreased both at the side close to the water source and on the opposite as well. For the CEM III/B sample (Figure 5.14*c*), the waterfront stopped in the middle after 1 day, then the water content decreased.

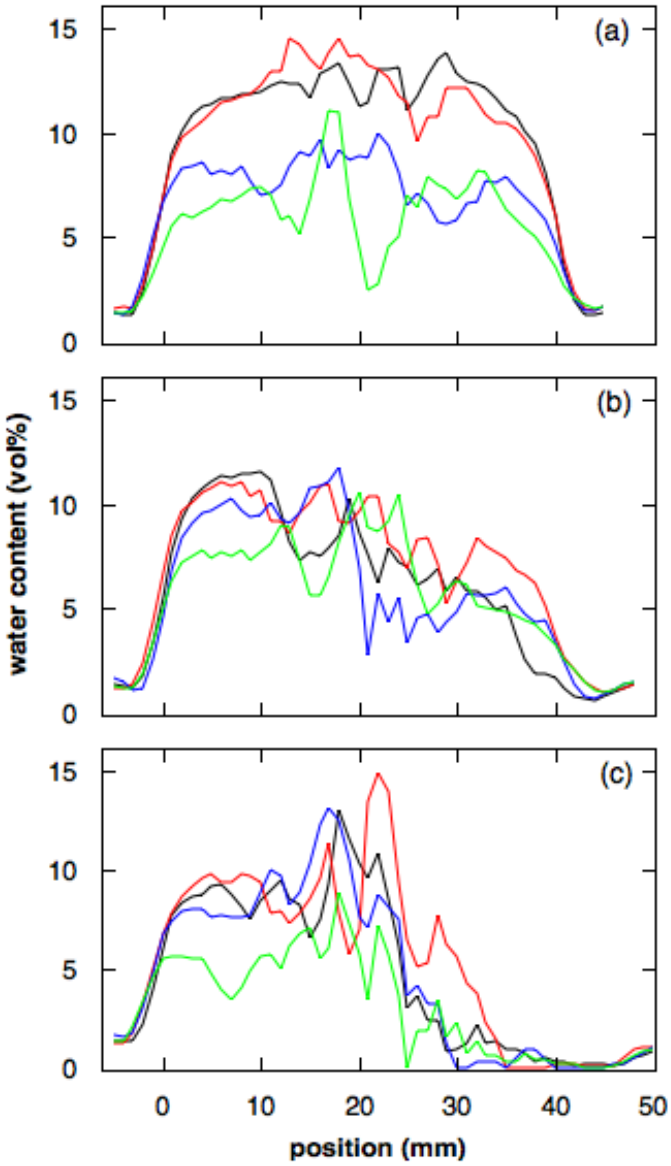


Figure 5.14 NMR profiles for CEM I (a), CEM I + Si (b) and CEM III/B (c) after 1 (black), 2 (red), 14 (blue) and 28 days (green) of capillary absorption

The conventional sorptivity measurement showed the same behaviour for all three samples, though the reason behind the water uptake slowing down after 1 day was different for the CEM I and the CEM III/B sample: one due to being saturated, the other due to the waterfront stopping in the middle.

## 5.3 Permeability

### 5.3.1 Test setup

According to the EN 12390-8 standard, the samples are cured in water then placed under pressure for 72 hours. The equipment is housed in a laboratory environment, in air. Therefore, the surface of the sample dries during the experiment. As the Surface GARField profile is a one dimensional depth profile, it is the sum of all water of a certain area at a given depth. If the water evaporates on the surface, the extra water that penetrated in the middle cannot be determined.

The usual setup was changed to overcome the problem of drying on the surface. Two 150 mm cubes were sealed in plastic during the experiment with a hole cut where the water pressure was applied (*Figure 5.15*). The third cube that was simultaneously tested was left on air with the surface drying.

Figure 5.15 Permeability experiment setup and hole to apply water pressure on sealed 15 cm cube samples. There is a sealing ring where water is applied at the bottom of the sample

One sample sealed in plastic and the reference sample left on air during the permeability measurement was split. The water penetration depth was measured in both cases by visual observation. This procedure was repeated twice with concrete from the same batch. The plastic sealing kept the samples wet, with no visible drying on the surface. However, there was some condensation on the inner side of the plastic. For initial testing, both sealed sample were measured by NMR: the one that was split after the permeability measurement and the other that was kept intact. When the samples were split, they had to be taken out from the plastic sealing. There was surface drying on the outside of the cubes as well as the split surface where the visual waterfront

was observed and marked. The expected change in water content saturation was small as underwater (standard) cured samples were used. Therefore the intact sample was more suitable for the NMR measurement as it was less affected by surface drying and easier to detect small changes in water content.

### 5.3.2 Concrete testing

The initial testing was carried out on CEM I samples with 0.5 and 0.6 w/c ratios, for the same paste volume. The maximum penetration depth was about 15 mm both stored in plastic and in air during the experiment (*Figure 5.16*). The water line could not be determined easily for the sealed specimen. The mix design was changed to a higher w/c, 0.6 for larger porosity. The penetration depth was 40 mm. The NMR profiles measured before and after the test showed no change in water content with the old coil.

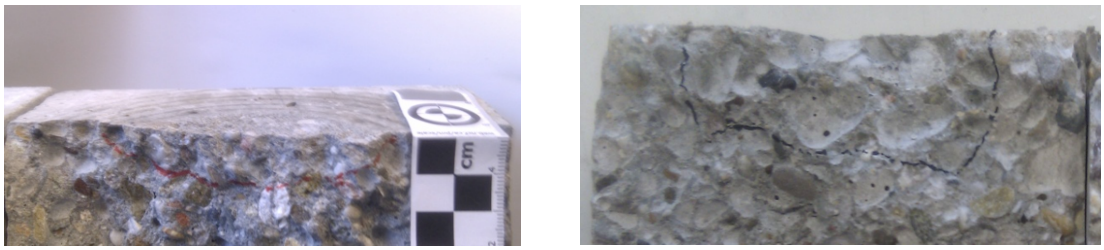

Figure 5.16 0.5 (left) and 0.6 w/c (right) water penetration after permeability. A centimetre scale is shown on the left. The right figure has the same scale as the figure on the left. The waterline was drawn after splitting. Maximum water penetration was about 2 cm for the 0.5 and about 4 cm for the 0.6 w/c

As discussed previously in *Section 4.3.1*, the optimised mix was 0.55 w/c ratio. The penetration depth was about 18-20 mm, still within the limit of 25 mm of the NMR magnet with the maximum amount of large porosity. Results obtained with the improved NMR coil had better signal to noise ratio. NMR profiles were acquired again before and after the penetration test and were very similar (*Figure 5.17*). The larger amount of water close to the surface layer is an artefact of the normalisation process (see *Section 3.7.1*). Spot measurement of relaxation time at 3 mm depth was also included in the experiment and was recorded before and after the permeability test. The echo train did not change, almost all the echo intensities were the same before and after (*Figure 5.18*).

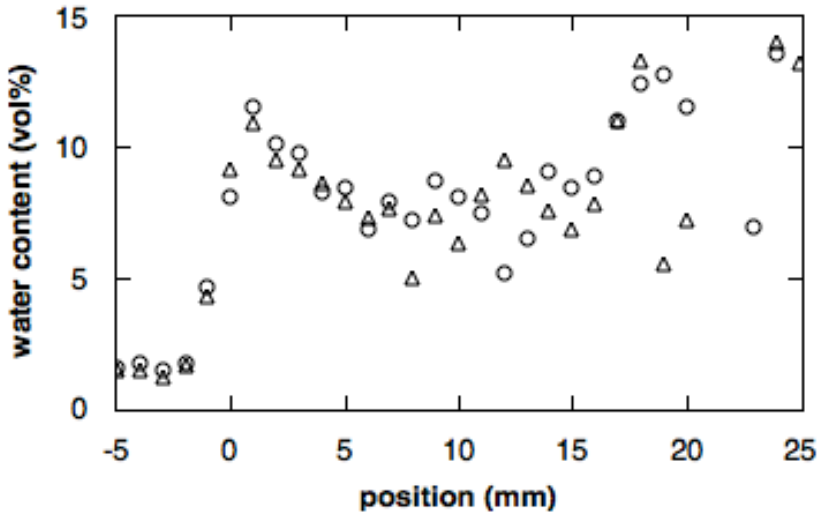


Figure 5.17 Water profiles before (circle) and after permeability test (triangle) on samples with 0.55 w/c

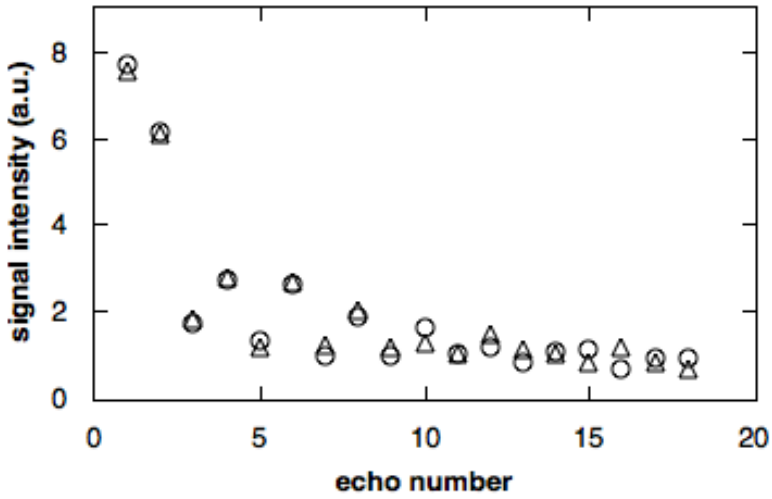


Figure 5.18 CPMG echo train of relaxation time spot measurement at 3 mm depth before (circle) and after (triangle) of permeability test

After several attempts with the old coil and various w/c ratios and the optimised w/c on the new coil, the conclusion was that any water saturation change that occurred across the visible colour change line was too small to detect by the Surface GARField NMR.

### 5.3.3 Effect of sample size, curing and testing duration

To further investigate the permeability measurement, the standard testing procedure was modified. The pressure is applied in a smaller area, than the sample itself, on a 70 mm in diameter circle. When the sample is split, the darker area where the water penetrated is wider than where the pressure is

applied and lateral water penetration occurs as well. Therefore, the effect of sample diameter on the water penetration depth was investigated.

Cylinders of 75, 100, 120, 150 and 190 mm diameter were prepared to have uniform distance between the sample surface and the penetrated area. The smallest, 75 mm samples leaked during the penetration depth and were eliminated from the data analysis.

The standard specifies underwater curing and therefore the saturation of the samples are high even before the permeability testing. The waterline is usually not easily determined. Sealed cured samples were also prepared to investigate the effect of initial water content on the penetration depth. In the original paper describing the water penetration under pressure as a measure of permeability [121] the author used samples that were underwater cured then left in laboratory air to dry for 7 days for clearer waterlines.

Therefore, samples with 3 curing methods were used: underwater cured (according to EN 12390-8), sealed cured (comparison) and underwater cured with air-drying of 7 days (according to[121]). For the standard underwater curing, all the above mentioned sizes were tested, with 100, 150 and 190 mm sealed cured and 150 mm underwater with air-drying. 3 samples were tested for each size and curing. An additional three samples were prepared for the 100 mm underwater cured samples and three for the 150 mm underwater cured ones for repeat.

Results are presented as the average with the standard error of the mean for different sample sizes on *Figure 5.19*.

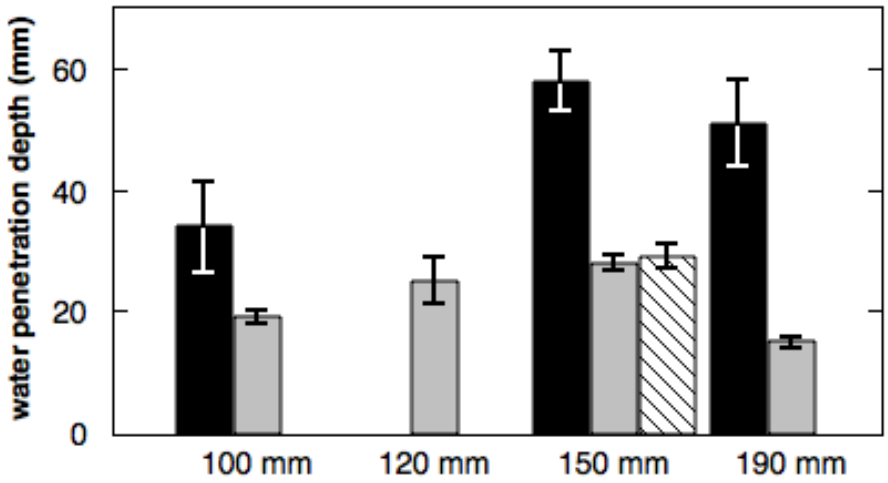


Figure 5.19 Permeability testing on different sample sizes and curing. Sealed (black), underwater cured (grey) and underwater cured with air drying (hashed shading)

Sample size affects the penetration depth. There is an increase in the case of underwater cured samples for larger samples. The water penetration depth increased from 19±1 mm for the 100 mm to 28±1 mm for the 150 mm diameter sample, However, the 190 mm sample had significantly lower water penetration, 15±1 mm. Air-drying of underwater cured samples had no effect on the water penetration depth compared to the standard underwater curing. However, sealed curing and therefore reduced saturation compared to standard testing increased the water penetration depth significantly due to the greater available unfilled porosity.

The water penetration depth was proportional to the duration the pressure was applied for in [121]. 15 cm concrete cubes were prepared for testing. 6 samples were used for each testing time. Pressure was applied for 24, 48, 72, 96 and 192 hours. Then the cube was split and the maximum penetration depth measured.

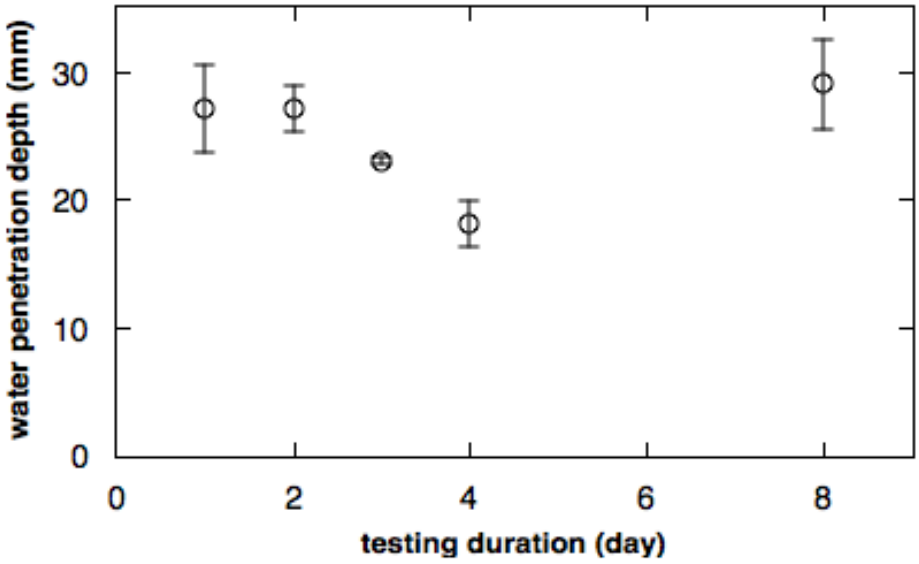


Figure 5.20 Permeability testing up to 8 days on 15 cm cubes

*Figure 5.20* shows that there is no obvious correlation between the water penetration depth and the duration for which the pressure was applied. The minimum was at 4 days of testing but this may represent an anomaly. The results from Murata [121] with a trend of increasing penetration depth by longer applied pressure could not be reproduced.

### 5.3.4 Testing on mortar

Further testing was carried out on the Large GARField using mortar samples. The samples were 18 mm in diameter and 15 cm length drilled from 150 mm cubes. The Large GARField can measure gel water and capillary water. The echo time was 64 µs, about half compared to the Surface GARField and therefore more echoes could be used in the CPMG experiment and more accurate fitting for relaxation time analysis was possible. Two underwater cured CEMI mortar samples were tested. Hydrostatic pressure was applied in a vessel for 72 hours (*Figure 5.21*). The pressure was kept at 5±0.5 bars constantly. The sample mass was measured before and after the pressure test to determine water uptake. Also, photographs (*Figure 5.21*) were taken before and after the test with a reference dry sample so that the colour change could be compared.

However, the surfaces of the samples dried very quickly and both measurements were difficult. The NMR results could be affected by the surface drying, though it represented only a very small volume compared to the overall sample.


Figure 5.21 Permeability vessel (left) and samples before experiment with reference dry sample on the left (right)

Sample mass was measured before and after the permeability testing. Samples were dried at 60°C after the permeability measurement till constant mass to be able to determine the water content before testing. The two samples had 6.6 and 6.5 g of water initially (this is equal to 17 vol% of water filled

porosity). After 3 days under pressure, the water content increased 0.26 and 0.22 g respectively, about 3.5% increase compared to initial water content.

CPMG was acquired with 2 mm steps. A total of 15 positions were measured both before and after the pressure test. The average of the middle 10 measurements were used for data analysis for better signal to noise ratio. Several fitting parameter sets were investigated, including 2 fixed relaxation times with a baseline and 2 components where the relaxation time was in the range of 150-450 µs for gel and 1000-3000 µs for capillary with a baseline. As an example, *Figure 5.22* shows two different analyses of one of the mortar samples measured before and after the permeability test. The fitting parameters for fixed relaxation times were 250 µs for gel, 1500 µs for capillary and baseline between 0-5 for water in larger air voids. For the variable parameters, the relaxation times were 236 and 2092 µs before and 215 and 2740 µs after the permeability measurement. Baseline for both before and after was set to a maximum of 2.

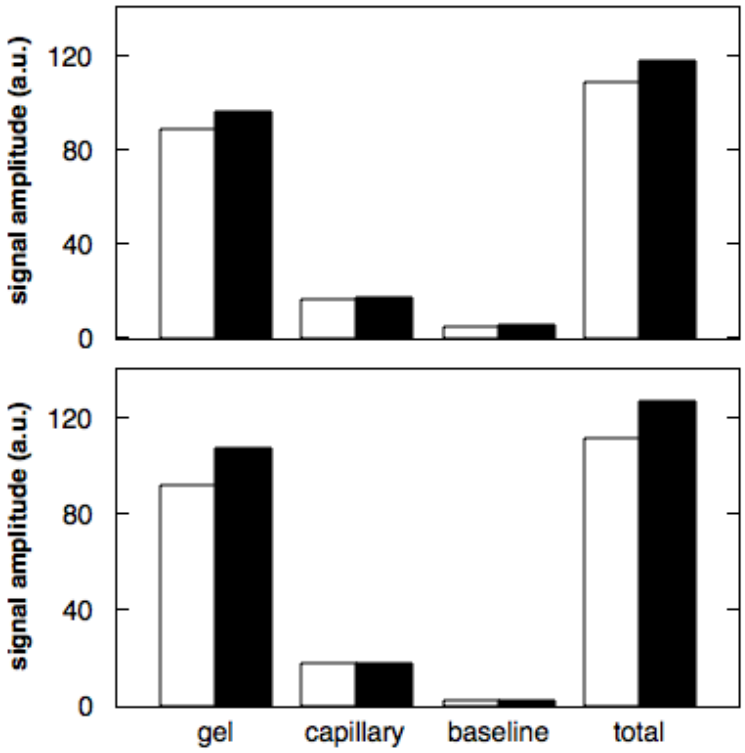


Figure 5.22 Water content of a CEM I mortar sample before (white) and after (black) the permeability test. Data is average of 10 positions. Top was analysed with fixed relaxation times of 250 and 1500 µs plus baseline, bottom with varied relaxation time 150-450 µs and 1000-3000 µs plus baseline

Figure 5.22 shows a small increase for gel and capillary water after permeability testing with both fittings. The baseline increases where the relaxation times were fixed. The baseline reached the maximum for the variable relaxation time analysis. The increase in the large porosity, the capillary and the baseline representing air voids was expected as capillary force only cannot fill the largest voids and hence they are only filled under pressure. The increase in gel porosity was unexpected. The gel porosity was never emptied as samples were never dried and hence the gel was assumed full even before pressure was applied.

Overall, the NMR signal increased after pressure was applied. The increase was between 2% and 8% depending on the fitting parameters. In all cases, mostly the long component increased. However, the error of the measurement was about 2-4%, therefore the difference in NMR signal was only slightly larger then the error. The results indicated a slight increase in water content. Kowalczyk et al [122] showed that the largest pores (relaxation time longer than 10 ms) in underwater cured 0.46 w/c cement pastes are empty after 50 days of curing and capillary force only is not able to fill those due to Kelvin-Laplace effects (see *Section 7.5*). Although cement capillary pore structure of pastes is different from mortars, it is probable that the very large pores are empty and were only filled by applying pressure.

## 5.4 Concluding remarks

Capillary absorption was carried out on concretes with different microstructures. The results were reproducible for both the conventional absorption test and the NMR profiling. Measurements after 1 day of capillary absorption showed reduced water uptake for all mixes. The conventional test method only shows the change in water uptake, but the reason behind was different for 40 mm thick CEM I and CEM III/B samples. The former was saturated after 1 day, the waterfront reached the other side of the sample. In case of the latter, the waterfront stopped in the middle and NMR profiles showed decrease in water. Thus the conventional sorptivity test only tells half of

the story and thy cannot differentiate between the different reasons of slower water uptake that can be observed using NMR methods.

Sealed cured and underwater cured CEM I samples showed that curing did not effect the water uptake by mass. The NMR profiles of the two were very similar as well. 0.8 w/c ratio CEM I samples showed about 20% higher water uptake than the 0.5 w/c CEM I concretes. NMR profiles also showed about 20% higher water content for the 0.8 compared to the 0.5 w/c ratio. Therefore the additional porosity created by increased w/c ratio was indeed capillary porosity that was measured by the Surface GARField.

The sample thickness affected the water uptake by mass only for the CEM I samples. The CEM I + SI showed a slightly increased water uptake by mass for thicker samples and CEM III/B mixes showed no change. The CEM I 40 mm thick sample was saturated after 1 day, therefore further water uptake was not expected. The NMR profiles of the CEM I + Si samples showed similar behaviour to the CEM I samples, though the water ingress was slower. The gravimetry showed that the 40 mm thick sample had slightly less water uptake, about 5-10% less than the thicker samples. It is probable, that overall behaviour of the CEM I + Si samples were similar to that of the CEM III/B and that the waterfront stopped after 1 day of capillary absorption. In case of the CEM III/B, the water uptake by gravimetry was the same for all sample sizes and the NMR profiles showed that the waterfront stopped in the middle of the 40 mm thick sample after 1 day of capillary absorption.

Sorptivity was measured on all mixes up to 4 weeks. NMR profiles show reduced water content after 1-4 days despite constant/increasing mass. The results suggest desorption in spite of continuous water source. Further investigations of this phenomena are found in *Chapter 6*. As many mortar and concrete water transport tests are based on visual observation, the colour change in relation to moisture content was further investigated and results are presented in *Chapter 7.*

Water penetration under pressure test was compared to NMR profiles on concrete samples. The NMR data showed no change in water content. Therefore, the change in saturation of the sample was lower than the sensitivity of the NMR measurement. The limitation of the permeability test procedure was

that the pressure was applied on a smaller surface than the side of the sample. Smaller samples leaked during the experiment. The Surface GARField measured a 15x15 cm area and the darker area was about 10-12 cm in diameter, about 40% of the surface area of the sample. The change in water content was small and made it more difficult to measure as only part of the measured volume was affected.

Further measurements on mortar samples with the Laboratory GARField showed a small increase in water content after the permeability measurement compared to the reference sample, though the change was just above the error of the measurement. Comparison of colour was not possible as the surface dried too quickly. The water content of both measured samples increased by about 3.5% after the pressure was applied based on gravimetry.

There was no clear relationship between the testing duration (how long the pressure was applied) and the visible water penetration depth. Therefore the test is not appropriate to work as a simpler test to measure permeability.

# 6 Long-term sorptivity

## 6.1 Introduction

Usually, sorptivity measurements are carried out up to 1 or 2 days, as after that the results deviate from the linear relationship between water uptake and square root of time. In this case, sorptivity measurements were carried out for up to 4 weeks, hence the “long-term” is used. A sorptivity anomaly was noted for all mixes when tested beyond 4-7 days, the water uptake slowed down significantly Despite constant mass being achieved (as confirmed by gravimetry), NMR profiling suggested a decrease in capillary water content was occurring (*Figure 6.1*). Further investigations were carried out to investigate the phenomena on concrete and mortar samples using the Laboratory GARField.

## 6.2 CEM I

*Figure 6.1* shows the water uptake measured by gravimetry and NMR of a 4 cm thick CEM I sample measured for a period of four weeks. Details of the experiment methodology employed are presented in *Section 3.7.1*. Water uptake by NMR was calculated from the echo sum profile summed over the full cross section of the sample.

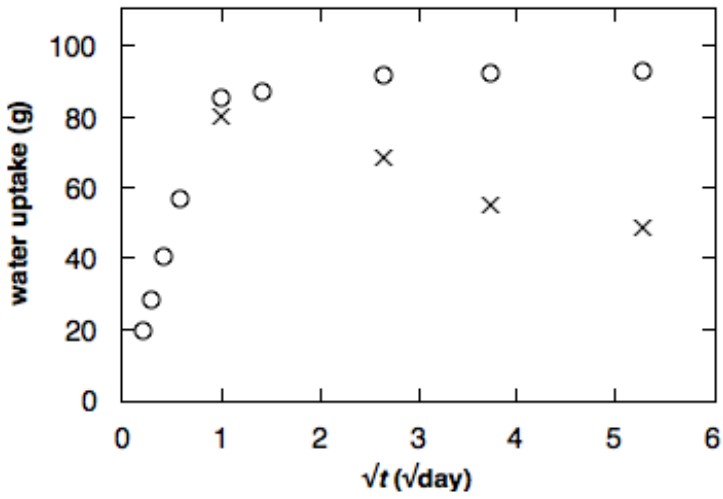


Figure 6.1 Water uptake measured by gravimetry (circles) and NMR (crosses) of a sealed cured 4 cm thick CEM I sample. Water uptake by NMR was the sum of the NMR profile and first measured after 1 day

*Figure 6.1* clearly shows that the sample exhibits a mass increase over the first day, which is a linear function of the square root of time. Thereafter, the mass is almost constant with only about 5-7% increase of water content from 1 to 28 days. The NMR cannot reliably measure the water content on a timescale of less than 24 hours as the NMR profiling measurement takes about 6.5 hours. After the first measurement at 24 hour of capillary sorption, the integrated intensity of the profile, representing the capillary adsorbed water, as seen in *Figure 6.1,* decreases with time to about 50% of the 1 day value at circa 28 days of adsorption despite the mass of the sample remaining constant. This is an apparent anomaly.

However, the calibration employed is affected by changes in relaxation time as the profile uses echo sum. The correction factor compensates for the difference in relaxation time of the saturated sandstone reference and the concrete. As the relaxation time of concrete decreases, the difference of relaxation time between sandstone and concrete increases. In order to account for this, the correction factor has to be increased. Therefore, all echo sum profiles acquired beyond 1 day of capillary sorption used a separate correction factor based on the measured relaxation time from the spot measurement for water content values. For long-term sorptivity experiments, at each measurement time, both a spot measurement for relaxation time and an NMR profile was acquired. This correction has been included in *Figure 6.1*. Indeed, all the profiles that showed datasets measured beyond 1 day of capillary absorption in *Section 5.2* were corrected with individual correction factors calculated from the spot measurements. If the original correction factor described in *Section 3.7.1* was used, the trend was the still the same. However, the results are not that accurate as the calibration was based on a relaxation time measured after 1 day of capillary absorption.

*Figure 6.2* shows spot measurement of the $T_2$ relaxation decay acquired at 3 mm depth at 1, 7, 14 and 28 days of capillary absorption of the same CEM I sample as shown on *Figure 6.1*. Both the amplitude and the signal lifetime decreased after 1 day with only small changes beyond 2 weeks. Echoes 3-20 were fit to a single $T_2$ decay representing the capillary and inter-hydrate water in

the sample. The first echo was discarded due to artefact effects and the second because it contains a significant element of gel-pore water. The standard error in the mean of the fitting of one sample measured five times was about 1.2 % for the intensity and approximately 2.5 % for the $T_2$ relaxation time.

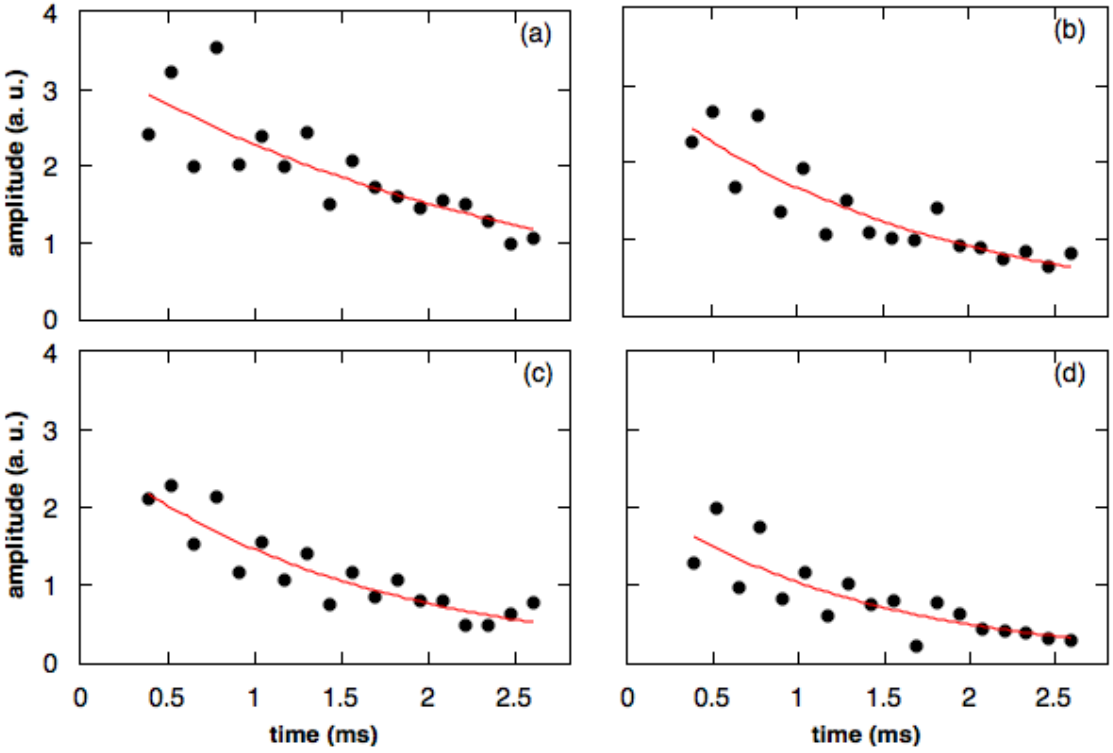


Figure 6.2 CPMG echo decay of 0.5 w/c sealed CEM I sample at (a) 1 day, (b) 7 days, (c) 14 days and (d) 28 days of capillary absorption with single exponential fit (red)

The NMR profiles up to 4 weeks of capillary absorption for the same sealed cured CEM I sample shown in *Figure 6.1* and *Figure 6.2* is presented on *Figure 6.3.* The water content decreased up to 4 weeks, though the change in water content by NMR was small beyond 2 weeks. The increased uncertainty at the middle of the profile around 15-25 mm is due to the lower signal intensity and therefore lower signal to noise ratio. The uncertainty became more significant as the total signal decreased after 28 days of capillary absorption.

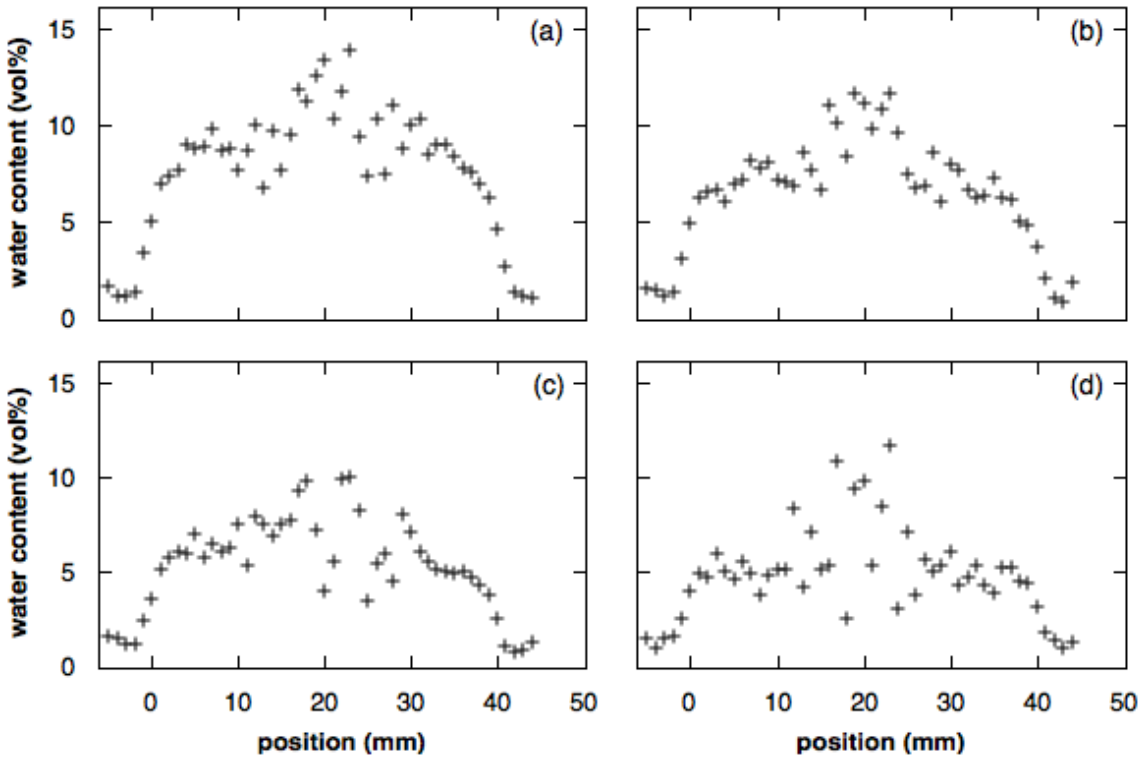


Figure 6.3 NMR profiles of sealed cured CEM I sample at (a) 1 day, (b) 7 days, (c) 14 days and (d) 28 days of capillary absorption, water uptake from left side

Underwater cured samples were also investigated so that the initial water content, as cured, could be measured. *Figure 6.4* shows the top 25 mm of the "as-cured", "dry" and after absorption profiles of an underwater cured CEM I sample. The "as-cured" profile was acquired with 2 mm steps (*Figure 6.4a*). Standard error of the mean was calculated from 5 repeats of the same measurement and is shown for 1 day of capillary absorption in *Figure 6.4c* at 4, 9 and 14 mm depth. The error bar is not clearly visible at 4mm because it was too small, about 1.5% of the water content value. The error increases significantly with depth due to the lower sensitivity of the instrument. The "dry" sample showed water beyond 10 mm depth. The analysis software was written that it will fit a Gaussian/sinc function for every slice (see *Section 3.6.3*). So when the data is inherently noisy, e.g. the sample is dry, there will be a non-zero value for each slice that has to be manually corrected. This shows some of the limitations of the Surface GARField measurement.

The water content after 1 day of capillary absorption was significantly larger than "as-cured". The water content after 1 day of capillary absorption between position 10-20 mm was twice as much compared to the "as-cured" of the same

section. Then the water content decreased towards the amount in the never dried, “as-cured” material.

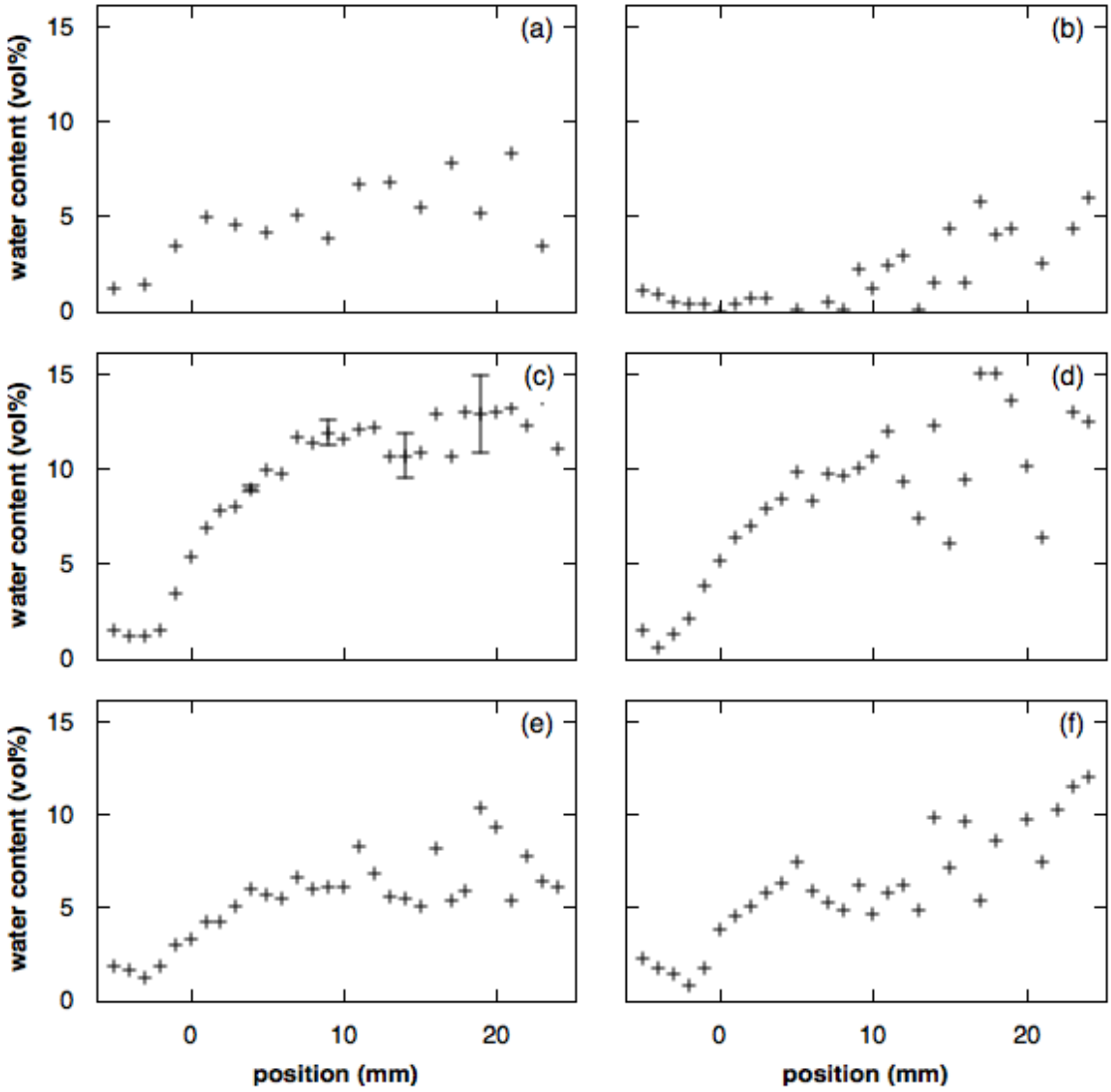


Figure 6.4 NMR profiles of underwater cured concrete before and after drying and at different times of capillary absorption. Representative error bars are shown for the 1 day data at 4, 9, 14 and 19 mm depth. (a) “as-cured”, (b) dried, (c) 1 day, (d) 2 days, (e) 7 days and (f) 14 days capillary absorption

High, 0.8 w/c ratio sealed samples were also tested to investigate the effect of gel to capillary porosity ratio on the sorptivity anomaly. Relaxation time measurements up to 4 weeks are shown on *Figure 6.5*. The dry measurement is shown on *Figure 6.5a*.

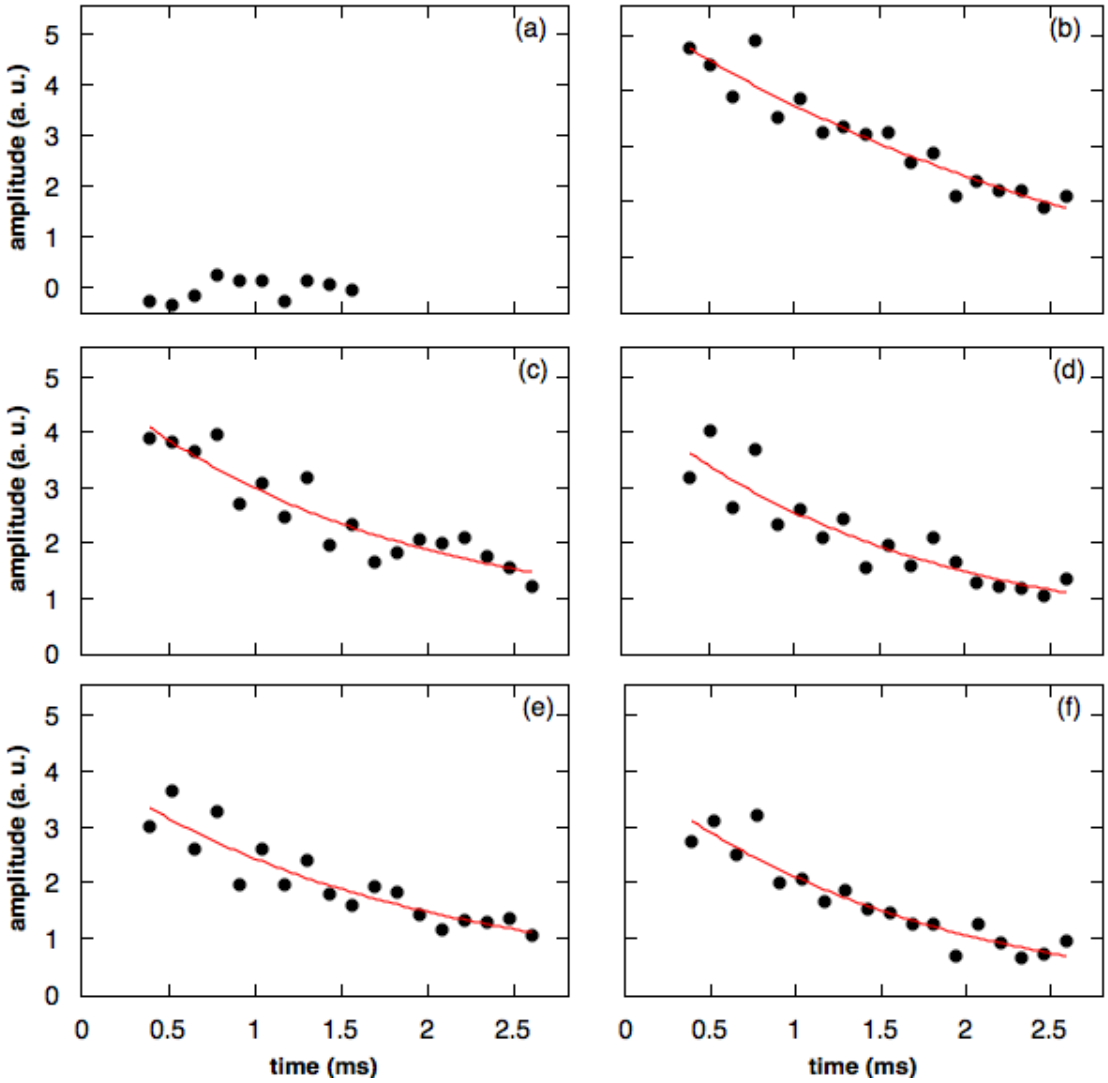


Figure 6.5 CPMG echo decay of 0.8 w/c CEM I sample at 3 mm from the wet surface at different times of capillary absorption single exponential fit (red), (a) dried, (b) 1 day, (c) 2 days, (d) 7 days, (e) 14 days and (f) 28 days

Average signal intensities and $T_2$ relaxation times with standard error of all three CEM I mixes after 1 day of capillary absorption is shown in *Table 6.1*.

Table 6.1

| **NMR data** | **Signal intensity (a.u.)** | **Relaxation time (μs)** |
|---|---|---|
| 0.5 w/c underwater cured | 3.86±0.07 | 1910±130 |
| 0.5 w/c sealed cured | 4.15±0.23 | 2240±80 |
| 0.8 w/c sealed cured | 5.20±0.22 | 2410±30 |

The change in the signal intensity and $T_2$ relaxation time is shown for all CEM I mixes on *Figure 6.6*. The relaxation time varied from sample to sample. To better capture the change of each sample, all data was first normalised to

the signal intensity and relaxation time measured after 1 day of capillary absorption. The results are the average of minimum of 3 samples for each mix and curing and standard error of the mean is also included.

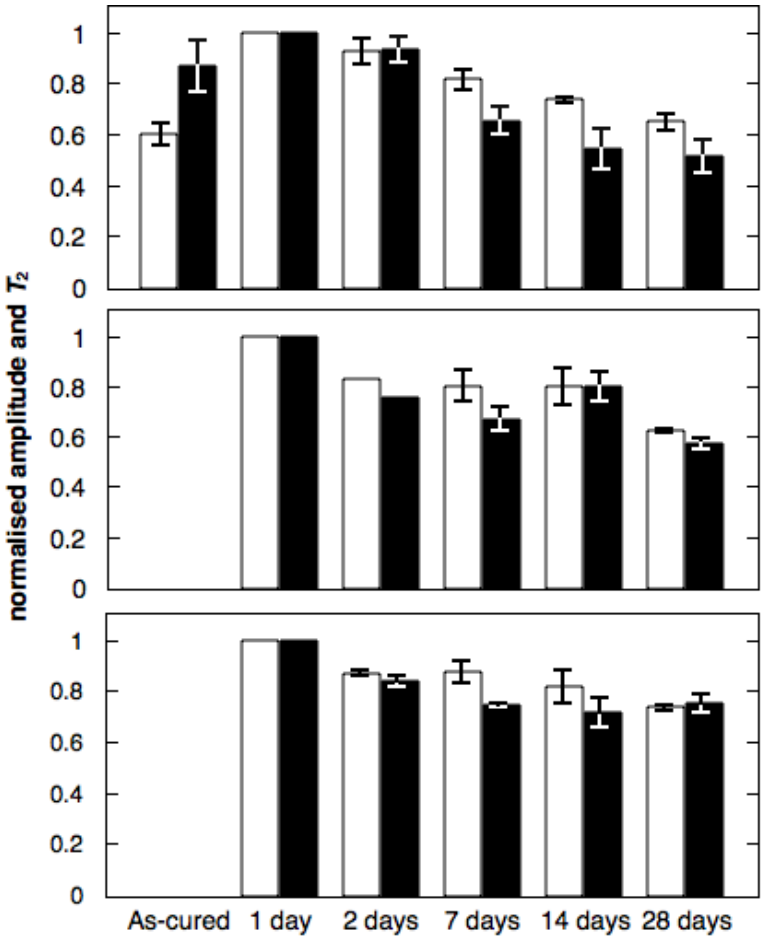


Figure 6.6 Normalised signal intensity (left bars) and $T_2$ relaxation time (right) at 3 mm depth as a function of capillary absorption time for, from top,0.5 *w*/*c* underwater cured and 0.5 and 0.8 *w*/*c* sealed cured concrete. Data are mean results within each group. Error bars show the error in the mean.

All three CEM I sample groups showed a decrease in both the signal intensity and the relaxation time. So both the amount of water and the pore size decreased. The underwater cured sample showed that in the “as-cured” material, the water content and the relaxation time was lower than that of 1 day. The water content was similar in the “as-cured” material as the dried and rewetted sample after 2 weeks of capillary absorption.

It seems that water first penetrates large capillary porosity, and then somehow desorbs despite a constant water source and constant sample mass. These results suggest that additional capillary porosity was created by the drying process that then returned to the original amount as a result of rewetting.

Also, the water filled pore size increased when rewetted for 1 day returning to close to the original, "as-cured" level after 1 week, although the absolute change observed was not that significant.

## 6.3 CEM I + Si and CEM III/B

CEM I with 10% silica fume and CEM III/B sealed cured samples were also tested up to 4 weeks of capillary absorption. Spot measurements were taken at 3 mm depth, same as for the CEM I samples. 6 samples were measured for CEM I + Si and 6 samples for CEM III/B. However, not all times were recorded for all samples, but there was a minimum of 3 samples tested for each time. Average signal and relaxation time with standard error for CEM I + Si and CEM III/B after 1 day of capillary absorption is shown in *Table 6.2*.

Table 6.2

| **NMR data** | **Signal intensity (a.u.)** | **Relaxation time (**μs) |
|---|---|---|
| CEM I + Si | 4.66±0.13 | 2250±60 |
| CEM III/B | 4.12±0.27 | 1640±80 |

The signal intensity and relaxation time data is shown on *Figure 6.7*. The data was first normalised to 1 day of capillary absorption, then the mean calculated as the relaxation times varied from sample to sample but the rate of change was similar.

Both of the blended cements tested show similar behaviour to the CEM I samples. Both the signal intensity and the $T_2$ relaxation time decreased with time. The decreasing amplitude indicating that less water is measured. The decreasing value of measured $T_2$ means the size of water filled porosity is decreasing. The rate of change varied for the three binders, but the trend was the same suggesting a similar mechanism despite the different microstructures that might be expected.

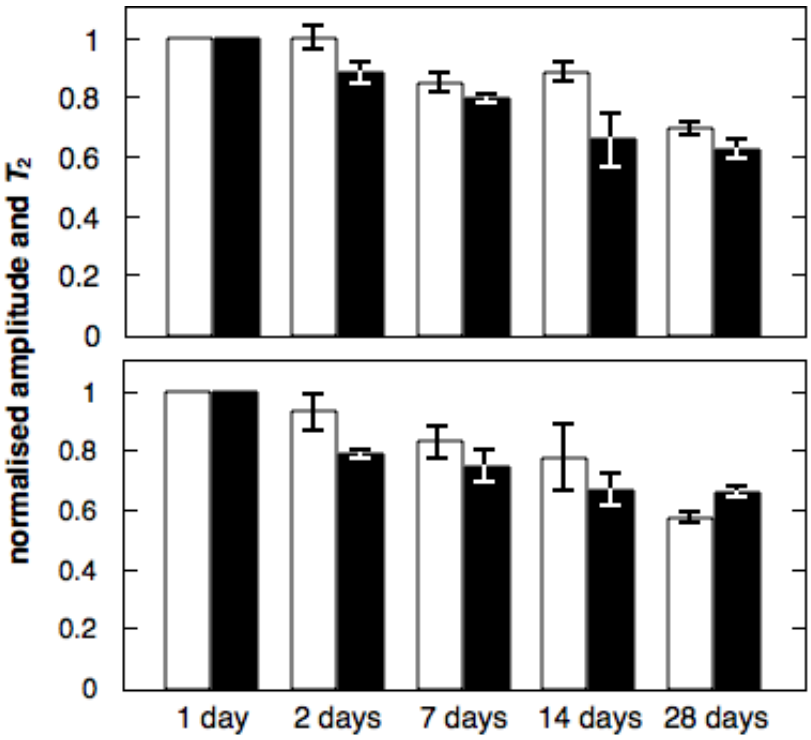


Figure 6.7 Normalised signal intensity (left bars) and $T_2$ relaxation time (right) at 3 mm depth as a function of capillary absorption time for CEM I + Si (top) and CEM III/B (bottom). Data are mean results within each group. Error bars show the error on the mean.

In order to gain further insight, and hence explain this anomaly, experiments were moved to the Laboratory GARField where it was expected that the gel pore water could also be seen. As the maximum sample diameter is limited for that equipment, mortar samples were used instead of concrete.

## 6.4 CEM I mortar

Mortar samples were tested on the Laboratory GARField at the University of Surrey. Both gel and capillary porosity can be measured with this technique because the echo time achievable is about half that compared to the Surface GARField. Hence it is possible to record signal from smaller pores with shorter relaxation times. However, the maximum sample diameter is 18 mm and maximum measured sample length with this maximum diameter is about 30-35 mm.

Water uptake of a sealed cured sample is shown on *Figure 6.8*. Water content increased linearly with the square root of time up to about 4 days, then slowed down.

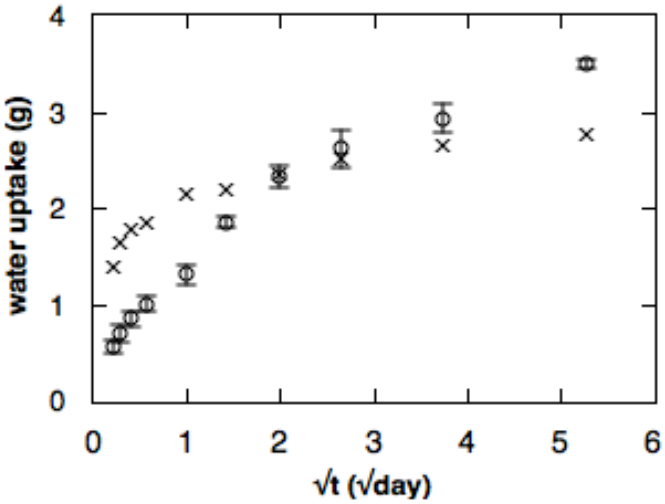


Figure 6.8 Average water uptake by gravimetry of sealed cured CEM I mortar sample (circles) with standard error of the mean and gravimetric water uptake of an underwater cured sample (crosses)

NMR profiles were acquired with 2 mm steps for dried samples and 1 mm steps for rewetted samples. The CPMG experiment was carried out at each position. For profiling, the mortar data was fitted with 2 components and a baseline: a short component between 150-500 μs and a long component 1000-3000 μs plus a baseline 0-1. The baseline maximum was 1, about 1% of the total signal, as real phased data was fitted and longer components than 3000 μs was not seen in any analysis, but higher values for baseline introduced artefacts in the capillary fitting. Fitting the last part of the echo train then subtracting the fitted part from the front half of the echo train (stripping) did not work well with the mortar sample probably due to lower signal to noise than paste samples used previously with the Laboratory GARField.

NMR profiles of a sealed cured sample up to 2 weeks of capillary absorption are shown on *Figure 6.9*. Profiles are the total amount of water measured by the Laboratory GARField: the sum of gel and capillary and the baseline after $T_2$ analysis. The total water content increased after 1 day of capillary absorption and became constant after about 4 days. The water content is in arbitrary units, a.u., (based on signal intensity) as calibrating the measurement for the true water content (in gram or vol%) is not straightforward and was only limited time

available. However, the units are the same for all Surface GARField measurements.

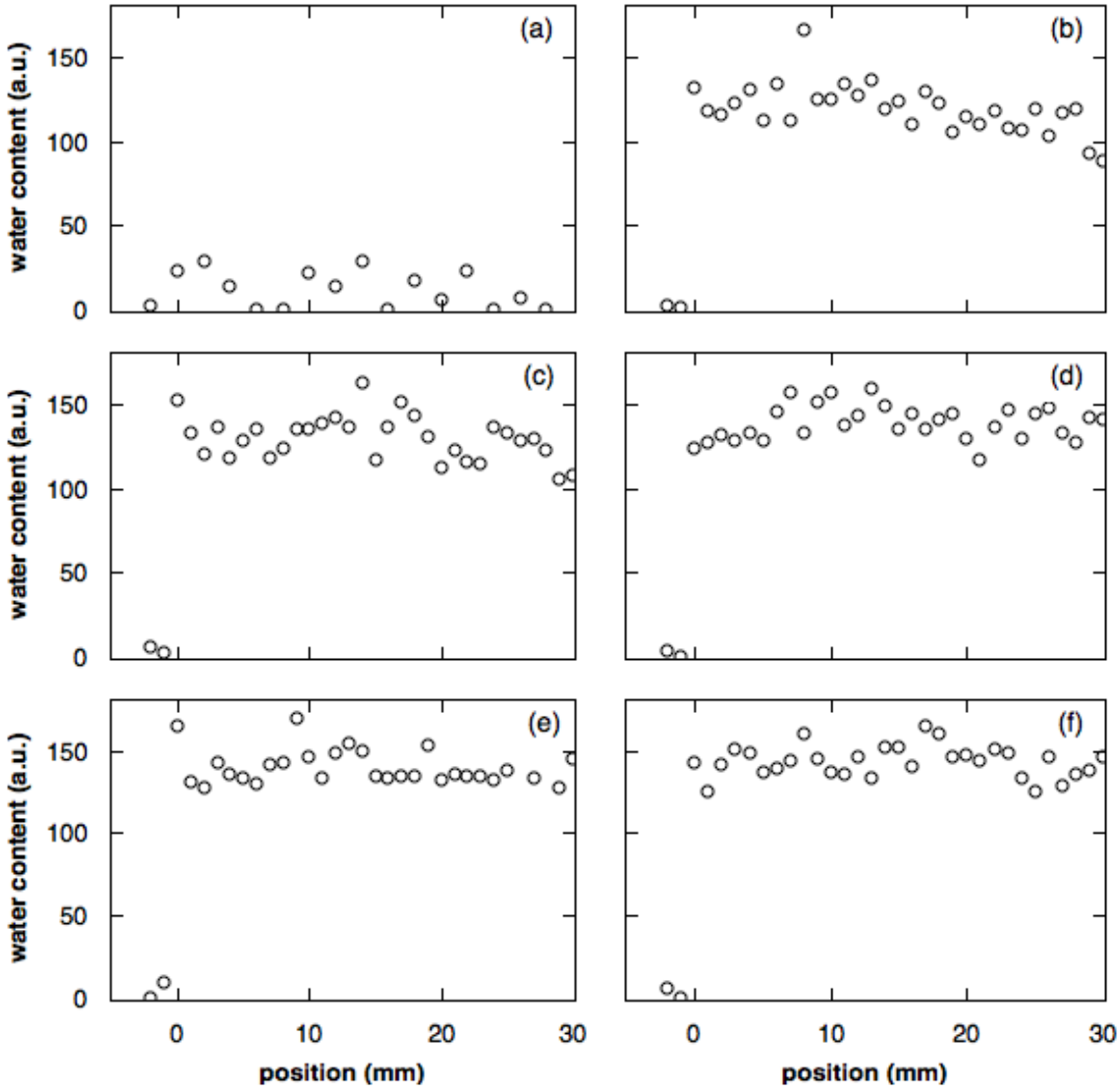


Figure 6.9 NMR total water profile (gel + capillary + baseline) of a sealed cured mortar sample (a) dry, (b) 1 day, (c) 2 days, (d) 4 days, (e) 7 days and (f) 14 days of capillary absorption. Surface in contact with water was at 0 mm

The average of 11 depth resolved slices was used for exponential fitting in order to improve the signal to noise ratio. The top 4 slices were not used to avoid surface effects. The data was fitted with 2 components at fixed relaxation times plus a baseline. The absolute signal intensities in the long and short components depend critically on the choice of $T_2$ values used in the analysis. For example, fitting with a shorter relaxation time will increase the total. Therefore the analysis was repeated for different fixed pairs of $T_2$ values including 250 µs and 1500 µs, and the original ranges used for profiles.

Although the absolute signal fractions changed, the trend of decreasing amount of large filled pore spaces and an increasing ratio of filled small pore spaces to large pore spaces during capillary absorption remained the same. The difference between the 250/1250/baseline and 250/1500/baseline and varied parameters fitting for gel water content was 5-6%, 5-10% for capillary water content and 3-5% for the total.

The chosen 2 components were 250 μs and 1250 μs plus a baseline. These values were chosen based on literature reports [101, 123] and on multiple different fitting analyses.

*Figure 6.10* shows the change in water content ratio up to 4 weeks of capillary absorption of the same sealed cured sample as on *Figure 6.9*. Data is normalised to 1 day total (gel + capillary + baseline) water content.

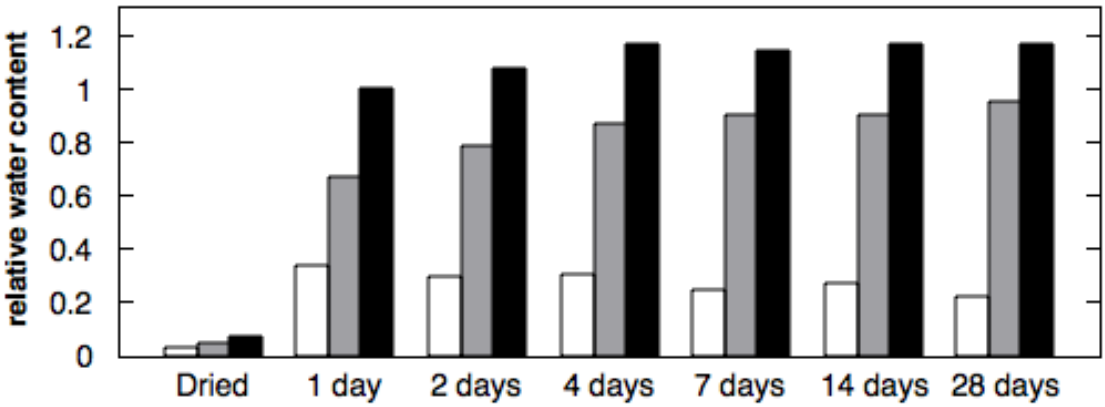


Figure 6.10 Relative water content of a sealed cured mortar sample. Data was normalized to total water after 1 day. Total water (black bars), gel water (grey) and capillary water (white) up to 4 weeks of capillary absorption

Underwater cured mortar samples were also investigated. Three samples were investigated. The water uptake by gravimetry varied significantly, between 0.72 and 2.13 g after 24 hours of capillary absorption. One possible cause is that the samples were transported wet from Germany to the University of Surrey in January and the cold conditions caused microstructural damage.

Average echo decay of 11 slices with 2 component exponential fitting plus a baseline offset is shown on *Figure 6.11*. The semi-logarithmic scale shows the increase in uncertainty at the end of the echo train. The maximum signal amplitude was constant at all measured times except for the dry sample. However, the relaxation time of the signal varied by time.

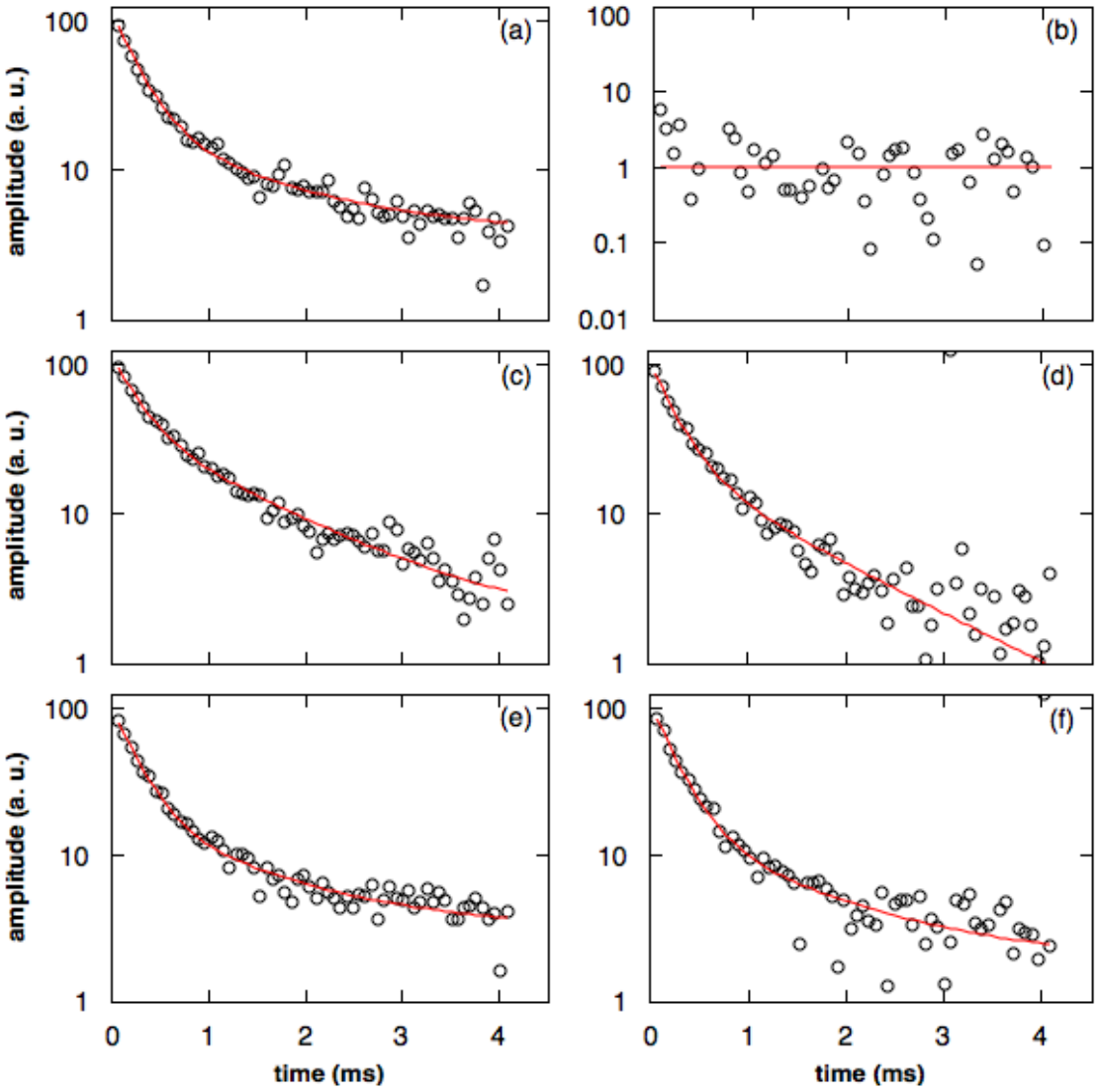


Figure 6.11 Average echo decays of an underwater cured mortar sample (a) “as-cured”, (b) dried and after (c) 1 day, (d) 2 days, (e) 7 days and (f) 14 days of water absorption. The data is fit to a two-component exponential decay function plus baseline offset

The total water content, gel to total and capillary to total water ratio is shown on *Figure 6.12*. The data was normalised to 1 day total water content. The standard error of the mean was calculated where sufficient data was available.

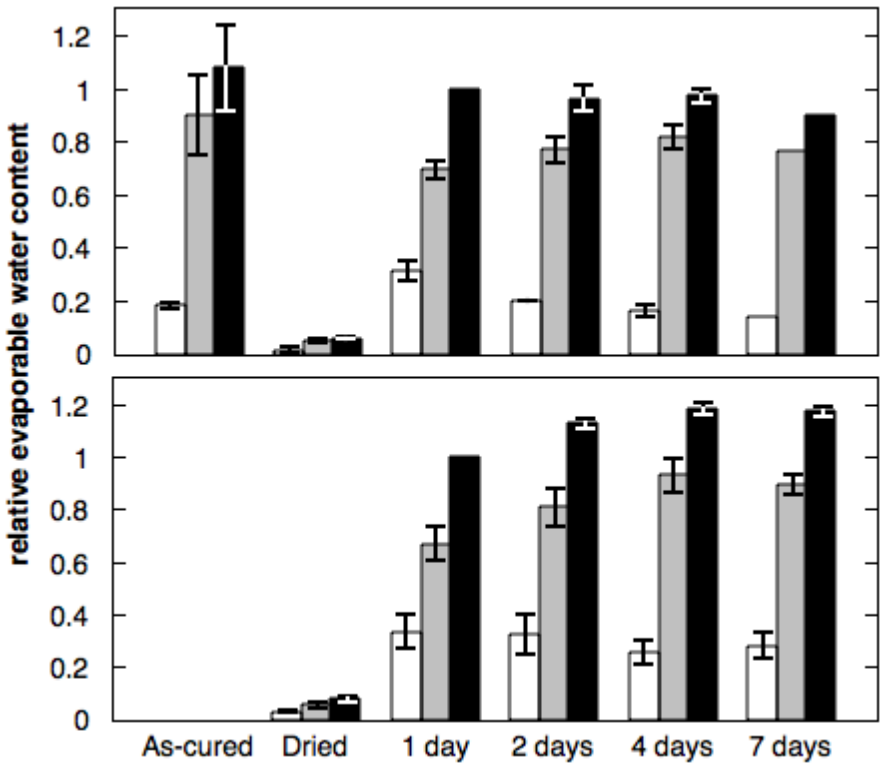


Figure 6.12. Water content normalised to the total for 1 day of capillary absorption for underwater cured (top) and sealed cured (bottom) samples, showing total (black bars), short (grey) and long (white) components by time.

## 6.5 CEM I + Si and CEM III/B mortars

Two CEM I + Si and two CEM III/B standard mortar samples were also investigated. Another CEM III/B sample was measured and discarded after 24 hours of capillary absorption due to suspiciously high water uptake by gravimetry. The water uptake after 1 day was double that of a CEM I sample. The water uptake for both binders varied significantly from sample to sample unlike the CEM I binder samples. It is possible that road transport in cold weather (January) could have affected the microstructure similar to the under water cured CEM I sample. The samples were wet cored. Therefore the initial moisture content before drying could not be usefully measured. *Figure 6.13* shows the average water uptake for CEM I + Si samples by gravimetry and a water uptake of a CEM III/B.

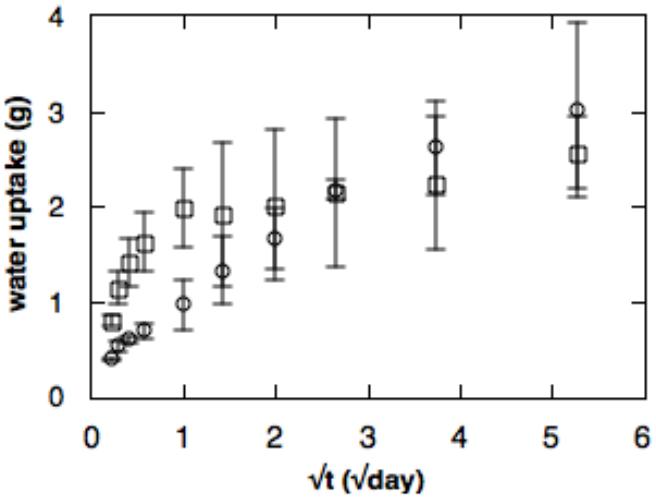


Figure 6.13. Water uptake by gravimetry for CEM I + Si (circle) and CEM III/B mortar samples. Standard error of the mean was large.

NMR profiles were acquired for all samples. An average of 11 slices were used for better signal to noise ratio. 2 fixed $T_2$ components plus a baseline were used for the analysis. However, the long component was different from the one used for CEM I mortars. The $T_2$ for capillary was different in the Surface GARField measurement. The 250 μs and 1250 μs plus baseline combination resulted in poor fitting. Therefore 1800 μs was used for the long component for CEM I + Si and 1500 μs for the CEM III/B. The fitting with longer capillary water component was significantly better than with 1250 μs for the blended cements. *Figure 6.14* shows the normalised water content by NMR for CEM I + Si and CEM III/B sealed cured mortar samples.

The total water content did not change significantly for either binder. There was a decrease in the capillary water content for both binders. Gel water slightly increase for CEM I + Si samples. CEM I + Si samples were tested up to 4 weeks. However, water content ratios (gel, capillary and total water compared to 1 day total water content) did not change significantly beyond 7 days.

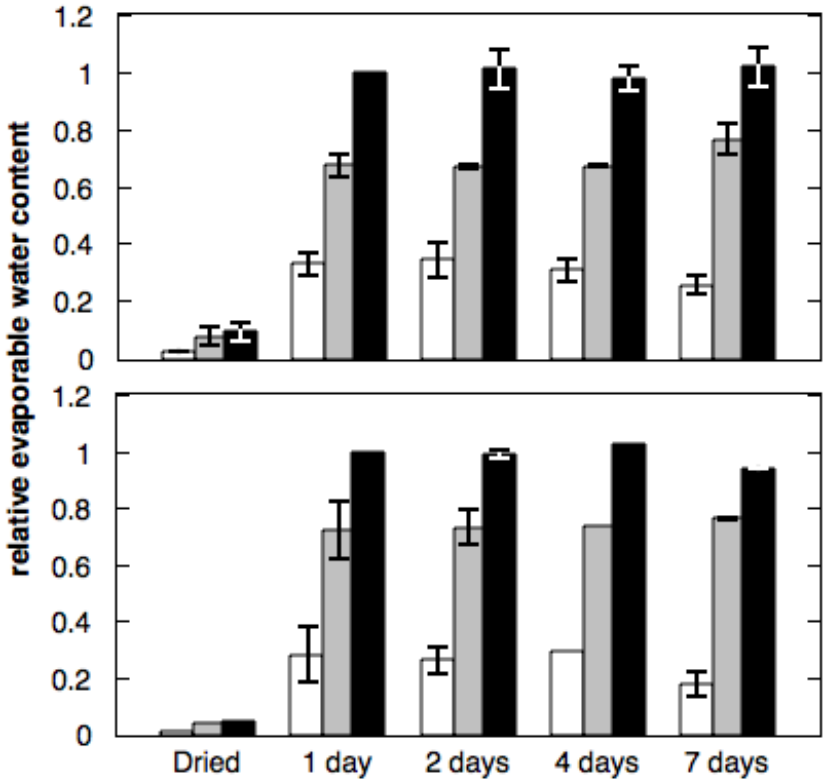


Figure 6.14. Water content normalised to the total for 1 day of capillary absorption for CEM I + Si (top) and CEM III/B (bottom) samples, showing total (black bars), short (grey) and long (white) components by time.

## 6.6 Comparison of results measured with different GARFields

To be able to compare results measured on two different GARField systems, concrete samples cored from 150 mm cubes were measured on the Laboratory GARField. The same batch was used as for the investigations on the Surface GARField. The maximum aggregate size was 8 mm for the CEM I concrete, therefore 18 mm diameter cylinders could be heavily affected by large aggregates for water uptake. Three samples were measured, two sealed cured and one underwater cured CEM I concrete. The sealed cured samples were taken from the same cube.

Water uptake varied significantly. The water uptake by gravimetry for all three samples tested is shown on *Figure 6.15*. One of the sealed cured samples had almost twice the water uptake compared to the other two concrete samples.

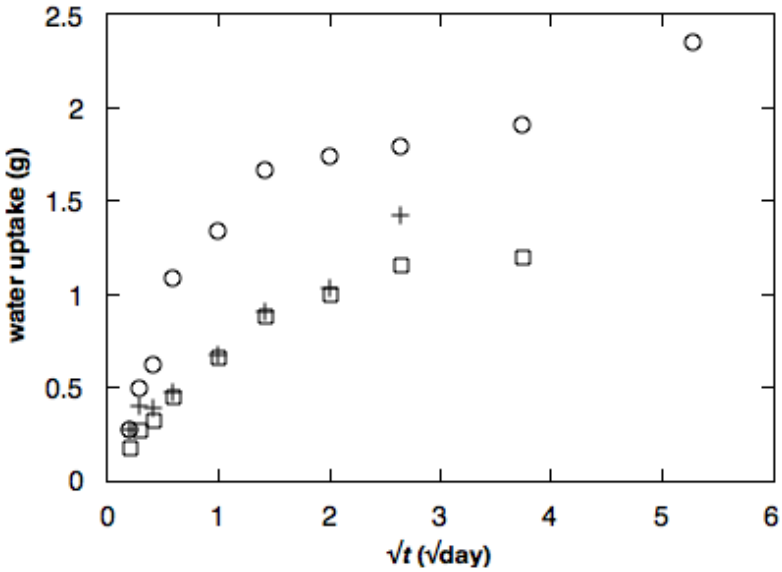


Figure 6.15. Water uptake by gravimetry of small CEM I concrete cylinders two sealed cured (circles and squares) and an underwater cured (crosses) sample was measured.

NMR profiles were acquired with 1 mm steps. An average of 11 slices were used for detailed analysis of relative water content change with the objective of partially averaging out the aggregate size effect. The echo train was fitted with 2 fixed $T_2$ components and a baseline, same parameters as the CEM I mortar samples. The relative water contents up to 7 days is shown for two sealed cured and one underwater cured CEM I concrete cylinders on *Figure 6.16*. The sealed cured sample shown below in the middle figure had the lower sorptivity by gravimetry on *Figure 6.15*.

The relative water contents of the CEM I concrete samples measured with the Laboratory GARField showed no decrease in capillary water content. The underwater cured sample showed significant decrease in total water content after 1 day of capillary absorption compared to the “as-cured” material. The gel and overall water content increased and almost returned to the “as-cured” level after 7 days. The sealed concrete sample at the bottom of *Figure 6.16* showed decrease in capillary water content. However, the water uptake by gravimetry was double that of the other two samples and in the region of the CEM I mortar samples that had a higher paste volume.

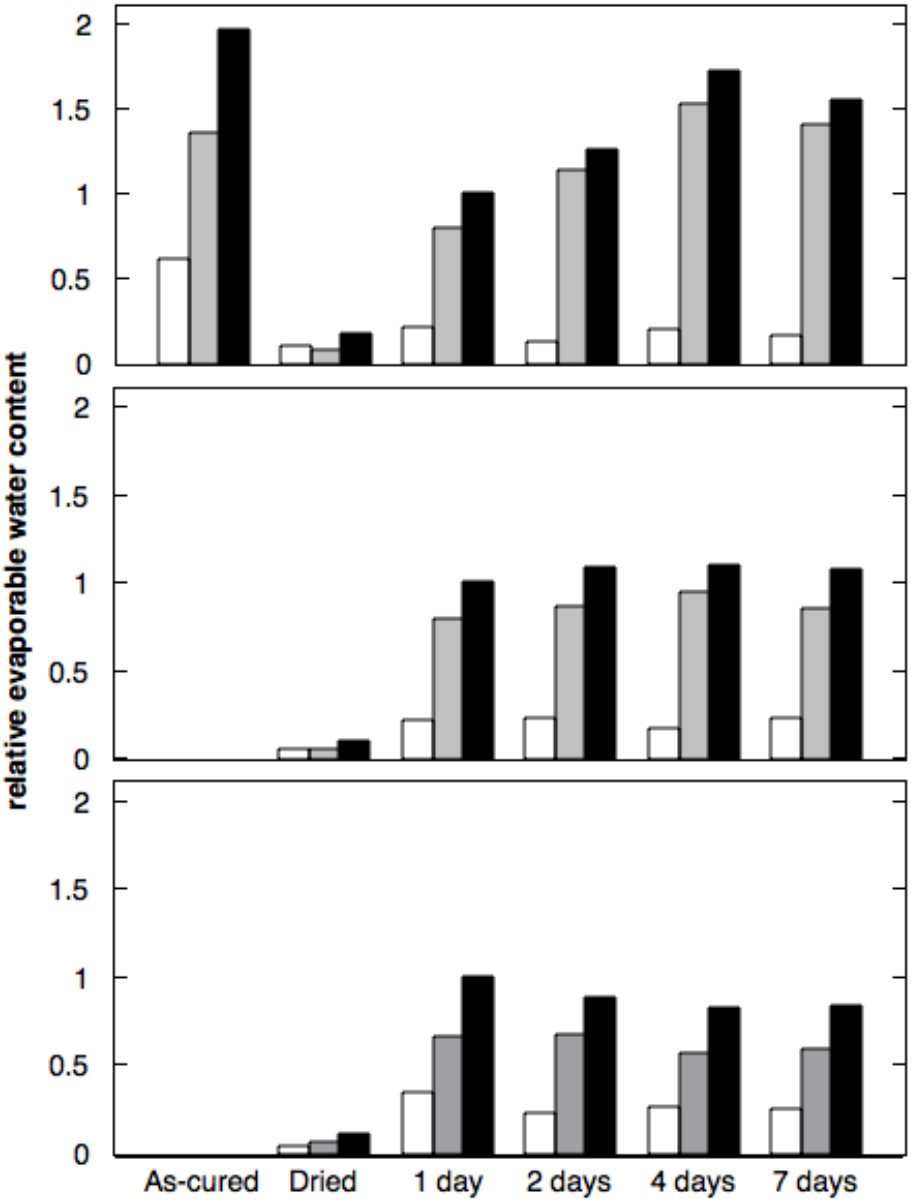


Figure 6.16. Water content normalised to the total for 1 day of capillary absorption for under water cured (top) and two sealed cured (middle and bottom) CEMI concrete samples, showing total (black bars), short (grey) and long (white) components by time.

Despite the attempts to obtain better comparison of concrete data measured on the Surface GARField and mortar measurements on the Laboratory GARField, the results were not conclusive. The reason is probably the large maximum aggregate size (8 mm) relative to the diameter (18 mm). The results from the same concrete batch measured with the Surface GARField on larger, 150x150 mm surface showed good reproducibility.

## 6.7 Possible causes for sorptivity anomaly

Three cements, two curing methods and two w/c ratios were investigated. All measured concrete samples measured with the Surface GARField and mortar samples measured with the Laboratory GARField showed a decrease in water filled capillary porosity regardless of binder or water-to-binder ratio by NMR. Underwater cured samples had lower initial capillary water than after drying and rewetting for 1 day. Measurement on mortar samples showed an increase in gel porosity by time. The possible causes are the following.

One possibility as noted in literature [61, 124] is delayed hydration at rewetting, which would reduce the capillary porosity by creating additional gel porosity. However, the timescale of capillary absorption was very different in those works. Further hydration was observed within the few hours of rewetting. NMR data in this work was first acquired after 24 hours. Also, the samples used were cured for a minimum of 3 months to reach a high degree of hydration and minimise changes in the microstructure and rewetting. The degree of hydration was measured for underwater cured CEM I concrete after 4 weeks of capillary absorption and on a reference sample after drying. XRD analysis carried out by the HeidelbergCement laboratory showed no change. The amount of unhydrated phases was the same for the dried and rewetted sample as the reference, only dried sample. The degree of hydration was 90±1% both before and after rewetting measured by quantitative analysis of all the different phases, including unhydrated clinkers. Therefore delayed hydration was discounted as the cause.

A second possibility was based on the XRD results that showed increased amount of ettringite after rewetting compared to the dried reference sample., from 1.1 w% to 3.3 w%. Ettringite decomposes at relatively low temperatures. The idea was that ettringite filled the capillary porosity during rewetting. However, the amount of other hydrate phases decreased slightly and the overall volume of hydrates did not change. Also, without macroscopic volume change data, it could not be assumed that change of the volume of solid phases necessarily lead to the same change in the pore space. The mortar sample results did not show a decrease in the overall evaporable water amount and reduced pore volume, therefore this possibility was unlikely.

A third possibility was that water first entered large pores and then the smaller pores filled with water from the large pores [62]. This could account for the more slowly increasing signal from the gel porosity in the mortars. The drying temperature was too low to empty the inter-layer pores and it is not expected that those were affected during rewetting. However, it seemed unreasonable that, the gel pores filled at the expense of water in the capillary pores in presence of a continued water source. Therefore, this was an unlikely explanation.

Based on this assessment the most reasonable explanation is that the change in both water content and pore size are due to swelling in the smaller gel porosity filling up the capillary space [63]. It was suggested by Parrott et al in 1980 [125] that capillary tension forces could cause small porosity to collapse on the first drying of alite pastes though most of the change was recoverable. In a more recent study, Maruyama et al [126] have also suggested that drying can result in a closing of gel porosity and increase of capillary.

Results showed in this work are consistent with both Parrott et al and Marayuma et al. During drying, the gel porosity partly collapses creating larger additional capillary pores. When the sample is rewet, the newly created larger spaces fill. However, with time, the network returns to nearer the original levels, so most of the change is reversible. The timescale of the swelling during capillary sorption is about 1 day.

The difference in the behaviour of the total signal intensity beyond one day of capillary sorption between underwater and sealed cured mortar samples cannot be explained solely from the results in this thesis. One possibility is that the different curing methods affect the internal stresses of the paste and how the large porosity is created during hydration [39]. The macroscopic shrinkage of the sealed cured mortar is significantly bigger than for the underwater cured mortar. It is possible that the pore network of the underwater cured sample is more refined, and so filling of the gel porosity from the capillary porosity is a slower process. Without knowing, the capillary and gel water content of samples cured both ways before drying (that could not be measured with the wet coring method used) it is not possible to fully explain the observed difference.

## 6.8 Concluding remarks

The sorptivity anomaly identified in cementitious materials has been investigated. Although it is a widely researched topic, no conclusive evidence has been found on the possible cause. Several ideas have been suggested, such as further hydration and swelling. This work provides a new insight to the phenomena and a probable answer to the anomalous behaviour.

NMR measurements show that the amount of inter-hydrate and capillary water of dried concrete and mortar samples first increased when rewetted, but then after 1 day of capillary absorption, decreased. In case of underwater cured concretes, the amount of capillary water increased substantially above the amount in the “as-cured” sample before returning close to the original level. As there is a constant supply of water, the results suggested a redistribution of porosity in favour of smaller pores not visible by the Surface GARField system. The decrease of capillary water beyond 1 day of capillary absorption was observed on all investigated mixes regardless of cement or w/c ratio.

Further measurements on mortars that included gel water as well as capillary water showed that in the case of underwater cured samples additional large porosity was created during drying. This was at the expense of gel water after 4 days of capillary absorption the small and large pore water volumes returned close to the original, never dried value. The total water content remained constant. In case in sealed cured mortar samples, the gel porosity increased and the capillary porosity slightly decreased beyond 1 day of capillary absorption. However, the total amount of water (gel and capillary) increased over time. The difference in total water content depending on curing is probably due to the different internal stresses when the microstructure was formed.

The data has been interpreted as evidence for C-S-H swelling in the dried material upon water ingress. The swelling of gel porosity and reduced amount of large porosity appears to be the most probable cause for the sorptivity anomaly observed.

The results imply that dried samples do not represent the original microstructure well, even when relatively gentle drying (at 60°C) is applied. It is

most probable, that water transport measurement on dry samples give higher values for transport then in real structures where the inner humidity of the sample is higher.

Another important result is that most of the changes are reversible and that the amount of gel and capillary porosity return the amount before drying in the case of underwater cured samples. Therefore the decrease in water uptake can be seen as not an anomaly, but as being representative of the sorptivity of a non-dried sample.

This work has been published in Cement and Concrete Research [127].

# 7 Colour change

## 7.1 Introduction

Visual observation of the colour change associated with the wetting (and drying) of cement-based materials is a commonly used method to determine the water penetration front in concrete and mortar. It is fundamental to water uptake test methods such as the sorptivity and the water penetration under pressure test[71]. However, there is no absolute evidence that the colour change observed is a good measure of the extent of water penetration or uptake.

In this chapter, the colour change front observed visually experiments are compared with the results of NMR water profiling to determine whether they are accurate measure of the actual “waterfront.”

## 7.2 Concrete samples

Capillary absorption tests were carried out on concrete samples following the procedures described in *Section 5.2*. After 1 day of sorptivity measurement and before the first NMR profile was acquired, digital (optical) photographs were taken of the sides of the concrete samples on which there was a visible colour change (darkening) region close to the wet surface. The sides of the slabs where the colour-change water front line was observed had a thin paste skin originating from casting. To ensure that this did not significantly affect the results, a slab was split in half to observe the internal waterfront. It was in good agreement with that observed at the surface.

It was found that for all three cement types investigated, the NMR profiles, acquired with the Surface GARField, showed the presence of liquid water beyond that darker area for all three binders.

*Figure 7.1* shows an NMR profile and a photograph of a sealed cured 40 mm thick CEM I sample after 1 day of capillary absorption. The profiles are echo

sums. Surface in contact with water was at 0 mm on the scale. The photographs of the cross-section of the samples are below the NMR profiles. The photographs are all greyscale and slightly enhanced for brightness and contrast. The NMR profile indicated that the whole sample was saturated. Although the profile is noisier between 15-25 mm due to uncertainty of the profiling at larger depth. The photograph showed a clear colour change boundary, though the whole sample is darker than observed on the dry sample before water ingress. The first 15 mm from the left side (that was in contact with water) was darker than the rest of the sample. The water content by NMR is slightly higher for the first 10-15 mm from the wet side, about the same depth as the darker region.

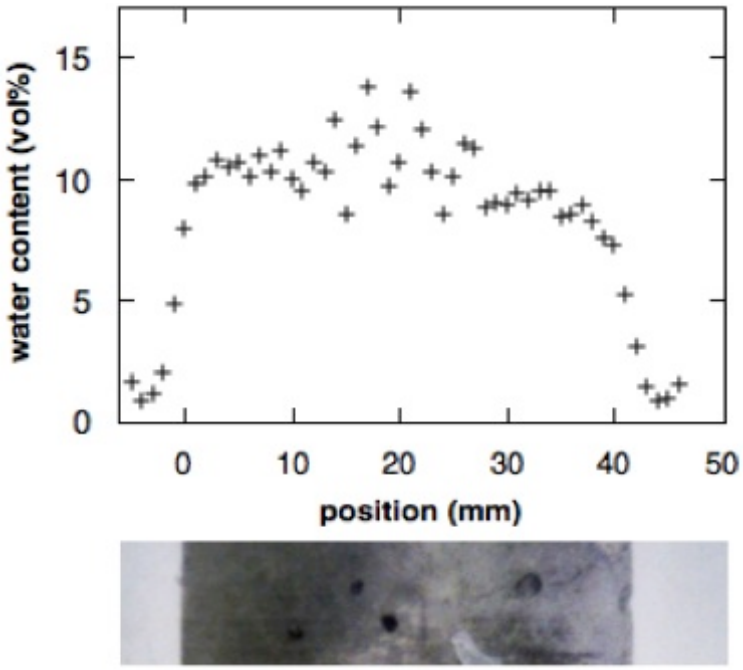


Figure 7.1. Echo sum NMR profile of a CEM I sealed cured concrete sample after 1 day of capillary absorption with photographic cross-section below.

*Figure 7.2* shows a similar experiment on CEM I + Si. There was an even clearer water line, about 10-15 mm from the wet surface. The water line was not straight. There was a 5-6 mm variation in the visual water penetration depth. However, the NMR profile showed water extending well beyond this dark region, up to about 25-30 mm from the wet surface. That is to say water penetrated about 15-20 mm further in the sample than it is indicated by visual observation of the colour change.

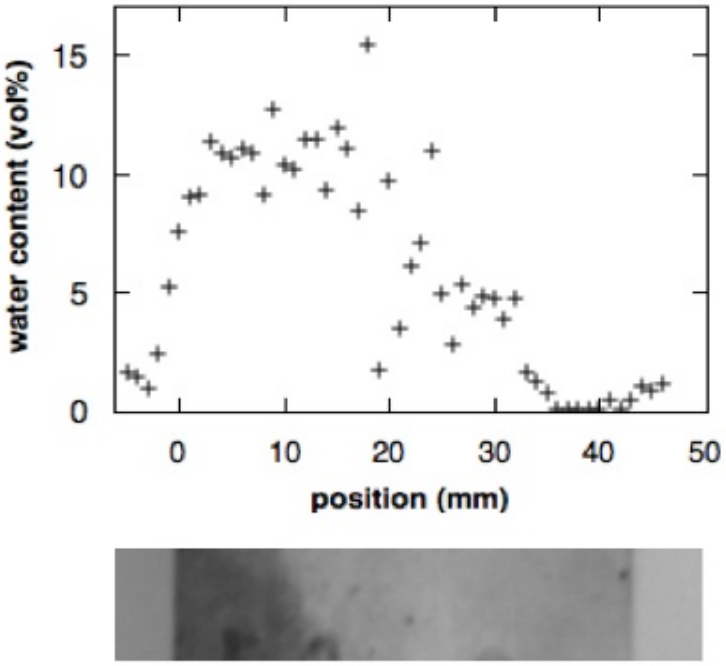


Figure 7.2. Echo sum NMR profile of a CEM I +Si concrete sample after 1 day of capillary absorption with photographic cross-section below.

*Figure 7.3* shows a CEM III/B sample. The echo sum NMR profile showed water ingress up to 30 mm. The uneven water profile between 5-20 mm is probably caused by uncertainty of the measurement due to overall low water content. The average water content of the wetted region of the other two mixes, CEM I and CEM I + Si were about 10-12 vol%. The water content for CEM III/B varied between 5 and 10 vol%. The signal to noise was lower because the noise level was the same for all mixes and samples, but in this case, the signal was lower due to the lower quantity of water. The photograph below the NMR profile shows that the visibly wet region was up to about 15-20 mm. Again, this is less than the depth of water penetration determined by NMR.

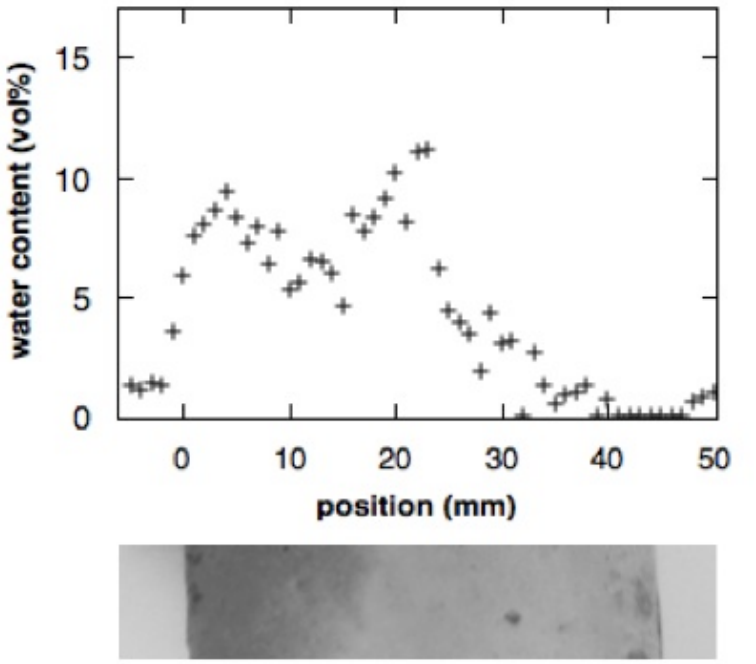


Figure 7.3. Echo sum NMR profile of a CEM III/B concrete sample after 1 day of capillary absorption with photographic cross-section below.

## 7.3 CEM I mortar

Cored mortar cylinders were investigated with the Laboratory GARField to further investigate the relationship between the “waterfront” observed visually on the surface of the sample and the actual waterfront as determined by NMR. The step size was normally 1 mm. At each step, a CPMG echo train was recorded. The $^{1}$H NMR frequency was 23.4 MHz and the $\pi/2$ pulse length was 6.5 µs. A total of 64 echoes with 64 µs echo spacing and 2048 averages were recorded at each step. Water profiles were constructed two different ways. One profile used echo sum by summing all echoes for each slice. For the other profile the data was fitted with two exponential decays and a baseline. The shorter component was allowed to vary between 150-500 µs and the longer between 1000-3000 µs. The baseline varied between 0-1 (about 0-1% of the total signal intensity). The echo sum profile is affected by the signal lifetime, and longer $T_2$ components are over-represented. Photographs of the same section of the cylinders, before and after capillary absorption, are shown immediately below the profile plots. The photographs were all greyscale and slightly

enhanced for brightness and contrast. All photographs were taken with the same white background.

*Figure 7.4* show NMR profiles of water in the first 32 mm of four sealed-cured CEMI mortar cylinders after 1 day of capillary absorption. All samples were cored from the same mortar cube. However, the top left and bottom right samples were cored and dried in August 2013. The top right and bottom left were cored and dried in January-February 2014. Bottom right sample was measured in August 2013 immediately after drying. The top left sample was left dried until January and measured parallel with the other two samples. The exposed surface was at 0 mm on the scale. Both profiles are shown, circles (left axes) were exponential fitting for total water content and crosses (right axes) for echo sums. Typically for the parameters used most of the signal occurred in the first 10-12 echoes. Hence the echo sum is about ten times the initial amplitude, though both were in arbitrary units.

*Figure 7.4a* shows water ingress beyond the measured 33 mm. The visual waterline was however at about 18 mm into the sample, with slightly darker area beyond. According to the echo sum data, there was a significant gradient in concentration across the invaded region after 1 day of capillary absorption. However, it was much less evident in the intensity derived from the total water content profiles. *Figure 7.4b* shows that NMR measurements estimate that water ingress exceeds beyond 32 mm. Indeed, the waterfront was beyond the range of the measurement. However, the photograph below showed a clear colour change (i.e. waterfront) at about 25 mm.

*Figure 7.4c* and *Figure 7.4d* show two more samples. The former has a dark area about 5 mm in the sample and a slightly darker area beyond. It is not clear why there are two visual waterfronts. Though whichever is chosen, it underestimates the water ingress determined by NMR. *Figure 7.4d* has a visual waterfront at 10 mm. For both samples, NMR showed water ingress of 20-22 mm. In *Figure 7.4d*, the profile was acquired with 1 mm steps close to the wet front, then with 2 mm steps. The sample was investigated in the orientation testing hence the different resolution.

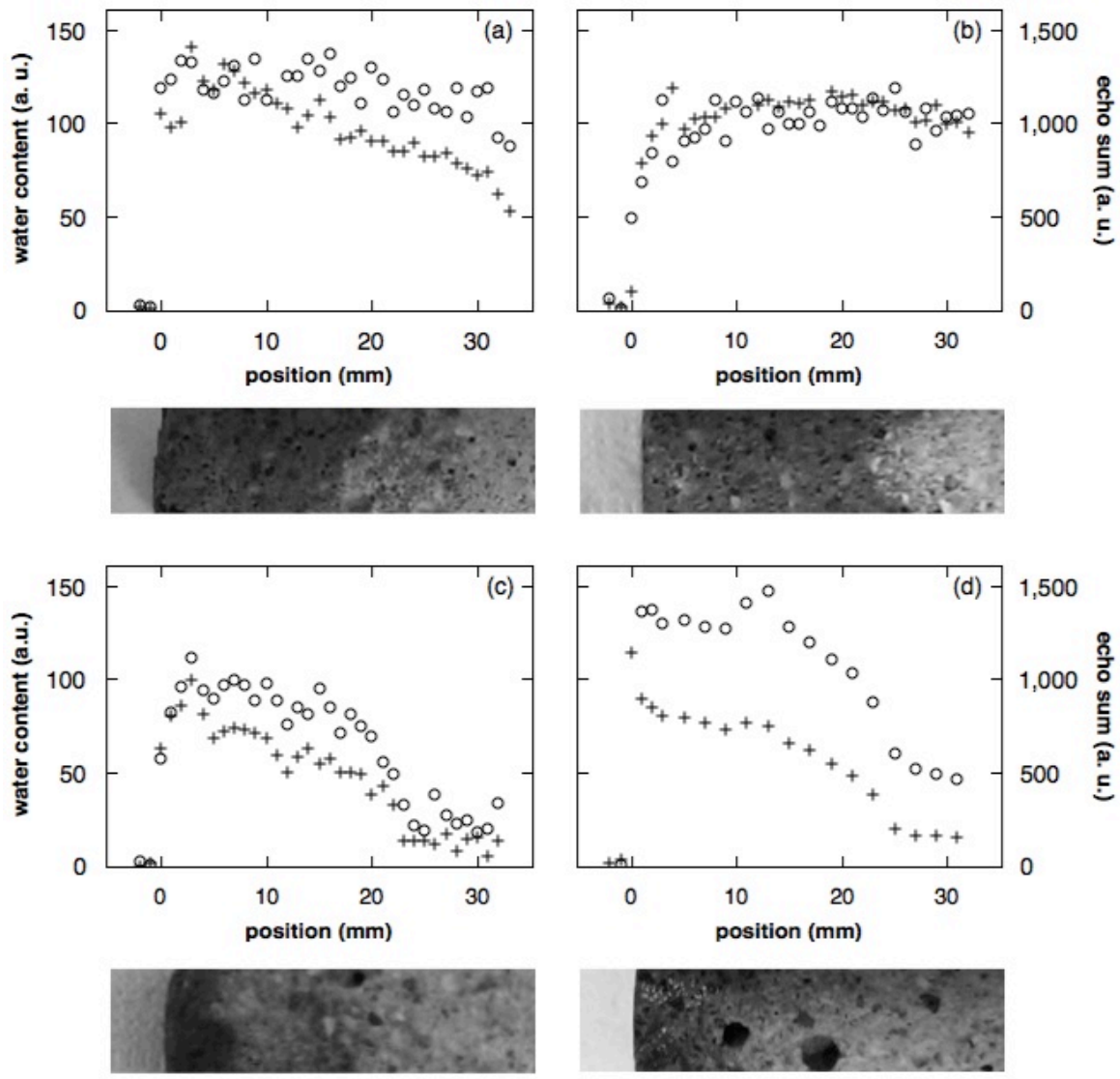


Figure 7.4 NMR profiles and photographs of 4 sealed cured CEM I mortar cylinder after 1 day of capillary absorption. The profiles are constructed from echo sums (crosses, right hand axes) and exponential fitting intensities (circles, left hand axes). All cylinders were cored from the same cube of mortar.

For all samples, the position of the “waterfront” determined by NMR was beyond the position indicated by the visibly wet region. In some cases, there was more than one visual waterfront. However, there seems to be no direct connection between the water content and the colour change boundary. However, the echo sum profile showed a change in gradient suggesting a change in the water filled pore size. Echo sum profiles are sensitive to the signal decay time. The longer the signal lifetime, the more echoes can be recorded with the same echo spacing and therefore the sum of those echoes increase, even when the signal amplitude is constant. With a small amount of very large pores filing, the total water content would not change significantly.

However, it will affect the echo sum as the relaxation time of a very large pore is long and contributes to all echoes.

*Figure 7.5* shows a sealed cured CEM I sample from dry (a), after 1 (b) 2 (c) and 4 (d) days of capillary absorption. The dry sample was uniformly light grey. The visual waterfront moved forward by time, from 5 mm at 1 day with a second waterfront at about 15 mm to 27-28 mm at 2 days and beyond the 33 mm measured by NMR at 4 days of capillary absorption. Again, the position of the waterfront determined by NMR was consistently at a greater distance than that indicated by the visible waterfront.

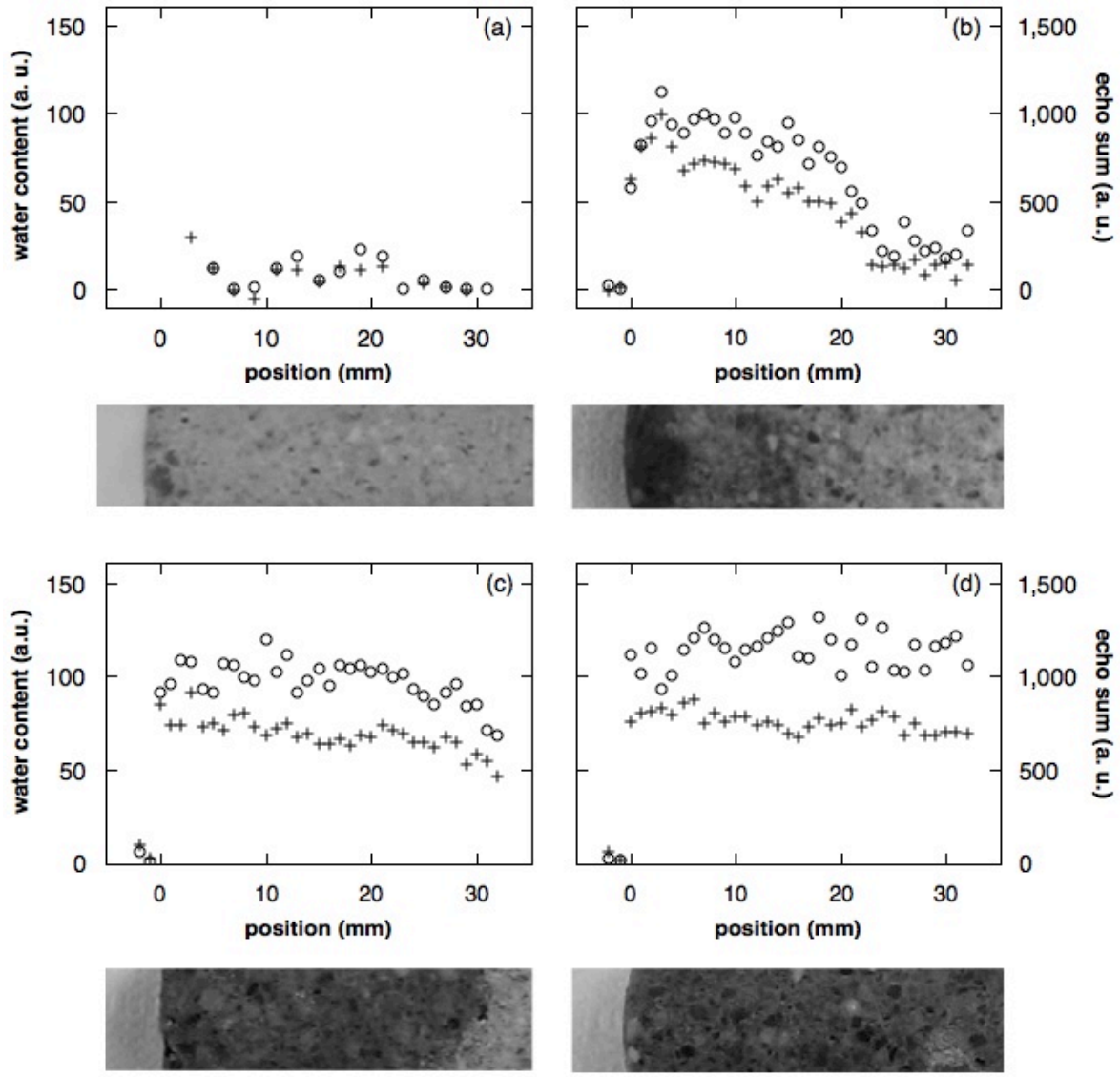


Figure 7.5. NMR profiles and photographs of a sealed cured CEM I mortar cylinder used in sorptivity experiments: (a) dry, (b) after 1 day, (c) after 2 days and (d) after 4 days of capillary absorption. The profiles are constructed from echo sums (crosses, right hand axes) and exponential fitting intensities (circles, left hand axes)

Two under water cured CEM I mortar samples were also investigated. *Figure 7.6* shows the underwater cured mortar samples. However, the water uptake by gravimetry was suspiciously low for one sample (*Figure 7.6 left*). The visual waterfront was not easily visible for either of the samples. Photographs show a small change in darkness. There was no significant change in colour as in the case of sealed cured mortar samples.

One possible explanation is that the sample on the left of *Figure 7.6* had significantly lower water content than the sealed samples. Water ingress by visual observation was about 25 mm for the sample. The NMR profile show water up to about 25-27 mm, although the maximum water content was anomalously low up to that depth.

The sample on the right showed water ingress by NMR up to about 30 mm with a visual waterfront at about 23 mm. The water content by NMR was higher than the other water cured sample. However, the visual waterfront was not as clear as in the case of sealed cured samples.

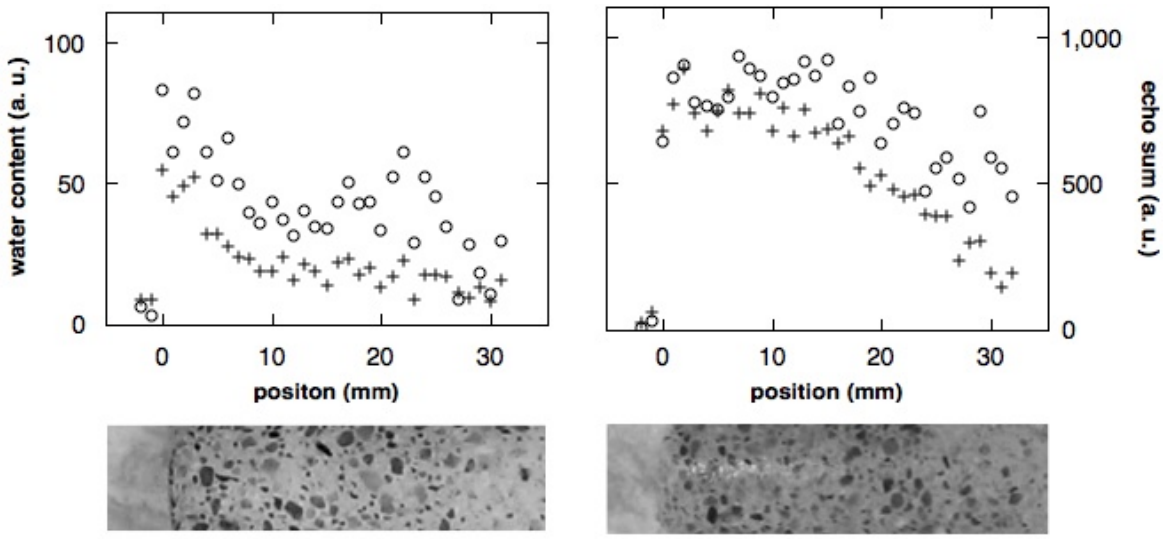


Figure 7.6. NMR profiles and photographs of two underwater cured CEM I mortar cylinders with photographs below after 1 day of capillary absorption. Visual waterfront was not clearly visible. The profiles are constructed from echo sums (crosses, right hand axes) and exponential fitting intensities (circles, left hand axes)

## 7.4 Blended mortar

In total, three CEM I + Si and three CEM III/B mortar cylinders were investigated. One CEM I + Si and one CEM III/B were part of the initial investigations with the Laboratory GARField where 2 mm steps were used,

*Figure 7.7* shows two CEM I + Si sealed cured mortar cylinders after 1 day of capillary absorption with photographs below. The clear visual waterfront was about 5 mm (left) and 8 mm (right). The NMR water profile showed water ingress up to about 20 mm for both samples with a sharp boundary between the wet and dry regions of the sample. Again, the position of the waterfront determined by NMR was 10-15 mm beyond the visual waterfront. As observed previously, there is no obvious change in the total water content or the echo sum NMR profiles before and after the position indicated by the visual waterfront.

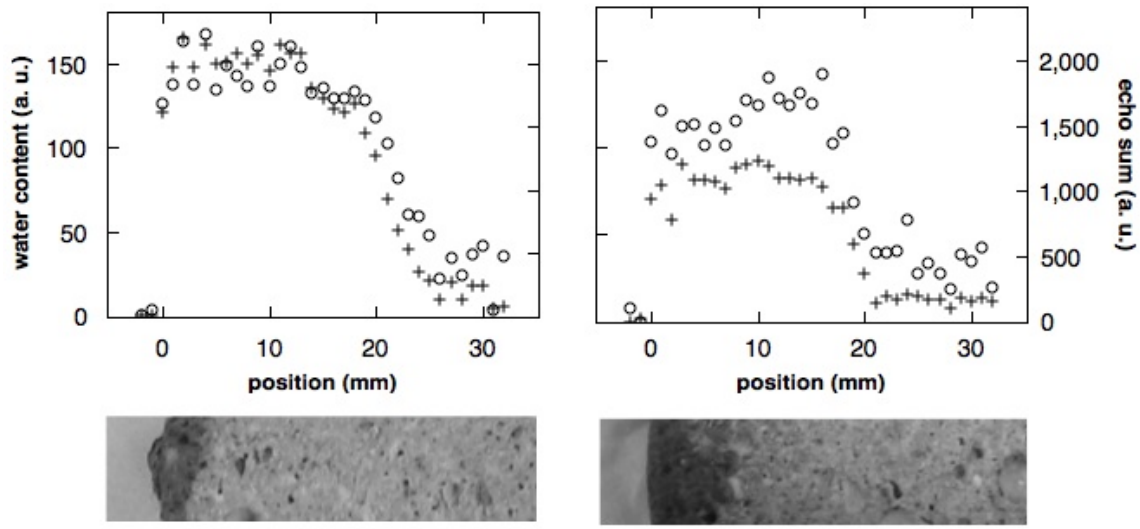


Figure 7.7. NMR profiles and photographs of two sealed cured CEM I + Si mortar cylinders with photographs below after 1 day of capillary absorption. The profiles are constructed from echo sums (crosses, right hand axes) and exponential fitting intensities (circles, left hand axes).

*Figure 7.8* shows a CEM III/B mortar cylinder up to 7 days of capillary absorption. NMR profiles showed that the waterfront stopped at about 25 mm depth. The visual waterfront also stopped, but at 12 mm. There is no clear indication of the visual waterfront after 1 day of capillary absorption (*Figure 7.8a*) in the NMR profiles. There was a decrease in the echo sum profiles (crosses) at b) 2 days, c) 4 days, and d) 7 days where the visual waterfront was

at 15 mm for 2 days and at 10 mm for 4 and 7 days. Again, at all times, the position of the NMR waterfront was beyond that determined visually.

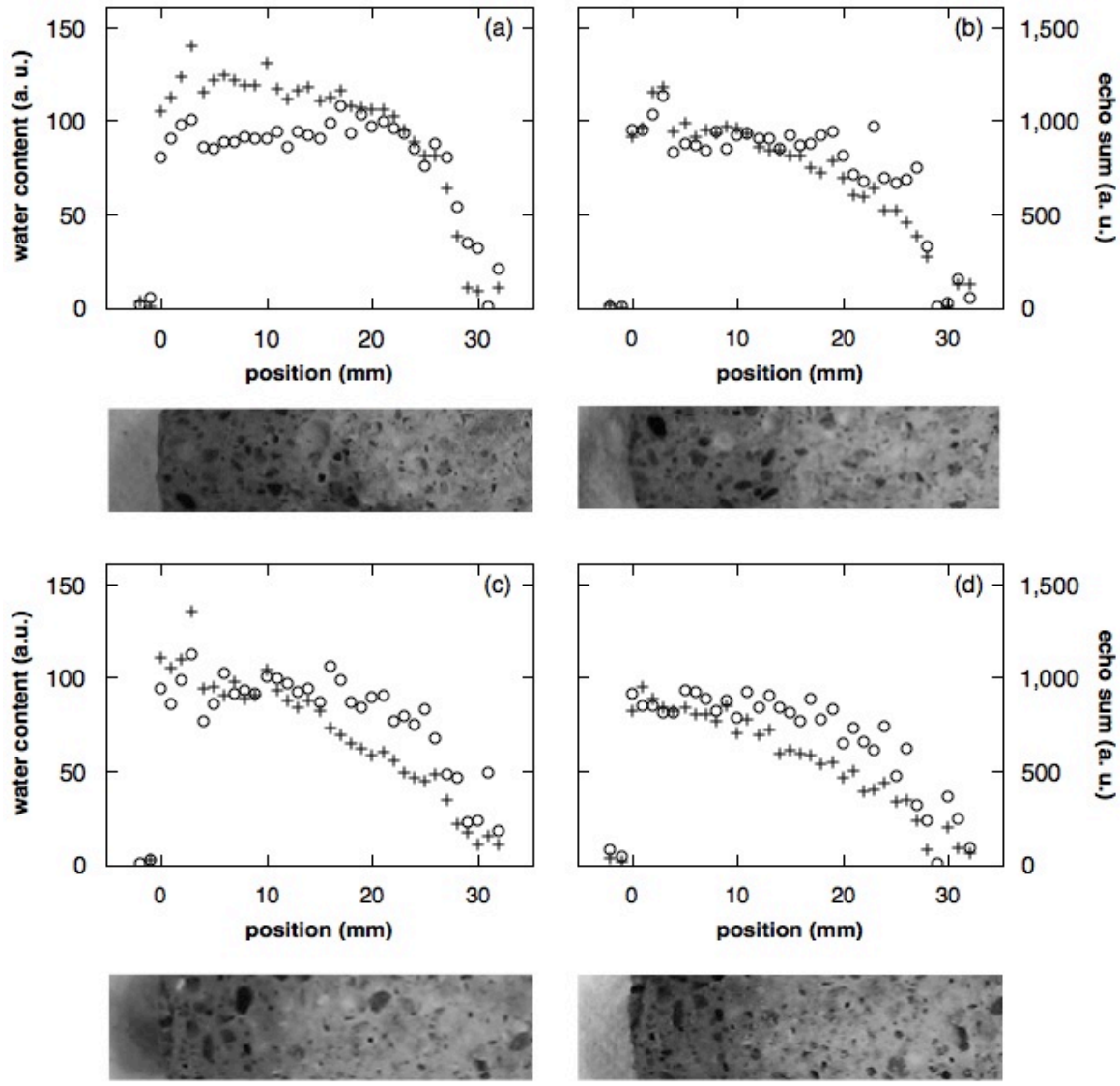


Figure 7.8. NMR profiles and photographs of a sealed cured CEM III/B mortar cylinder with photographs below after (a) 1 day, (b) 2 days, (c) 4 days and (d) 7 days of capillary absorption. The profiles are constructed from echo sums (crosses, right hand axes) and exponential fitting intensities (circles, left hand axes)

## 7.5 Cause of visual change

In a capillary uptake experiment, there is a (non-linear) gradient of internal relative humidity in the sample from 100% where the sample is in contact with liquid water down to the ambient value at the exposed end.

The observed colour change is associated with the wetting of pores of size comparable to the wavelength of light, i.e. circa 400-700 nm, which is the size of a larger capillary pore. The Kelvin equation (see *equation 2.7*) determines the pore radius filled at a certain RH. For optical wavelengths, and using parameters for water and assuming that water wets cement, this suggests that the colour change occurs at relative humidities exceeding 99.7%.

The NMR measurements were sensitive to water in gel pores, inter-hydrate pores and larger capillary pores due to chemical shrinkage and air voids. Using the Kelvin equation, pore width representative sizes of 3, 30, 300 and 3000 nm would fill at relative humidities of 70, 96, 99.6% and >99.9% respectively. NMR senses water across a very wide range of pore sizes, and hence relative humidities.

The colour change can be associated with 99.7% RH, the range where large capillary pores and air voids, of size about equal to the wavelength of light, fill with water. The overall volume of those large pores is small compared to the amount of gel and inter-hydrate pores. The relaxation time associated with the very large capillary pore associated with the colour change is in the range of 40-70 ms. In case of the CPMG experiments in this work, this very long relaxation time can be associated with small changes in the baseline.

Therefore a sharp feature in the NMR water profile at the colour change boundary cannot be expected, but there may be an indication in the echo sum profiles due to the increased sensitivity to long relaxation time.

## 7.6 Concluding remarks

It was noted during the concrete capillary absorption tests, that the visual waterline on the sides of the samples was not where the real waterfront was. The waterfront measured by NMR profiling was beyond the darker, visibly wet region for all samples and the NMR results showed that colour change is an inaccurate measure of the actual waterfront. The experiment had limitation as the samples had a thin paste skin on the sides and only echo sum profiles could be acquired with the Surface GARField NMR due to low signal to noise ratio.

Also, despite a water line in water penetration under pressure testing, NMR could not detect a change in water content after the test. The error of the measurement was about 3%.

Further experiments using drilled mortar cylinders on the Laboratory GARField showed that the position of the waterfront determined by NMR was beyond the visual waterline for all samples. There was no obvious change in saturation at the position of the waterfront identified visually although echo sum profiles suggested a small change in the water filled pore size. The colour change probably occurs when a very large pore size, about 500 nm, (in the range of the wavelength of visible light) fills. The fraction of these very large pores compared to the total capillary and gel porosity is very small, and so the change in water content is very small and could not be easily detected by NMR.

The visual waterfront underestimated the true water penetration depth for all investigated binders, the difference could be more than 10 mm between the two waterfronts. The difference in distance between the visual water line and the real waterfront depended on binder and varied from sample to sample. Therefore the use of visual observation as a comparison test between samples with different cement types is questionable.

Based on the results from the capillary sorptivity test, the real water penetration depth could exceed the visual front in the water penetration under pressure test as well.

The results of this work suggest caution when using the colour boundary or water line in testing of concrete water permeability or how far water penetrates the system. Especially that the darker region has about the same water saturation level as just beyond the visual front.

This work has been published in Magazine of Concrete Research [128].

# 8 Conclusion and future work

## 8.1 Introduction

Water transport in concrete is important as many of the degradation processes of concrete are connected to the presence and transport of water within the pore structure of the cement paste and other pores and cracks. The move towards complex binder systems including supplementary cementitious materials requires long-term predictions of the performance of concretes made with new binders. Therefore, a thorough understanding of the transport phenomena that occur in known systems is essential. Spatially resolved NMR provided better understanding of the physical mechanisms that occur during accepted water transport test procedures and provide new insight into processes of potential water/structure interaction that can occur during those tests.

## 8.2 Conclusions

### 8.2.1 GARField measurement

The Surface GARField NMR measurement was optimised and calibrated for assessing the presence and distribution of liquid water in concrete. Although the measurement technique has limitations, it worked on range of microstructures and provided useful insight into conventional water transport tests. The measurement is calibrated for a 15x15 cm surface area, though it could be applied to larger samples as the signal loss between large slabs and the calibrated surface was 5% and can be taken into account in calibrating measurements. However, the signal decay by depth was different for the reference saturated sandstone and the investigated concretes. This caused artefacts in the profiling resulting in under/over estimates of the water content at different locations. To make this more complicated, samples cured underwater

and never subjected to drying and dried and rewetted concrete samples showed a different signal decay by depth. Therefore, accurate compensation for signal loss by depth requires knowledge of the curing and history of the sample. This is not necessarily a problem in laboratory use, but will be a limitation of the measurement on site when older, existing structures are investigated.

### 8.2.2 Conventional water transport tests

Capillary absorption of three different binders, two curing methods and two w/c ratios were investigated. NMR profiling by the Surface GARField of concrete revealed the limitations of the simple gravimetric measurement. The conventional sorptivity test only tells half the story. The water uptake slowed down for all investigated concrete mixes, though the reason behind varied for the different binders: the thin (4 cm) CEM I samples were saturated after 1 day, the CEM III/B samples of the same size though were only half way wet and the waterfront stopped.

The EN 12390:8 water penetration under pressure test was also investigated. The change in the water content was too small to detect with the Surface GARField and results using mortar samples and the Laboratory GARField are not conclusive even though they showed a slight increase in water content. The testing parameters were varied for better understanding of the test. The effect of the sample diameter and the testing duration were investigated. The water penetration depth increased for larger samples. There was no clear relationship between testing duration and visible water penetration depth.

When using conventional water transport tests the limitations of the simple test procedures revealed by NMR profiling should be the taken into account.

### 8.2.3 Long-term sorptivity

Following an initial increase, the measurement on concrete samples by the Surface GARField showed a decrease in absorbed capillary water content by time after 1 day of capillary absorption. Both the signal intensity and the

relaxation time decreased suggesting a reduction in the amount of capillary water in smaller pores at later times compared to 1 day. This phenomenon was present in all investigated samples regardless of binder, curing and w/c ratio. Samples cured underwater showed that the original level of capillary porosity was significantly lower than after drying and rewetting for 1 day and that after 4-7 days, the level returned to the “as-cured” level.

Measurements on sealed mortar samples with the Laboratory GARField showed that the gel porosity increased at the expense of the capillary porosity. Measurements on under water cured samples revealed that additional capillary porosity was created during drying at the expense of the gel porosity. From a different perspective, collapsing gel increased the larger porosity. This was mostly reversible and both gel and capillary water levels in under water cured samples returned to original levels after about 4 days of capillary absorption.

Several possible causes for this effect were considered of which, the most probable, is considered to be C-S-H swelling. The swelling could be a possible cause of the well-known sorptivity anomaly observed in the water uptake of cementitious materials.

### 8.2.4 Colour change

It was observed that during the capillary absorption experiment on concrete slabs the position of the visual waterfront present on the sides of the sample did not correspond to the moisture profile obtained by NMR with the Surface GARField. There was a significant amount of water penetrating beyond the visibly wet region with only a marginal change in saturation measured by NMR. Cored mortar cylinders were further investigated using the Laboratory GARField. Photographs of the samples were compared to the NMR profiles. There was no marked change in the degree of saturation gradient at the visual water line boundary.

The results showed that visual waterfront is a poor indicator of the water penetration depth. The wavelength of visible light corresponds to a very large capillary pore size that is only a very small fraction of the overall pore volume. The relative humidity to fill that pore size is very high, 99.7%.

NMR profiling showed evidence that the water penetrated beyond the visibly wet region for sorptivity measurement. Water penetration under pressure experiments (Chapter 5.3) also indicated no strong front by NMR either.

In many concrete tests, the real material property is difficult to measure. Hence an alternative is used with a simple measurement and then the material property estimated. From an engineering prospective, if a test procedure does not show the true value or material property then this is not major problem as long the test is conservative. In this case, the visual waterline underestimates the water penetration depth and hence it is not conservative. Therefore, all tests based on visual observation, such as the European standard water penetration pressure test are fundamentally flawed. As a consequence of their limited ability to accurately track the waterfront in concrete the results of such tests should be used with extreme caution.

## 8.3 Future work

### 8.3.1 GARField measurement

A full profile with the current settings takes about 6.5 hours to measure with 1 mm steps and 1 hour for acquiring a separate dataset for $T_2$ analysis. It is appropriate in laboratory use, but the acquisition time should be reduced for on-site use. Further tests are required with larger motor steps for quicker measurement with possibly more scans acquired at larger depth to compensate for the reduced signal to noise ratio.

### 8.3.2 Conventional water transport tests

More in-depth experiments of under-water cured mortar samples is needed to some of the tested samples showed anomalously low water content both by NMR and gravimetry.

Further investigations of the water penetration under pressure test are needed to better understand the changes in the water filled porosity. Water

pressured applied from one end to mortar samples would allow to investigate the visual waterfront and colour change by NMR profiling. The change in water content is small. A more sensitive measurement or increased number of scans for better signal to noise is needed.

### 8.3.3 Long-term sorptivity

The results of this work showed a redistribution of water between gel and interhydrate and capillary pores. However, several questions remain that are worth investigating. A key to better understanding this phenomenon is to couple the NMR results with macroscopic volume changes and also the possible chemical changes caused by drying and then by rewetting the sample. Another interesting possibility is to carry out the investigation using organic liquids. To date the sorptivity anomaly has only been observed during water absorption and not with organic liquids. Only the first drying and rewetting was investigated. As most of the microstructural changes occur in the first drying, investigation of further drying and rewetting cycles could be of interest.

In case of the sealed cured samples the original gel and capillary porosity fractions could not be determined. The porosity was not filled with water therefore could not be investigated by NMR. The original porosity ratios would be worth investigating by either wetting the samples before drying or using alternative pore-size distribution measurement technique.

Another interesting and yet unanswered question is the increasing overall water content in sealed cured mortar samples in contrast to the constant total volume of samples cured underwater. Macroscopic volume change measurement might shed light to the cause of the difference in behaviour.

### 8.3.4 Colour change

Due to time restrictions, only a limited number of samples were tested for colour change during capillary absorption. Some of the samples were discarded as the water uptake by gravimetry or the NMR profiles showed unusual and unexpected behaviour probably due to microstructural damage. Also, for some

samples, the water ingress way beyond the measurement range of the Laboratory GARField. Repeats of all investigated binders, especially under water cured CEM I mortars would be of use. The mix design and capillary absorption duration should be carefully chosen so that the water penetration is within the measurable depth with the Laboratory GARField

A better understanding of the colour change relating to a certain pore size filling is important as visual observation of the water front is widely used. The total volume and volume fraction of the pore size associated with the colour change is worth investigating and can be applied to current testing procedures.

## References


[1] M. Felice, "Material of the Month: Concrete," *Materials World Magazine,* vol. 2013, pp. 3rd November 2014, .

[2] "World Business Council for Sustainable Development, Cement Sustainability Initiative," *2014(24th June),* Available: http://wbcsdcement.org.

[3] R. Malinowski, "Ancient mortars and concretes. durability aspects," in *Symponsium on Mortars, Cements and Grouts used in the Conservation of Hystoric Buildings,* 1981, pp. 341.

[4] S. Chandra and L. Berntsson. "1 - historical background of lightweight aggregate concrete," in *Lightweight Aggregate Concrete*, S. Chandra and L. Berntsson, Eds. 2002, .

[5] C. Mukerji, "The politics of rediscovery in the history of science: Tacit knowledge of concrete before its discovery," in *Annual Meeting of the American Sociological Association,* 2005, .

[6] K. Scrivener, "Cement production," in *Nanocem Transcend First Training Course, Maastricht,* 2011, .

[7] N. Davey. *A History of Building Materials* 1961 Available: http://books.google.de/books?id=9WF8AAAAIAAJ.

[8] Encyclopædia Britannica Online, "concrete," vol. 2014, .

[9] P. Hewlett. *Lea's Chemistry of Cement and Concrete* 2003.

[10] W. P. Hughes, D. Ancell, S. Gruneberg and L. and Hirst, "Exposing the myth of the 1:5:200 ratio relating initial cost, maintenance and staffing costs of office buildings," in *20th Annual ARCOM Conference,* Heriot-Watt University, Edinburgh, 2004, pp. 373.

[11] H. F. W. Taylor. *Cement Chemistry* (2nd ed.) 1997.

[12] I. G. Richardson. The calcium silicate hydrates. *Cem. Concr. Res. 38(2),* pp. 137-158. 2008.

[13] K. Scrivener, "Influence of SCMs," in *Nanocem Transcend First Training Course, Maastricht,* 2011, .

[14] C. Tasdemir. Combined effects of mineral admixtures and curing conditions on the sorptivity coefficient of concrete. *Cem. Concr. Res. 33(10),* pp. 1637-1642. 2003.

[15] J. -. Escalante-Garcia and J. H. Sharp. The chemical composition and microstructure of hydration products in blended cements. *Cement and Concrete Composites 26(8),* pp. 967-976. 2004.

[16] E. Gueneyisi and K. Mermerdas. Comparative study on strength, sorptivity, and chloride ingress characteristics of air-cured and water-cured concretes modified with metakaolin. *Mater. Struct. 40(10),* pp. 1161-1171. 2007. Available: http://dx.doi.org/10.1617/s11527-007-9258-5.

[17] J. Gorce and N. B. Milestone. Probing the microstructure and water phases in composite cement blends. *Cem. Concr. Res. 37(3),* pp. 310-318. 2007.

[18] R. Siddique and J. Klaus. Influence of metakaolin on the properties of mortar and concrete: A review. *Appl. Clay. Sci. 43(3–4),* pp. 392-400. 2009.

[19] BS EN 12620:2013, "Aggregates for concrete," 2013.

[20] K. Scrivener, "Hydration and microstructure," in *Nanocem Transcend First Training Course, Maastricht,* 2011, .

[21] K. A. Khalil. Pore structure and surface area of hardened cement pastes containing silica fume. *Mater Lett 26(4–5),* pp. 259-264. 1996.

[22] B. Lothenbach, K. Scrivener and R. D. Hooton. Supplementary cementitious materials. *Cem. Concr. Res. 41(12),* pp. 1244-1256. 2011.

[23] T. C. Powers and T. L. Brownyard. *Studies of the Physical Properties of Hardened Portland Cement Paste* 1948.

[24] H. J. H. Brouwers. The work of powers and brownyard revisited: Part 1. *Cem. Concr. Res. 34(9),* pp. 1697-1716. 2004.

[25] H. J. H. Brouwers. The work of powers and brownyard revisited: Part 2. *Cem. Concr. Res. 35(10),* pp. 1922-1936. 2005.

[26] A. C. A. Muller, K. L. Scrivener, A. M. Gajewicz and P. J. McDonald. Densification of C-S-H measured by 1H NMR relaxometry. *J. Phys. Chem. C 117(1),* pp. 403-412. 2013. Available: http://dx.doi.org/10.1021/jp3102964.

[27] H. M. Jennings. A model for the microstructure of calcium silicate hydrate in cement paste. *Cem. Concr. Res. 30(1),* pp. 101-116. 2000.

[28] H. M. Jennings. Refinements to colloid model of C-S-H in cement: CM-II. *Cem. Concr. Res. 38(3),* pp. 275-289. 2008.

[29] P. J. McDonald, V. Rodin and A. Valori. Characterisation of intra- and inter-C–S–H gel pore water in white cement based on an analysis of NMR signal amplitudes as a function of water content. *Cem. Concr. Res. 40(12),* pp. 1656-1663. 2010.

[30] E. J. Garboczi and D. P. Bentz. Modelling of the microstructure and transport properties of concrete. *Constr. Build. Mater. 10(5),* pp. 293-300. 1996.

[31] A. Ulrik Nilsen and P. J. M. Monteiro. Concrete: A three phase material. *Cem. Concr. Res. 23(1),* pp. 147-151. 1993.

[32] G. Ramesh, E. D. Sotelino and W. F. Chen. Effect of transition zone on elastic moduli of concrete materials. *Cem. Concr. Res. 26(4),* pp. 611-622. 1996.

[33] P. Stroeven and M. Stroeven. Reconstructions by SPACE of the interfacial transition zone. *Cement and Concrete Composites 23(2–3),* pp. 189-200. 2001.

[34] G. Pang, S. Chae and S. Chang, "Predicting Model for Pore Structure of Concrete Including Interface Transition Zone between Aggregate and Cement Paste," *International Journal of Concrete Structures and Materials,* vol. 3, pp. 81-90, .

[35] P. Stroeven. A stereological approach to roughness of fracture surfaces and tortuosity of transport paths in concrete. *Cement and Concrete Composites 22(5),* pp. 331-341. 2000.

[36] Z. Wu, H. S. Wong and N. R. Buenfeld. Influence of drying-induced microcracking and related size effects on mass transport properties of concrete. *Cem. Concr. Res. 68(0),* pp. 35-48. 2015.

[37] P. Zhang, F. H. Wittmann, T. Zhao, E. H. Lehmann and P. Vontobel. Neutron radiography, a powerful method to determine time-dependent moisture distributions in concrete. *Nucl. Eng. Des. 241(12),* pp. 4758-4766. 2011.

[38] M. Geiker, "Porosity development and moisture fixation, mechanisms," *Nanocem Transcend 1st Training Course, Maastricht,* 21-25 February 2011, 2011.

[39] P. Acker. Swelling, shrinkage and creep: A mechanical approach to cement hydration. *Mater. Struct. 37(4),* pp. 237-243. 2004.

[40] C. Gallé. Effect of drying on cement-based materials pore structure as identified by mercury intrusion porosimetry: A comparative study between oven-, vacuum-, and freeze-drying. *Cem. Concr. Res. 31(10),* pp. 1467-1477. 2001.

[41] S. Diamond. A discussion of the paper “Effect of drying on cement-based materials pore structure as identified by mercury porosimetry—a comparative study between oven-, vacuum-, and freeze-drying” by C. gallé. *Cem. Concr. Res. 33(1),* pp. 169-170. 2003.

[42] A. Korpa and R. Trettin. The influence of different drying methods on cement paste microstructures as reflected by gas adsorption: Comparison between freeze-drying (F-drying), D-drying, P-drying and oven-drying methods. *Cem. Concr. Res. 36(4),* pp. 634-649. 2006.

[43] N. C. Collier, J. H. Sharp, N. B. Milestone, J. Hill and I. H. Godfrey. The influence of water removal techniques on the composition and microstructure of hardened cement pastes. *Cem. Concr. Res. 38(6),* pp. 737-744. 2008.

[44] P. C. Fonseca and H. M. Jennings. The effect of drying on early-age morphology of C–S–H as observed in environmental SEM. *Cem. Concr. Res. 40(12),* pp. 1673-1680. 2010.

[45] V. S. Ramachandran. "1 - concrete science," in *Handbook of Analytical Techniques in Concrete Science and Technology*, V. S. Ramachandran and J. J. Beaudoin, Eds. 2001, .

[46] P. A. M. Basheer. "16 - permeation analysis," in *Handbook of Analytical Techniques in Concrete Science and Technology*, V. S. Ramachandran and J. J. Beaudoin, Eds. 2001, .

[47] D. P. Bentz, E. J. Garboczi and E. S. Lagergren. Multi-scale microstructural modeling of concrete diffusivity: Identification of significant varibles. *Cement, Concrete and Aggregates 20(1),* pp. 129-139. 1998.

[48] F. Bernard and S. Kamali-Bernard. Predicting the evolution of mechanical and diffusivity properties of cement pastes and mortars for various hydration degrees – A numerical simulation investigation. *Computational Materials Science 61(0),* pp. 106-115. 2012.

[49] E. J. Garboczi and D. P. Bentz. Multiscale analytical/numerical theory of the diffusivity of concrete. *Adv. Cem. Based Mater. 8(2),* pp. 77-88. 1998.

[50] B. H. Oh and S. Y. Jang. Prediction of diffusivity of concrete based on simple analytic equations. *Cem. Concr. Res. 34(3),* pp. 463-480. 2004.

[51] M. Zhang, G. Ye and K. van Breugel. Modeling of ionic diffusivity in non-saturated cement-based materials using lattice boltzmann method. *Cem. Concr. Res. 42(11),* pp. 1524-1533. 2012.

[52] Z. Zhang, M. Thiéry and V. Baroghel-Bouny. A review and statistical study of existing hysteresis models for cementitious materials. *Cem. Concr. Res. 57(0),* pp. 44-60. 2014.

[53] V. Baroghel-Bouny. Water vapour sorption experiments on hardened cementitious materials. part II: Essential tool for assessment of transport properties and for durability prediction. *Cem. Concr. Res. 37(3),* pp. 438-454. 2007.

[54] E. W. Washburn. The dynamics of capillary flow. *Phys. Rev. 17(3),* pp. 273-283. 1921. Available: http://link.aps.org/doi/10.1103/PhysRev.17.273.

[55] C. Hall. Water movement in porous building materials—IV. the initial surface absorption and the sorptivity. *Build. Environ. 16(3),* pp. 201-207. 1981.

[56] C. Hall. Water movement in porous building materials—I. unsaturated flow theory and its applications. *Build. Environ. 12(2),* pp. 117-125. 1977.

[57] C. Hall and W. D. Hoff, *Water Transport in Brick, Stone, and Concrete.* Spon Press, 2009.

[58] V. Baroghel-Bouny. Water vapour sorption experiments on hardened cementitious materials: Part I: Essential tool for analysis of hygral behaviour and its relation to pore structure. *Cem. Concr. Res. 37(3),* pp. 414-437. 2007.

[59] B. B. Sabir, S. Wild and M. O'Farrell. A water sorptivity test for mortar and concrete. *Mater. Struct. 31(8),* pp. 568-574. 1998. Available: http://dx.doi.org/10.1007/BF02481540.

[60] C. Hall. Water sorptivity of mortars and concretes: A review. *Magazine of Concrete Research 41(Volume 41, Issue 147),* pp. 51-61(10). 1989. Available: http://www.icevirtuallibrary.com/content/article/10.1680/macr.1989.41.147.51.

[61] C. Hall, W. D. Hoff, S. C. Taylor, M. A. Wilson, B. Yoon, H. -. Reinhardt, M. Sosoro, P. Meredith and A. M. Donald. Water anomaly in capillary liquid absorption by cement-based materials. *J. Mater. Sci. Lett. 14(17),* pp. 1178-1181. 1995.

[62] N. S. Martys and C. F. Ferraris. Capillary transport in mortars and concrete. *Cem. Concr. Res. 27(5),* pp. 747-760. 1997.

[63] S. C. Taylor, W. D. Hoff, M. A. Wilson and K. M. Green. Anomalous water transport properties of portland and blended cement-based materials. *J. Mater. Sci. Lett. 18(23),* pp. 1925-1927. 1999. Available: http://dx.doi.org/10.1023/A%3A1006677014070.

[64] L. Hanžič and R. Ilić. Relationship between liquid sorptivity and capillarity in concrete. *Cem. Concr. Res. 33(9),* pp. 1385-1388. 2003.

[65] C. Hall. Anomalous diffusion in unsaturated flow: Fact or fiction? *Cem. Concr. Res. 37(3),* pp. 378-385. 2007.

[66] BS 1881-122:2011, "Testing concrete. Method for determination of water absorption," 2011.

[67] M. A. Wilson, S. C. Taylor and W. D. Hoff. The initial surface absorption test (ISAT): An analytical approach. *Magazine of Concrete Research 50(Volume 50, Issue 2),* pp. 179-185(6). 1998. Available: http://www.icevirtuallibrary.com/content/article/10.1680/macr.1998.50.2.179.

[68] L. Basheer, M. Basheer, A. Long, N. Harmon, L. Basheer, M. Basheer, A. Long and N. Harmon. Autoclam permeability system for measuring absorption and permeability of concrete in the laboratory and on site. 2005, .

[69] P. A. M. Basheer and É Nolan. Near-surface moisture gradients and in situ permeation tests. *Constr. Build. Mater. 15(2–3),* pp. 105-114. 2001.

[70] J. W. Figg. Methods of measuring the air and water permeability of concrete. *Magazine of Concrete Research 25(Volume 25, Issue 85),* pp. 213-219(6). 1973. Available: http://www.icevirtuallibrary.com/content/article/10.1680/macr.1973.25.85.213.

[71] BS EN 12390-8:2009, "*Testing hardened concrete - Part 8: Depth of penetration of water under pressure*," .

[72] W. Vichit-Vadakan and G. W. Scherer. Measuring permeability of rigid materials by a beam-bending method: III, cement paste. *J Am Ceram Soc 85(6),* pp. 1537-1544. 2002.

[73] H. Loosveldt, Z. Lafhaj and F. Skoczylas. Experimental study of gas and liquid permeability of a mortar. *Cem. Concr. Res. 32(9),* pp. 1357-1363. 2002.

[74] N. Hearn, R. J. Detwiler and C. Sframeli. Water permeability and microstructure of three old concretes. *Cem. Concr. Res. 24(4),* pp. 633-640. 1994.

[75] H. S. Wong, M. Zobel, N. R. Buenfeld and R. W. Zimmerman. Influence of the interfacial transition zone and microcracking on the diffusivity, permeability and sorptivity of cement-based materials after drying. *Magazine of Concrete Research 61(Volume 61, Issue 8),* pp. 571-589(18). 2009. Available: http://www.icevirtuallibrary.com/content/article/10.1680/macr.2008.61.8.571.

[76] K. S. Chia and M. Zhang. Water permeability and chloride penetrability of high-strength lightweight aggregate concrete. *Cem. Concr. Res. 32(4),* pp. 639-645. 2002.

[77] S. Tsivilis, J. Tsantilas, G. Kakali, E. Chaniotakis and A. Sakellariou. The permeability of portland limestone cement concrete. *Cem. Concr. Res. 33(9),* pp. 1465-1471. 2003.

[78] H. Hilsdorf and J. Kropp. *Performance Criteria for Concrete Durability* 2004Available: http://books.google.de/books?id=P6yp_9RLqFYC.

[79] B. Blümich. *Essential NMR: For Scientists and Engineers* 2005Available: http://books.google.de/books?id=N2JQfyCvk8sC.

[80] F. D'Orazio, S. Bhattacharja, W. P. Halperin, K. Eguchi and T. Mizusaki. Molecular diffusion and nuclear-magnetic-resonance relaxation of water in unsaturated porous silica glass. *Phys. Rev. B 42(16),* pp. 9810-9818. 1990.

[81] A. Valori, P. J. McDonald and K. L. Scrivener. The morphology of C–S–H: Lessons from 1H nuclear magnetic resonance relaxometry. *Cem. Concr. Res. 49(0),* pp. 65-81. 2013.

[82] S. Meiboom and D. Gill. Modified spin-echo method for measuring nuclear relaxation times. *Rev. Sci. Instrum. 29(8),* pp. 688-691. 1958.

[83] B. Blümich, J. Perlo and F. Casanova. Mobile single-sided NMR. *Prog Nucl Magn Reson Spectrosc 52(4),* pp. 197-269. 2008.

[84] G. Eidmann, R. Savelsberg, P. Blümler and B. Blümich. The NMR MOUSE, a mobile universal surface explorer. *Journal of Magnetic Resonance, Series A 122(1),* pp. 104-109. 1996.

[85] J. Perlo, F. Casanova and B. Blümich. Profiles with microscopic resolution by single-sided NMR. *Journal of Magnetic Resonance 176(1),* pp. 64-70. 2005.

[86] A. E. Marble, I. V. Mastikhin, B. G. Colpitts and B. J. Balcom. An analytical methodology for magnetic field control in unilateral NMR. *Journal of Magnetic Resonance 174(1),* pp. 78-87. 2005.

[87] P. J. McDonald, P. S. Aptaker, J. Mitchell and M. Mulheron. A unilateral NMR magnet for sub-structure analysis in the built environment: The surface GARField. *Journal of Magnetic Resonance 185(1),* pp. 1-11. 2007.

[88] P. J. McDonald, J. Mitchell, M. Mulheron, P. S. Aptaker, J. Korb and L. Monteilhet. Two-dimensional correlation relaxometry studies of cement pastes performed using a new one-sided NMR magnet. *Cem. Concr. Res. 37(3),* pp. 303-309. 2007.

[89] A. Valori, "Characterisation of Cementitous Materials by 1H NMR," 2009.

[90] Perlo, J., Casanova, F., Bluemich, B, "Ex situ NMR in highly homogeneous fields: H-1 spectroscopy," *Science,* vol. 315, pp. 1110-1112, 2007.

[91] B. Manz, A. Coy, R. Dykstra, C. D. Eccles, M. W. Hunter, B. J. Parkinson and P. T. Callaghan. A mobile one-sided NMR sensor with a homogeneous magnetic field: The NMR-MOLE. *Journal of Magnetic Resonance 183(1),* pp. 25-31. 2006.

[92] M. Nogueira d'Eurydice and P. Galvosas. Measuring diffusion–relaxation correlation maps using non-uniform field gradients of single-sided NMR devices. *Journal of Magnetic Resonance 248(0),* pp. 137-145. 2014.

[93] G. Bennett, J. -. Gorce, J. L. Keddie, P. J. McDonald and H. Berglind. Magnetic resonance profiling studies of the drying of film-forming aqueous dispersions and glue layers. *Magn. Reson. Imaging 21(3–4),* pp. 235-241. 2003.

[94] K. R. Brownstein and C. E. Tarr. Importance of classical diffusion in NMR studies of water in biological cells. *Phys. Rev. A 19(6),* pp. 2446-2453. 1979. Available: http://link.aps.org/doi/10.1103/PhysRevA.19.2446.

[95] W. P. Halperin, S. Bhattacharja and F. D'Orazio. Relaxation and dynamical properties of water in partially filled porous materials using NMR techniques. *Magn. Reson. Imaging 9(5),* pp. 733-737. 1991.

[96] J. C. MacTavish, L. Miljkovic, M. M. Pintar, R. Blinc and G. Lahajnar. Hydration of white cement by spin grouping NMR. *Cem. Concr. Res. 15(2),* pp. 367-377. 1985.

[97] G. Papavassiliou, F. Milia, M. Fardis, R. Rumm, E. Laganas, O. Jarh, A. Sepe, R. Blinc and M. M. Pintar. 1H nuclear magnetic resonance imaging of water diffusion in hardened cement pastes. *J Am Ceram Soc 76(8),* pp. 2109-2111. 1993.

[98] S. Bhattacharja, M. Moukwa, F. D'Orazio, J. Jehng and W. P. Halperin. Microstructure determination of cement pastes by NMR and conventional techniques. *Adv. Cem. Based Mater. 1(2),* pp. 67-76. 1993.

[99] E. W. Hansen, H. C. Gran, P. O. Kvernberg and B. Pedersen. Surface-to-volume ratio of porous materials obtained by a combined use of NMR and MIP. *J Phys Chem B 101(45),* pp. 9206-9214. 1997. Available: http://dx.doi.org/10.1021/jp971925c.

[100] P. Wang, M. M. Ferguson, G. Eng, D. P. Bentz, C. F. Ferraris and J. R. Clifton. 1H nuclear magnetic resonance characterization of portland cement: Molecular diffusion of water studied by spin relaxation and relaxation time-weighted imaging. *J. Mater. Sci. 33(12),* pp. 3065-3071. 1998. Available: http://dx.doi.org/10.1023/A%3A1004331403418.

[101] A. C. A. Muller, K. L. Scrivener, A. M. Gajewicz and P. J. McDonald. Use of bench-top NMR to measure the density, composition and desorption isotherm of C–S–H in cement paste. *Microporous and Mesoporous Materials 178(0),* pp. 99-103. 2013.

[102] P. J. Prado, B. J. Balcom, S. D. Beyea, T. W. Bremner, R. L. Armstrong and P. E. Grattan-Bellew. Concrete freeze/thaw as studied by magnetic resonance imaging. *Cem. Concr. Res. 28(2),* pp. 261-270. 1998.

[103] K. Hazrati, L. Pel, J. Marchand, K. Kopinga and M. Pigeon. Determination of isothermal unsaturated capillary flow in high performance cement mortars by NMR imaging. *Mater. Struct. 35(10),* pp. 614-622. 2002.

[104] S. D. Beyea, B. J. Balcom, T. W. Bremner, P. J. Prado, D. P. Green, R. L. Armstrong and P. E. Grattan-Bellew. Magnetic resonance imaging and moisture content profiles of drying concrete. *Cem. Concr. Res. 28(3),* pp. 453-463. 1998.

[105] M. Van Landeghem, J. d'Espinose de Lacaillerie, B. Blümich, J. Korb and B. Bresson. The roles of hydration and evaporation during the drying of a cement paste by localized NMR. *Cem. Concr. Res. 48(0),* pp. 86-96. 2013.

[106] A. J. Bohris, U. Goerke, P. J. McDonald, M. Mulheron, B. Newling and B. Le Page. A broad line NMR and MRI study of water and water transport in portland cement pastes. *Magn. Reson. Imaging 16(5–6),* pp. 455-461. 1998.

[107] J. Tritt-Goc, N. Piślewski, S. Kościelski and F. Milia. The influence of the superplasticizer on the hydration and freezing processes in white cement studied by 1H spin-lattice relaxation time and single point imaging. *Cem. Concr. Res. 30(6),* pp. 931-936. 2000.

[108] K. Friedemann, F. Stallmach and J. Kärger. NMR diffusion and relaxation studies during cement hydration—A non-destructive approach for clarification of the mechanism of internal post curing of cementitious materials. *Cem. Concr. Res. 36(5),* pp. 817-826. 2006.

[109] N. Nestle, A. Kühn, K. Friedemann, C. Horch, F. Stallmach and G. Herth. Water balance and pore structure development in cementitious materials in internal curing with modified superabsorbent polymer studied by NMR. *Microporous and Mesoporous Materials 125(1–2),* pp. 51-57. 2009.

[110] P. J. McDonald, J. -. Korb, J. Mitchell and L. Monteilhet. Surface relaxation and chemical exchange in hydrating cement pastes: A two-dimensional NMR relaxation study. *Phys Rev E. 72(1),* pp. 011409. 2005. Available: http://link.aps.org/doi/10.1103/PhysRevE.72.011409.

[111] L. Monteilhet, J. -. Korb, J. Mitchell and P. J. McDonald. Observation of exchange of micropore water in cement pastes by two-dimensional t_{2}-t_{2} nuclear magnetic resonance relaxometry. *Phys Rev E. 74(6),* pp. 061404. 2006. Available: http://link.aps.org/doi/10.1103/PhysRevE.74.061404.

[112] F. Barberon, J. -. Korb, D. Petit, V. Morin and E. Bermejo. Probing the surface area of a cement-based material by nuclear magnetic relaxation dispersion. *Phys. Rev. Lett. 90(11),* pp. 116103. 2003. Available: http://link.aps.org/doi/10.1103/PhysRevLett.90.116103.

[113] A. Valori, . Instruction manual to use the concrete suraface GARField. 2008

[114] M. D. Hürlimann and D. D. Griffin. Spin dynamics of Carr–Purcell–Meiboom–Gill-like sequences in grossly inhomogeneous B0 and B1 fields and application to NMR well logging. *Journal of Magnetic Resonance 143(1),* pp. 120-135. 2000.

[115] BS EN 206-1:2000, "Concrete. Specification, performance, production and conformity," 2000.

[116] BS EN 12350-5:2009, "Testing fresh concrete. Flow table test," 2009.

[117] BS EN 196-1:2005, "Methods of testing cement. Determination of strength," .

[118] BS EN 12390-2:2009, "Testing hardened concrete. Making and curing specimens for strength test," 2009.

[119] BS EN 12390-3:2009, "Testing hardened concrete. Compressive strength of test specimens," 2009.

[120] R. Loser, B. Lothenbach, A. Leemann and M. Tuchschmid. Chloride resistance of concrete and its binding capacity – comparison between experimental results and thermodynamic modeling. *Cement and Concrete Composites 32(1),* pp. 34-42. 2010.

[121] J. Murata, "Studies on the Permeability of Concrete," *Materials and Structures,* pp. 47-54, 1965.

[122] R. M. Kowalczyk, A. M. Gajewicz and P. J. McDonald. The mechanism of water-isopropanol exchange in cement pastes evidenced by NMR relaxometry. *RSC Adv. (40),* pp. 20709.

[123] S. Zamani, R. M. Kowalczyk and P. J. McDonald. The relative humidity dependence of the permeability of cement paste measured using GARField NMR profiling. *Cem. Concr. Res. 57(0),* pp. 88-94. 2014.

[124] D. A. Lockington and J. Parlange. Anomalous water absorption in porous materials. *J. Phys. D 36(6),* pp. 760. 2003. Available: http://stacks.iop.org/0022-3727/36/i=6/a=320.

[125] L. J. Parrott, W. Hansen and R. L. Berger. Effect of first drying upon the pore structure of hydrated alite paste. *Cem. Concr. Res. 10(5),* pp. 647-655. 1980.

[126] I. Maruyama, Y. Nishioka, G. Igarashi and K. Matsui. Microstructural and bulk property changes in hardened cement paste during the first drying process. *Cem. Concr. Res. 58(0),* pp. 20-34. 2014.

[127] N. Fischer, R. Haerdtl and P. J. McDonald. Observation of the redistribution of nanoscale water filled porosity in cement based materials during wetting. *Cem. Concr. Res. 68(0),* pp. 148-155. 2015.

[128] N. Fischer, R. Haerdtl and P. J. McDonald. Is colour change a good measure of a water penetration front? *(Magazine of Concrete Research),* pp. 1-6(5). Available: http://www.icevirtuallibrary.com/content/article/10.1680/macr.14.00354.